ADSORPTIVE REMOVAL OF SULFAMETHOXAZOLE AND TRIMETHOPRIM FROM AQUEOUS SOLUTIONS USING WHITE-ROT FUNGUS BIOCHAR, CORNCOB BIOCHAR, AND THEIR COMPOSITE MIXTURES

CHIPPOH KAUDZA

MASTER OF SCIENCE IN

SOIL AND WATER ENGINEERING

JOMO KENYATTA UNIVERSITY

OF

AGRICULTURE AND TECHNOLOGY

2026

Adsorptive Removal of Sulfamethoxazole and Trimethoprim from Aqueous Solutions Using White-Rot Fungus Biochar, Corncob Biochar, and Their Composite Mixtures

Chippoh Kaudza

A Thesis Submitted in Partial Fulfillment of Requirements for the Degree of Master of Science in Soil and Water Engineering of the Jomo Kenyatta University of Agriculture and Technology

2026

DECLARATION

This thesis is my original work and has not been presented for degree in any other University.

Signature ..... Date .....

Chippoh Kaudza

This thesis has been submitted for examination with our approval as the University Supervisors:

Signature ..... Date .....

Prof. James Raude, PhD

JKUAT, Kenya

Signature ..... Date .....

Dr. Elijah Ngumba, PhD

JKUAT, Kenya

DEDICATION

I dedicate this work to Almighty God, whose divine guidance and boundless grace have sustained me throughout this academic journey. Without his blessings, this achievement would not have been possible. I also dedicate this work to my dear parents, Mr. Enos Senior Kaudza and Mrs. Bertha Kaudza, whose unconditional love, sacrifices, and unwavering support have been the foundation of my success. Their encouragement has inspired me to persevere and reach this milestone. To God and my parents, I dedicate this work with gratitude.

ACKNOWLEDGEMENT

I express my sincere gratitude to my supervisors, Prof. Eng. James M. Raude and Dr. Elijah Ngumba from Jomo Kenyatta University of Agriculture and Technology (JKUAT) for their guidance and support throughout my studies. I would also like to thank Dr. Jared O. Nyang'au, from Aarhus University, Denmark, to whom I owe gratitude for supporting in the elemental analysis of samples at the Department of Biological and Chemical Engineering, Aarhus University, Denmark. I appreciate Dr. Eng. Joseph Sang, who was my academic adviser throughout my studies. I appreciate the staff at the Department of Soil Water and Environmental Engineering (SWEED), Department of Chemistry, Department of Civil Engineering and Department of Food Science and Technology respectively, for their guidance in sample analysis. I am grateful to Josephine Ouma, Joel Klement Ogilo, Faith Chepkony, Annitah Agasa, and Mary Nyambura Mwangi for their guidance and support in conducting adsorption experiments. Finally, I am grateful to my parents, siblings and friends, for not only offering me overwhelming support and encouragement, but also enduring my absence during my studies.

TABLE OF CONTENTS

LIST OF TABLES

LIST OF FIGURES

LIST OF APPENDICES

ABBREVIATION, ACRONYMS AND SYMBOLS

ARE	Average relative error
ARGs	Antibiotic Resistant Genes
ANOVA	Analysis of Variance
BOD	Biological Oxygen Demand
CB700	Corncob biochar
CCD	Central Composite Design
CHNS	Carbon, Hydrogen, Nitrogen, and Sulfur
CO_2	Carbon dioxide
COD	Chemical Oxygen Demand
$CoFe_2O_4$	Cobalt iron oxide
CFD	Computational Fluid Dynamics
D	Desirability function
D-R	Dubinin-Radushkevich
FTIR	Fourier Transform Infrared Spectroscopy
HCl	Hydrochloric acid
HC	Hydrothermal Carbonization
H_2O	Water
H_3PO_4	Phosphoric acid
IPD	Intra-Particle Diffusion
JKUAT	Jomo Kenyatta University of Agriculture and Technology
KBr	Potassium bromide
KMD	Kenya Meteorological Department
KNO_3	Potassium nitrate
LC-MS/MS	Liquid Chromatography-Tandem Mass spectrometry
NaOH	Sodium hydroxide
NSAIDs	Nonsteroidal Anti-Inflammatory Drugs
PCs	Pharmaceutical compounds

PFO	Pseudo-first-order
pH_{pzc}	Point of zero charge
PKa_1	First acid dissociation constant expressed as a negative logarithm
PKa_2	Second acid dissociation constant expressed as a negative logarithm
PSO	Pseudo-second-order
RSM	Response surface methodology
SDG	Sustainable Development Goal
SEM	Scanning Electron Microscopy
SMX	Sulfamethoxazole
S/N	Signal-to-Noise ratio
TC	Total carbon
TMP	Trimethoprim
TOC	Total organic carbon
WR700	White-rot fungus biochar
WWTP	Wastewater Treatment Plant
XRD	X-ray diffraction
$\boldsymbol{a}$	Number of rows (runs)
α	Adsorption rate during the initial phase
α_0	Value of the fixed response at the center point of the design
α_i	Linear effect regression term
α_{ii}	Quadratic effect regression term
α_{ij}	Interaction effect regression term
$\boldsymbol{a_S}$	Constant related to adsorption affinity
$\boldsymbol{A}$	Mass percentage of ash
$\boldsymbol{AC}$	Ash content
$\boldsymbol{A_T}$	Temkin isotherm constant
$\boldsymbol{AC}$	Ash content

$\boldsymbol{B}$	Constant related to the heat of adsorption
$\boldsymbol{b}$	Number of levels
$\boldsymbol{\beta}$	Desorption constant
$\boldsymbol{\beta_S}$	Parameter that indicates surface heterogeneity
$\boldsymbol{C}$	Mass percentage of carbon
$\boldsymbol{c}$	Number of center point replicates
$\boldsymbol{C_1}$	Concentration of stock solution
$\boldsymbol{C_2}$	Concentration of working solution
$\boldsymbol{C_e}$	Concentration of adsorbate at equilibrium time
$\boldsymbol{C_{ip}}$	Intra-particle diffusion constant
$\boldsymbol{C_t}$	concentration of adsorbate at time t
$\boldsymbol{C_0}$	Initial adsorbate concentration
$\boldsymbol{\varepsilon}$	Random error
$\boldsymbol{f}$	Number of columns (factors)
g/cm^3	Gram per cubic centimeter
g/L	Gram per liter
$\boldsymbol{H}$	Mass percentage of hydrogen
$\boldsymbol{K}$	Dubinin-Radushkevich constant
$\boldsymbol{k}$	Number of studied factors
$\boldsymbol{k_1}$	Pseudo-first order rate constant
$\boldsymbol{k_2}$	Pseudo-second-order rate constant
$\boldsymbol{K_F}$	Freundlich constant
$\boldsymbol{k_{ip}}$	Measure of the diffusion coefficient
$\boldsymbol{K_L}$	Langmuir isotherm constant
mg/L	Milligram per liter
mg/g	Milligram per gram
$\boldsymbol{m}$	Mass of adsorbent
$\boldsymbol{M_1}$	Mass of wet biochar

M_2	Mass of dry biochar
M_3	Mass after heating at 550°C
M_4	Mass after heating at 700°C
$M_{Biochar}$	Mass of biochar
$M_{Biomass}$	Mass of precursor
MC	Moisture content
n	Number of measurements
N	Mass percentage of nitrogen
N_E	Total number of experiments
ng/L	Nanogram per liter
o	Total number of observations
O	Mass percentage of oxygen
OA	Orthogonal array
q_e	Adsorption capacity at equilibrium time
$q_{e,calc}$	Calculated equilibrium adsorption capacity
$q_{e,meas}$	Measured equilibrium adsorption capacity
$q_{e,exp}$	Experimental equilibrium adsorption capacity
q_{max}	Maximum adsorption capacity
q_t	Adsorption capacity at time t
R	Gas constant
R^2	Determination coefficient
R_L	Separation factor
s	Adsorption intensity or surface heterogeneity
S	Mass percentage of sulfur
t	Time in minutes
T	Absolute temperature
µg/L	Microgram per liter
µm	Micrometer

$\boldsymbol{v}$	Number of independent variables
$\boldsymbol{V_1}$	Volume of stock solution to be drawn
$\boldsymbol{V_2}$	Volume of working solution
$\boldsymbol{V}$	Volume of solution
$\boldsymbol{VM}$	Volatile matter
$\boldsymbol{x_i}$	level of the independent variable
$\boldsymbol{x^2}$	Chi-square
$\boldsymbol{y}$	Predicted response variable
$\boldsymbol{z_i}$	Observed value
$\boldsymbol{\lambda_{max}}$	Maximum absorbance wavelength

ABSTRACT

Pharmaceutical residues, particularly antibiotics, are emerging contaminants of environmental concern because of their persistence in aquatic environments and their contribution to antibiotic resistance. Adsorption using biochar has attracted considerable attention as a sustainable and cost-effective treatment technology. This study evaluated the removal of sulfamethoxazole (SMX) and trimethoprim (TMP) from aqueous solutions using phosphoric acid-activated white-rot fungus biochar (WR700), corncob biochar (CB700), and their mixtures. Specifically, the study characterized the physicochemical properties of WR700 and CB700, evaluated their adsorption behavior using kinetic and equilibrium studies, and assessed the performance of their mixtures under varying operating conditions using a Taguchi L25 orthogonal array. Biochar characterization using scanning electron microscopy (SEM), Fourier-transform infrared spectroscopy (FTIR), elemental analysis, proximate analysis, and zeta potential analysis confirmed that both WR700 and CB700 possessed porous structures, oxygen-containing functional groups, and favorable surface characteristics for adsorption. Batch adsorption experiments showed that WR700 achieved maximum removal efficiencies of 99.5% for SMX and 89.8% for TMP, while CB700 achieved maximum removal efficiencies of 89.8% for SMX and 87.7% for TMP. The maximum adsorption capacity of WR700 was 0.22 mg g^{-1} for both antibiotics, whereas CB700 achieved adsorption capacities of 0.12 mg g^{-1} for SMX and 0.15 mg g^{-1} for TMP. Adsorption was influenced by solution pH, contact time, and adsorbent dosage, with kinetic and equilibrium analyses indicating that both physical and chemical interactions contributed to antibiotic removal. The mixtures of WR700 and CB700 did not improve adsorption performance. Instead, maximum removal efficiencies of 65.56% for SMX and 27.37% for TMP were obtained, indicating an antagonistic interaction between the two biochars. Overall, the study demonstrates that WR700 and CB700 are effective adsorbents for the removal of sulfamethoxazole and trimethoprim from aqueous solutions, whereas combining the two biochars does not enhance adsorption performance. These findings provide useful information for the development of sustainable biochar-based technologies for antibiotic removal from contaminated water.

CHAPTER ONE

INTRODUCTION

1.1 Background Information

The contamination of aquatic environments by pharmaceutical compounds (PCs) has emerged as a global environmental concern due to their continuous release into water bodies and persistence behavior in the environment (Chauhan et al., 2022). Pharmaceuticals enter aquatic systems through wastewater discharged from pharmaceutical manufacturing industries, effluents from wastewater treatment plants, household waste, landfill leachates, and the excretion of unmetabolized drugs by humans and animals (Chmielewski et al., 2023; Kümmerer, 2010). Consequently, pharmaceutical residues have been detected in surface water, groundwater, wastewater, and even the cryosphere, indicating their widespread distribution across aquatic environments (Chauhan et al., 2022).

The presence of pharmaceutical compounds in aquatic ecosystems poses significant risks to both environmental and public health. Continuous exposure to these contaminants has been associated with endocrine disruption, metabolic disorders, alterations in microbial communities, chronic toxicity, and the development of antibiotic resistance (Khasawneh & Palaniandy, 2021; Wilkinson et al., 2022). Among these impacts, antibiotic resistance has become particularly concerning because the presence of antibiotics in aquatic environments creates selective pressure on microorganisms, accelerating the emergence and spread of resistant strains (Wilkinson et al., 2022). These adverse effects demonstrate the urgent need for effective technologies capable of removing pharmaceutical contaminants from wastewater before discharge into the environment.

However, the management of pharmaceutical contaminants remains particularly challenging in developing regions. In many developing countries, including those in Sub-Saharan Africa, the challenge is worsened by inadequate wastewater treatment infrastructure, limited monitoring of pharmaceutical contaminants, and increasing consumption of antibiotics (Ali & Gujiba, 2024; Barasa et al., 2024). Consequently, pharmaceutical residues may enter rivers and lakes that serve as sources of domestic water, irrigation water, and aquatic food resources (Sikder et al., 2024). These conditions increase the need for affordable treatment technologies capable of removing pharmaceutical contaminants before wastewater is discharged into the environment.

Several technologies have been developed to remove pharmaceutical contaminants from wastewater, including conventional biological treatments such as the Activated Sludge Process, constructed wetlands, advanced oxidation processes, membrane filtration technologies, electrocoagulation, and adsorption (Abdel-raouf et al., 2019; Chauhan et al., 2022). Although many of these technologies achieve high removal efficiencies, they often require high capital investment, intensive energy consumption, and expensive operation and maintenance, limiting their widespread application, particularly in developing countries (Adeoye et al., 2024; Mutegoa, 2024). Consequently, there is growing interest in developing treatment technologies that are both efficient and economically sustainable.

Among the available treatment technologies, adsorption has attracted considerable attention because of its high removal efficiency for a broad spectrum of pharmaceutical compounds, operational simplicity, absence of toxic by-products, scalability, and relatively low operational cost (Adeoye et al., 2024; Chauhan et al., 2022). For example, Vona et al. (2015) compared adsorption using activated carbon with ultrafiltration, nanofiltration, biological treatment, and chlorine dioxide oxidation for the removal of selected pharmaceuticals. Their study demonstrated that adsorption achieved higher removal efficiencies for Ibuprofen, Diclofenac, Sulfamethoxazole, Clonazepam, and Diazepam, whereas the other treatment methods showed limited performance for several of the investigated pharmaceuticals. These findings highlight adsorption as one of the

most promising approaches for removing pharmaceutical contaminants from aqueous systems.

The efficiency of adsorption largely depends on the characteristics of the adsorbent employed. Consequently, there is increasing interest in developing sustainable, low-cost adsorbents from waste biomass. Biochar has emerged as one of the most promising adsorbents because it possesses a porous structure, high surface area, diverse surface functional groups, and can be produced from abundant agricultural residues and biological wastes (Anfar et al., 2020; Grisales-Cifuentes et al., 2021). Furthermore, converting agricultural residues into biochar contributes to waste valorization and may reduce greenhouse gas emissions associated with biomass disposal (Sarfaraz et al., 2021).

Numerous agricultural biochars have been investigated for the removal of pharmaceutical contaminants from water. For example, rabbit manure biochar has demonstrated a maximum adsorption efficiency of 96.8% for ciprofloxacin removal due to its porous structure and oxygen-containing functional groups (Huang et al., 2020). Rice hull biochar demonstrated a maximum adsorption efficiency of 97% for sodium diclofenac (Filipinas et al., 2021). Corncob biochar has been successfully applied for the adsorption of ciprofloxacin, ofloxacin, delafloxacin, sulfamethoxazole, and trimethoprim through π-π interactions, hydrogen bonding, and pore-filling mechanisms (Dang et al., 2020; Li et al., 2022). Similarly, oil palm fiber biochar has exhibited strong adsorption capacities of 7.3 mg/g and 100.9 mg/g acetaminophen and diclofenac, respectively (Grisales-Cifuentes et al., 2021). These studies demonstrate that agricultural residues are promising feedstocks for producing efficient and sustainable adsorbents for pharmaceutical removal.

Among these agricultural feedstocks, corncob biochar has received considerable attention because corncobs are generated in large quantities worldwide, possess relatively high lignocellulosic content, and can produce biochar with well-developed porosity after pyrolysis (Kaudza et al., 2026; Li et al., 2022). Since maize is cultivated in approximately

165 countries, corncobs represent an abundant, inexpensive, and renewable feedstock suitable for large-scale biochar production (Dang et al., 2020).

Although agricultural biochars have demonstrated excellent performance, there is growing interest in exploring biochars derived from alternative materials with unique physicochemical properties. White-rot fungi are well known for their ability to degrade a broad spectrum of xenobiotic compounds through ligninolytic enzymes such as laccase, manganese peroxidase, and lignin peroxidase (Torres-Farradá et al., 2024). While numerous studies have investigated living white-rot fungi for biosorption and biodegradation of contaminants, comparatively few have explored biochar produced from white-rot fungi for pharmaceutical adsorption. This limited knowledge hinders understanding of its adsorption capacity, adsorption mechanisms, and potential application in water treatment.

Therefore, investigating the adsorption performance of white-rot fungus biochar and corncob biochar is essential for expanding the range of sustainable adsorbents available for wastewater treatment. Evaluating their physicochemical characteristics, adsorption behavior, and removal mechanisms for pharmaceutical contaminants will provide valuable information for developing efficient, low-cost, and environmentally sustainable technologies for mitigating pharmaceutical pollution in aquatic environments.

Although previous studies have examined corncob biochar for pollutant removal, the reported biochar properties vary considerably. These differences arise from variations in pyrolysis temperature, residence time, and activating agent ratio, all of which significantly influence adsorption behavior (Putranto et al., 2022; Tsarpali et al., 2024). Furthermore, most existing studies have employed unrealistically high antibiotic concentrations. Therefore, this work focuses on environmentally relevant concentration ranges (0–6 mg/L) to better reflect real-world conditions.

1.2 Statement of Problem

The continuous release of pharmaceutical compounds (PCs), particularly antibiotics, into aquatic environments has become has become a significant environmental and public health challenge. Although these contaminants are generally detected at ng/L to μg/L concentrations, their persistence and biological activity can adversely affect aquatic organisms and promote the development and dissemination of antibiotic-resistant bacteria and antibiotic resistance genes (ARGs), thereby reducing the effectiveness of antibiotics used to treat infectious diseases in humans and animals (Adeoye et al., 2024; Kümmerer, 2010). Conventional wastewater treatment technologies, including activated sludge systems and other biological treatment processes, are often unable to remove these contaminants completely, resulting in their continuous discharge into receiving water bodies.

Adsorption using biochar has emerged as a promising, environmentally friendly, and cost-effective approach for removing pharmaceutical contaminants because biochar possesses high surface area, well-developed porosity, and abundant surface functional groups while being produced from renewable biomass (Chauhan et al., 2022; Sarfaraz et al., 2021). Previous studies have demonstrated the effectiveness of agricultural residue-derived biochars, including corncob biochar, for removing antibiotics from water. However, the adsorption performance of these materials varies considerably depending on feedstock characteristics and production conditions, indicating the need to explore alternative biochar materials and strategies for improving adsorption efficiency.

White-rot fungi possess unique lignocellulosic composition and ligninolytic enzyme systems that distinguish them from conventional agricultural feedstocks, yet biochar derived from non-edible white-rot fungi has received little attention as an adsorbent for pharmaceutical removal. Furthermore, although individual biochars have been extensively investigated, no studies have evaluated the synergistic adsorption performance of white-rot fungus biochar combined with corncob biochar for the removal

of sulfamethoxazole and trimethoprim from aqueous solutions. Addressing this knowledge gap is important for developing efficient, sustainable, and low-cost biochar-based technologies for pharmaceutical removal from contaminated water.

1.3 Objectives

1.3.1 Main Objective

The main objective of this study was to evaluate the removal of sulfamethoxazole and trimethoprim from aqueous solutions using white-rot fungus biochar, corncob biochar, and their mixtures.

1.3.2 Specific Objectives

The specific objectives of this study were to:

a) Prepare white-rot fungus biochar and corncob biochar and characterize their proximate composition, elemental composition, functional groups, surface morphology, and surface charge using gravimetric analysis, an elemental analyzer, Fourier-transform infrared spectroscopy (FTIR), scanning electron microscopy (SEM), and zeta potential analysis, respectively.
b) Evaluate the adsorption kinetics, equilibrium isotherms, and adsorption mechanisms of sulfamethoxazole and trimethoprim on white-rot fungus biochar and corncob biochar using appropriate kinetic and isotherm models, complemented by biochar characterization results.
c) Evaluate the removal performance of white-rot fungus biochar and corncob biochar mixtures for sulfamethoxazole and trimethoprim under varying operating conditions.

1.4 Research Questions

i. What is the proximate composition, elemental composition, functional groups, surface morphology, and surface charge characteristics of white-rot fungus biochar and corncob biochar?
ii. What is the adsorption kinetics, equilibrium isotherms, and underlying adsorption mechanisms involved in the removal of sulfamethoxazole and trimethoprim by white-rot fungus biochar and corncob biochar?
iii. What are the removal efficiencies and synergistic adsorption effects of white-rot fungus biochar and corncob biochar mixtures on sulfamethoxazole and trimethoprim under different operating conditions?

1.5 Justification of the Study

Sustainable Development Goal (SDG) 6 emphasizes the availability and sustainable management of water and sanitation for all, while SDG 3 and SDG 14 highlight the importance of protecting human health and aquatic ecosystems from environmental contaminants (FAO, 2015). Achieving these goals requires the development of effective and sustainable approaches for removing emerging contaminants, including pharmaceutical compounds, from wastewater before their release into aquatic environments.

Although adsorption has demonstrated considerable potential for pharmaceutical removal, the performance of biochar-based adsorbents depends strongly on feedstock characteristics, production conditions, and surface properties. Therefore, exploring alternative biochar materials with unique physicochemical characteristics is necessary to improve the efficiency and sustainability of adsorption-based treatment approaches.

White-rot fungi possess unique lignocellulosic structures and functional properties associated with their lignin-degrading capabilities; however, biochar derived from white-rot fungi remains relatively unexplored for pharmaceutical contaminant removal. In addition, limited information exists regarding the combined application of white-rot fungus biochar and corncob biochar for the removal of sulfamethoxazole and trimethoprim. Investigating the synergistic effect of these biochars provides an opportunity to understand how their mixture influence adsorption performance and mechanisms.

Therefore, this study contributes to the development of sustainable biochar-based wastewater treatment technologies by evaluating the characteristics, adsorption behavior, and removal mechanisms of white-rot fungus biochar, corncob biochar, and their mixtures. The findings may provide valuable information for researchers, water treatment practitioners, and developing regions seeking affordable and environmentally sustainable approaches for mitigating pharmaceutical contamination in water resources.

1.6 Scope and Limitations of the Study

The study was conducted in laboratories located at Jomo Kenyatta University of Agriculture and Technology, Kenya. This site was chosen because most of the laboratories needed for conducting the experiments and analyzing the sample are located there. Additional analysis was also performed in an external laboratory at the Department of Biological and Chemical Engineering, Aarhus University, Denmark.

The study focused on preparation of phosphoric acid-activated white-rot fungus biochar and corncob biochar, characterization of each biochar, evaluation of each biochar's performance in removing sulfamethoxazole and trimethoprim from synthetic water, and the evaluation of their mixtures in removing these antibiotics from synthetic water. However, the study did not evaluate the performance of each biochar in complex matrices, such as wastewater, nor did it assess their reusability potential.

CHAPTER TWO

LITERATURE REVIEW

2.1 Occurrence and Persistence of Pharmaceutical Compounds

Pharmaceutical compounds (PCs) are widely used in human and veterinary medicine for the treatment and prevention of diseases, enhancement of feed production, and improvement of livestock growth rate (Khasawneh & Palaniandy, 2021). However, their extensive consumption and incomplete removal during wastewater treatment have resulted in their continuous introduction into aquatic environments, where they may persist and exert biological effects on non-target organisms (Chauhan et al., 2022; Kümmerer, 2010). This occurrence has raised significant concerns among researchers because of the potential impacts of PCs on human health and aquatic ecosystems. Although the short-term effects of many pharmaceutical contaminants remain insufficiently understood, increasing evidence suggests that prolonged exposure may contribute to adverse outcomes, including antibiotic resistance, endocrine disruption, metabolic disturbances, and chronic toxicity (Fauziyen et al., 2024; Wilkinson et al., 2023). Consequently, understanding the occurrence, fate, and distribution of PCs in the environment has become an important area of environmental research.

Pharmaceutical Compounds have been detected in various environmental matrices, including surface water, groundwater, wastewater, and sediments, typically at concentrations ranging from ng/L to μg/L (Adeoye et al., 2024; Chauhan et al., 2022; Kümmerer, 2010). Their environmental concentrations vary depending on regional socioeconomic conditions, patterns of pharmaceutical consumption, physicochemical properties of individual compounds, and the efficiency of wastewater treatment systems (Khasawneh & Palaniandy, 2021). Table 2.1 presents the maximum concentrations of selected PCs reported in different countries. Currently, thousands of active pharmaceutical ingredients are approved for global use, including antibiotics, nonsteroidal anti-

inflammatory drugs (NSAIDs), anticonvulsants, antidepressants, β-blockers, hormones, lipid regulators, and antidiabetic drugs (Wilkinson et al., 2023). However, only a limited proportion of these compounds have been extensively evaluated for their environmental toxicity. This knowledge gap is particularly pronounced in low- and middle-income countries due to limited financial resources, inadequate analytical infrastructure, and insufficient environmental monitoring capacity (Wilkinson et al., 2023). Therefore, research on pharmaceutical contaminants often prioritizes compounds with high consumption rates, frequent detection in environmental samples, and known or suspected ecological risks.

Table 2.1: Maximum Concentrations of Various Pharmaceutical Compounds Detected in Different Countries

Therapeutic class	Pharmaceutical Compound	Maximum concentration (µg/L)	Sample source	Countries	References
Antibiotics	Sulfamethoxazole	2.146	Wastewater Treatment Plant (WWTP)	Southern California (USA)	Khasawneh & Palaniandy (2021)
		13.8	River water	Kenya	Ngumba et al. (2016)
	Trimethoprim	1.021	WWTP	Southern California (USA)	Khasawneh & Palaniandy, (2021)
		2.65	River water	Nairobi, Kenya	Ngumba et al. (2016)
	Ciprofloxacin	14000	WWTP	India	Silori & Tauseef (2021)

		0.509	River water	Kenya	Ngumba et al. (2016)
Stimulant	Caffeine	0.007	Surface water	United States of America (USA)	Sanusi et al. (2023)
		0.931	Groundwater	Taiwan	Sanusi et al. (2023)
	Cocaine	2.89	River water	Brazil	Jin et al. (2022)
Analgesics	Paracetamol	1110	Hospital effluent	Ghana	Otoo et al. (2022)
		3200	Drinking water		Otoo et al. (2022)
	Ibuprofen	300	Hospital effluent	Ghana	Otoo et al. (2022)
		500	Drinking water		Otoo et al. (2022)
		0.022	Surface water	Indonesia	Sudaryanto et al. (2023)

2.2 Environmental Impacts of Antibiotics

Antibiotics are chemical compounds used to treat and prevent bacterial diseases in both humans, plants, and animals (Boeckel et al., 2015; Chauhan et al., 2022). Their global use has increased substantially due to the growing demand for food and animal products, which has led to greater reliance on antibiotics to maintain animal and plant health and sustain agricultural productivity (Mshana et al., 2021). Depending on their mode of action, antibiotics are classified as either bactericidal, which kill bacteria, or bacteriostatic, which inhibit bacterial growth (Fauziyen et al., 2024). Although antibiotics are widely used in

human medicine, the majority are consumed in food animal production. For example, in the United States, approximately 80% of the antibiotics consumed annually are used in food animals. Globally, antimicrobial consumption in food animal production was estimated at 63,151 (±1,560) tons in 2010 and was projected to increase to 105,596 (±3,605) tons by 2030 (Boeckel et al., 2015).

The extensive use of antibiotics has resulted in their release into aquatic environments through pathways such as groundwater contamination, improper disposal of unused medications, and effluent discharges from wastewater treatment plants (Kümmerer, 2010). Consequently, antibiotic residues have become emerging contaminants of concern because they contribute to the development of antibiotic resistance, degrade water quality, and pose ecological risks to aquatic organisms, including algae and fish, as well as potential health risks to humans (Otoo et al., 2022; Sanusi et al., 2023).

2.3 Antibiotic Resistance and Public Health Risks

Sulfamethoxazole has been identified as one of the most frequently detected antibiotics in municipal wastewater treatment plants worldwide, particularly in Asia (Khasawneh & Palaniandy, 2021). It is commonly prescribed in combination with trimethoprim because the two antibiotics exhibit synergistic antimicrobial activity (Huang et al., 2024; Ngumba et al., 2016). Consequently, both compounds are often detected together in municipal wastewater. Following consumption by humans and animals, approximately 50–90% of administered antibiotics are excreted unchanged or as active metabolites, allowing them to enter aquatic environments through raw wastewater (Zhou et al., 2024). The widespread release of these antibiotics into the environment has raised significant concerns because of their adverse effects on both human health and aquatic ecosystems.

Continuous exposure to antibiotic residues in the environment promotes the emergence and spread of antibiotic-resistant bacteria and antibiotic resistance genes, reducing the effectiveness of antibiotics in treating bacterial infections (Wilkinson et al., 2022). This

has become a major global public health concern, as antibiotic resistance has been reported in every country. According to Kasimanickam et al. (2021), antibiotic-resistant infections are responsible for approximately 700,000 deaths annually worldwide, and this figure is projected to increase to 10 million deaths per year by 2050. Therefore, effective strategies to reduce antibiotic contamination in the environment are urgently needed to help mitigate the spread of antibiotic resistance.

2.4 Specifics of Sulfamethoxazole and Trimethoprim

2.4.1 Sulfamethoxazole

Sulfamethoxazole (SMX), also known as 4-amino-N-(5-methyl-1,2-oxazol-3-yl) benzenesulfonamide, is an antibiotic belonging to the sulfonamide group (Prasannamedha & Kumar, 2020; Zhou et al., 2024). Other antibiotics within the sulfonamide group include sulfaquinoxaline-Na, sulfisoxazole, sulfamethoxypyridazine, sulfathiazole, and sulfamethizole (Puhlmann et al., 2024). Among these compounds, SMX has received considerable attention due to its frequent detection as a contaminant in municipal wastewater treatment plants worldwide and in various environmental matrices (Khasawneh & Palaniandy, 2021; López-Cabeza et al., 2024). Notably, Wilkinson et al. (2022) reported that, among the 61 active pharmaceutical ingredients investigated in their study, SMX exhibited the highest concentrations in rivers worldwide. At 140 monitoring sites, SMX concentrations exceeded the predicted no-effect concentration, highlighting its potential ecological risk. This widespread occurrence is largely attributed to the extensive use of SMX for treating bacterial infections in humans, livestock, and aquaculture (Fauziyen et al., 2024).

The molecular structure of SMX, consisting of an aromatic benzene ring, a sulfonamide ($-SO_2NH-$) functional group, an amino ($-NH_2$) group, and an isoxazole ring, is illustrated in Figure 2.1. These structural features determine the physicochemical properties and environmental behavior of SMX, including its ionization characteristics, solubility, and

interactions with environmental matrices (Esteki et al., 2020; Fauziyen et al., 2024). The aromatic rings within the SMX molecule facilitate π–π electron donor–acceptor interactions with carbonaceous adsorbents, such as biochar, while the amino and sulfonamide functional groups contribute to hydrogen bonding and other polar interactions with oxygen-containing functional groups on adsorbent surfaces (Ambaye et al., 2020; Jha et al., 2023). In addition, SMX is an ionizable compound whose predominant molecular form changes with solution pH, influencing electrostatic interactions, adsorption capacity, and environmental transport behavior (Grimm et al., 2022). Therefore, understanding the molecular structure and functional groups of SMX is essential for explaining its persistence in aquatic environments and the mechanisms governing its removal through adsorption processes.

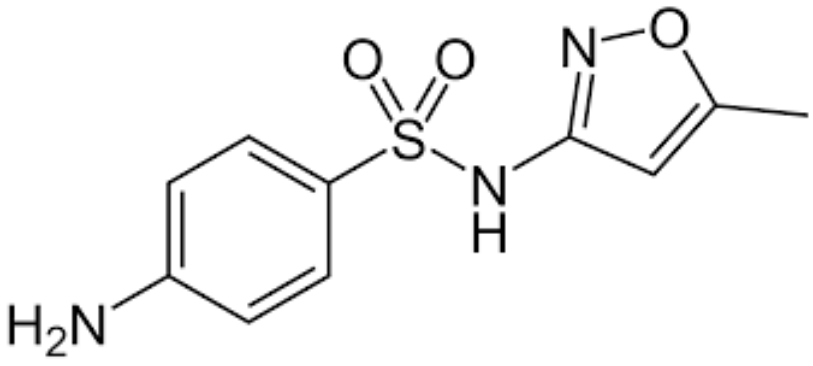

Figure 2.1: Molecular Structure of SMX

2.4.2 Trimethoprim

Trimethoprim (TMP), also known as 2,4-diamino-5-(3,4,5-trimethoxybenzyl) pyrimidine, is a synthetic antibiotic belonging to the diaminopyrimidine class (Kneis et al., 2023; Swedberg & Sundström, 2010). TMP exerts its antibacterial activity by inhibiting the

enzyme dihydrofolate reductase, thereby preventing the formation of tetrahydrofolic acid, an essential cofactor required for bacterial DNA synthesis (Diogo et al., 2024). Similar to sulfamethoxazole (SMX), TMP has been widely used for more than five decades and is commonly co-administered with SMX because the combination provides enhanced antimicrobial efficacy (Huang et al., 2024; Ngumba et al., 2016). In clinical practice, the two antibiotics are formulated as co-trimoxazole, typically in a ratio of 5:1 of SMX to TMP (Diogo et al., 2024; Ngumba, Gachanja, et al., 2016).

The extensive use of TMP has contributed to its widespread occurrence in aquatic environments. A global assessment of pharmaceutical pollution in rivers reported that TMP was among the 14 pharmaceuticals detected on every continent except Antarctica (Wilkinson et al., 2022). Although TMP generally exhibits relatively low toxicity to aquatic organisms, its continuous presence in the environment may promote the development and spread of antibiotic-resistant bacteria and antibiotic resistance genes, thereby reducing the effectiveness of antimicrobial therapies (Diogo et al., 2024, 2025; Kneis et al., 2023). Consequently, the removal of TMP and SMX from aqueous environments has become an important research priority because these antibiotics frequently co-occur in municipal wastewater and other aquatic systems.

The molecular structure of TMP, consisting of a pyrimidine ring, a trimethoxybenzyl group, and two amino (-NH_2) functional groups, is illustrated in Figure 2.2. These structural features influence the physicochemical properties of TMP, including its ionization behavior, solubility, and adsorption characteristics. The aromatic ring promotes π–π interactions with carbonaceous adsorbents such as biochar, while the amino and methoxy functional groups facilitate hydrogen bonding and other polar interactions with oxygen-containing surface functional groups (Ambaye et al., 2020; Jha et al., 2023). Furthermore, the ionization state of TMP varies with solution pH, influencing its electrostatic interactions, mobility, and adsorption behavior in aquatic environments (Grimm et al., 2022). Table 2.2 summarizes and compares the key physicochemical properties of TMP and SMX, including their color, molecular formula, negative

logarithmic acid dissociation constants (pKa_1 and pKa_2), water solubility, and density. These properties are important because they influence the environmental fate, transport, and adsorption behavior of both antibiotics, thereby providing a basis for understanding their removal from aqueous solutions using biochar-based adsorbents.

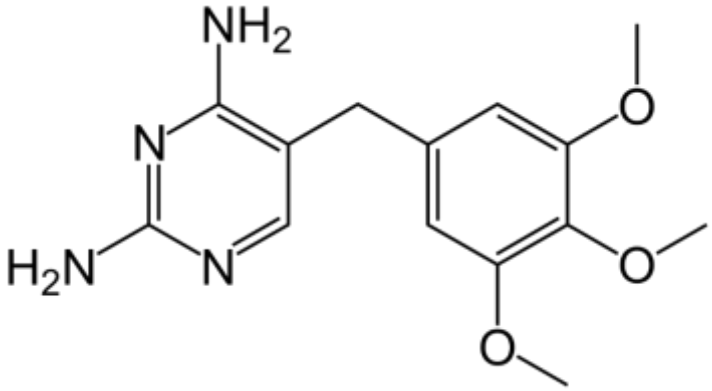

Figure 2.2: Molecular Structure of TMP

Table 2.2: Physicochemical Properties of Sulfamethoxazole and Trimethoprim

PC	Color	Molecular formula	$pKa_{1,2}$	Water solubility (mg/L)	Density (g/cm^3)	References
SMX	White	$C_{10}H_{11}N_3O_3S$	1.7, 5.6	610	1.179	Esteki et al. (2020)
TMP	White	$C_{14}H_{18}N_4O_3$	1.32, 7.45	400	1.165	Fauziyen et al. (2024) Ngumba et al. (2016) (Esteki et al., 2020)

2.5 Wastewater Treatment

Wastewater contains a wide range of pollutants, including heavy metals, dyes, pharmaceuticals, oil, and plastics, depending on the nature of human activities and industrial processes generating the effluent (Saravanan et al., 2021). The composition and concentration of contaminants vary considerably with the wastewater source. For example, textile industry effluents are often characterized by high dye concentrations, whereas pharmaceutical wastewater contains significant levels of pharmaceutical compounds (PCs). Consequently, the release of untreated wastewater into aquatic environments can deteriorate water quality, limiting its suitability for domestic consumption, agricultural applications, and ecosystem functioning. The accumulation of contaminants can increase biological oxygen demand (BOD) and chemical oxygen demand (COD), resulting in reduced dissolved oxygen levels and adverse effects on aquatic organisms (Saravanan et al., 2021). Additionally, wastewater pollutants can alter important water quality parameters, including pH, faecal coliform levels, and electrical conductivity (Hoogendijk et al., 2023).

Given the potential environmental and public health risks associated with wastewater contamination, effective treatment processes are necessary to reduce pollutant loads before discharge or reuse. Wastewater treatment involves a series of processes designed to remove contaminants, protect aquatic ecosystems, and facilitate the safe reuse of treated water where applicable (Abdel-raouf et al., 2019). These treatment approaches are generally categorized into physical, chemical, and biological methods. Mechanical processes, such as screening and filtration, are commonly incorporated within physical treatment systems because they rely primarily on physical separation mechanisms (Abdel-raouf et al., 2019). In practical applications, multiple treatment approaches are often integrated to improve overall pollutant removal efficiency and address the limitations of individual methods.

2.5.1 Physical Treatment Methods

Physical treatment methods involve the application of physical forces to separate contaminants from wastewater without causing significant biological degradation or chemical transformation. These processes primarily rely on mechanisms such as size exclusion, gravity separation, and phase separation to remove suspended solids and particulate matter (Ahmed et al., 2022). Common physical treatment techniques include screening, sedimentation, flow equalization, flotation, degasification, and filtration (Ahmed et al., 2022; Saravanan et al., 2021). However, although these approaches are effective for removing larger suspended particles, their efficiency is often limited for dissolved organic pollutants and emerging contaminants such as pharmaceutical compounds because these substances remain in the aqueous phase (Ghazal et al., 2022). Sedimentation, for example, facilitates the removal of settleable solids through gravitational separation but has limited effectiveness for small particles and dissolved micropollutants, including antibiotics (Anand et al., 2022; Ghazal et al., 2022).

2.5.2 Biological Treatment Methods

Biological treatment methods involve the use of microorganisms to degrade dissolved and suspended organic pollutants in wastewater under suitable environmental conditions, thereby enhancing the natural self-purification process (Abdel-raouf et al., 2019). These methods rely on microbial metabolic activities and include aerobic treatment, anaerobic treatment, disinfection, and phytoremediation approaches (Ahmed et al., 2022). Biological processes are widely applied in wastewater treatment because they can achieve effective organic matter removal with relatively lower operational costs compared with some advanced treatment technologies. However, their efficiency depends on factors such as wastewater characteristics, microbial activity, and the nature of the contaminants present (Ahmed et al., 2022). Conventional biological systems, including activated sludge processes and sequencing batch reactors, were primarily developed for the removal of organic matter and nutrients rather than emerging contaminants such as antibiotics

(Oberoi et al., 2019). Consequently, these systems often demonstrate limited or moderate removal efficiencies for antibiotic compounds, allowing some pharmaceuticals to persist in treated wastewater (Oberoi et al., 2019).

2.5.3 Chemical Treatment Methods

Chemical treatment methods involve the use of chemical reactions or reagents to remove pollutants from wastewater (Abdel-raouf et al., 2019). Common chemical treatment techniques include coagulation, flocculation, ozonation, chemical precipitation, and adsorption (Abdel-raouf et al., 2019; Saravanan et al., 2021). These methods are particularly effective for removing dissolved contaminants and fine particles, making them suitable for the treatment of pharmaceutical compounds, including antibiotics. However, some chemical treatment processes, particularly coagulation, flocculation, and adsorption, may generate residual sludge or spent adsorbents that require appropriate disposal to minimize secondary environmental pollution (Saravanan et al., 2021). Table 2.3 summarizes the pharmaceutical compound removal efficiencies reported in various studies. While physical and biological treatment processes generally exhibit low to moderate removal efficiencies, chemical treatment methods, particularly adsorption, consistently achieve high removal efficiencies, highlighting their potential for the effective removal of pharmaceutical contaminants.

Table 2.3: Pharmaceutical Removal Efficiencies of Specific Type of Wastewater Treatment Process Within Each Treatment Category

Wastewater treatment method	Specific type	Removal efficiency (%)	PC	References
Physical	Sand and anthracite sand biofiltration	<20	Amoxicillin, Clarithromycin, Oxytetracycline, Sulfamethoxazole	Xu et al. (2021)

			(SMX), Trimethoprim (TMP)	
	Sand filtration	0	SMX	Göbel et al. (2007)
		17-23	Macrolides	
		74±14	TMP	
	Reverse osmosis	>99	Caffeine, SMX, Omeprazole	Matin et al. (2023)
	Commercial nanofiltration	40-95	Caffeine, SMX, Omeprazole	Matin et al. (2023)
Biological	Sequencing batch reactor	37	SMX	Oberoi et al. (2019)
		21	TMP	
	Phytoremediation:			
	Green algae Nannochloris	32	TMP	Bai & Acharya (2016)
		0	SMX	Stando et al. (2022)
		100	Triclosan	
	Limnobium laevigatum	96	SMX	
		75.4	TMP	
	Aerobic granular sludge	~30	TMP	Barros et al. (2021)
		~60	SMX	

Chemical	Adsorption:			
	Corncob xylose residue biochar	98.52	SMX	Li et al. (2022)
	Miscanthus giganteus biochar	80	SMX	Burdová et al. (2024)
		91	TMP	
	Integrated coagulation and sorption	70.4-86.5	SMX	Macherzyński et al. (2021)
		54.7-94.7	TMP	
	Ozonation	100 in < 30 minutes	SMX, TMP, Sulfadimethoxine, Oxytetracycline	Gorito et al. (2022)

2.6 Adsorption Technology

Adsorption is one of the most preferred methods for the removal of pharmaceuticals from aqueous solutions due to its ability to remove a wide range of pharmaceutical compounds, its low cost, and its environmental friendliness (Abdel-raouf et al., 2019). The technology employs various adsorbents that serve as binding sites for the adsorbates (Otieno, 2023; Singh et al., 2018). The interaction between the adsorbent and the adsorbate may occur through either physical (physisorption) or chemical (chemisorption) mechanisms (Ehiomogue et al., 2021). These interactions are commonly analyzed using kinetic and isotherm models, which describe the adsorption rate and the adsorption behavior of the adsorbent (Bellahsen et al., 2021; Ehiomogue et al., 2021).

2.7 Application of Adsorbents for Pharmaceutical Adsorption

In recent years, various adsorbents have been applied in the treatment of wastewater containing pharmaceutical compounds (PCs). Materials such as algae, bacteria, industrial wastes, and agricultural wastes are commonly used to remove pollutants from aqueous solutions (Li et al., 2017; Martins et al., 2018; Zhao et al., 2021). These materials are generally affordable, biodegradable, and renewable, with treatment costs ranging from approximately US$10 to US$200 per million liters of water, depending on the type of adsorbent employed (Adewuyi, 2020).

Adsorbents can be used either in their natural form or after modification to enhance their performance. However, unmodified adsorbents may increase chemical oxygen demand (COD), biological oxygen demand (BOD), and total organic carbon (TOC) due to the release of organic compounds into the treated water. In contrast, conversion into biochar or other modified forms reduces the organic matter content of adsorbents, improves surface charge, and enhances porosity, thereby increasing adsorption efficiency (Adewuyi, 2020; Reza et al., 2020).

Despite numerous studies on the removal of PCs using individual adsorbents, research on the application of adsorbents such as white-rot fungus biochar and its mixtures with corncob biochar remains limited. Investigating these adsorbents for the removal of sulfamethoxazole and trimethoprim could contribute to the development of more efficient adsorption systems that overcome the limitations associated with single-adsorbent approaches.

2.7.1 Adsorbents from Agricultural Waste

Agricultural wastes are increasingly being used as adsorbents for the removal of pharmaceutical compounds from wastewater. Besides being affordable and renewable, their utilization provides a sustainable approach to waste management by converting agricultural residues into value-added products and reducing environmental pollution. For

example, the decomposition of agricultural wastes releases greenhouse gases such as carbon dioxide and methane into the atmosphere, whereas their conversion into adsorbents helps mitigate these emissions (Sarfaraz et al., 2021).

The adsorption performance of agricultural waste-derived adsorbents depends largely on the physicochemical characteristics of the feedstock, particularly its lignin, cellulose, and hemicellulose composition, as well as its surface chemistry. During pyrolysis, agricultural wastes with relatively high lignin content generally produce biochar with higher carbon content and lower ash content than low-lignin feedstocks (Weber & Quicker, 2018). These differences influence the surface chemistry and adsorption behavior of the resulting biochar. For instance, biochars with higher carbon content typically possess fewer oxygenated functional groups, which may reduce adsorption through hydrogen bonding and electrostatic interactions while promoting π–π interactions and hydrophobic interactions (Yang et al., 2023).

Corncob is one of the most widely studied agricultural wastes for biochar production because of its abundance and favorable physicochemical properties. Corncobs account for approximately 18% of the total corn biomass (Blandino et al., 2016; Liu et al., 2014). Given that global annual corn production exceeds 1.17 billion metric tons, an estimated 211 million metric tons of corncobs are generated each year, providing a continuous and readily available feedstock in more than 165 countries (Dang et al., 2020; Gandam et al., 2022). Structurally, corncobs consist of an outer woody ring, glume, and chaff surrounding an inner pith, and are composed primarily of cellulose (33–43%), hemicellulose (26–36%), and lignin (17–21%) (Gandam et al., 2022). Owing to their relatively high cellulose and hemicellulose contents and lower lignin content, corncobs undergo substantial thermal decomposition at moderate pyrolysis temperatures. Hemicellulose is the least thermally stable component, decomposing at approximately 220–315°C, followed by cellulose and lignin (Weber & Quicker, 2018). Consequently, corncob biochar is commonly produced at moderate pyrolysis temperatures and residence times; for example, Dang et al. (2020) prepared corncob biochar at 600°C for 1 h.

The removal efficiency and adsorption capacity of selected agricultural waste-derived adsorbents investigated for the removal of pharmaceuticals from aqueous solutions are presented in Table 2.4. The reported studies demonstrate that agricultural wastes, particularly when converted into biochar, are capable of removing a wide range of pharmaceutical contaminants, including antibiotics, analgesics, anti-inflammatory drugs, and stimulants. However, adsorption capacities and removal efficiencies vary considerably among adsorbents due to differences in feedstock composition, biochar production conditions, and operating parameters such as solution pH, initial adsorbate concentration, and adsorbent dosage (Anastopoulos et al., 2020; Dang et al., 2020). Consequently, the adsorption performances presented in Table 2.4 should be interpreted as indicative rather than directly comparable.

Table 2.4: Agricultural Waste-based Adsorbents used in the Removal of Pharmaceuticals from Wastewater

Adsorbents	Form used	Pharmaceuticals	Removal efficiency (%)/Adsorption capacity (mg/g)	Reference(s)
Corncobs	Biochar	Ciprofloxacin	0.4 mg/g	Dang et al. (2021)
		Ofloxacin	0.306 mg/g	
		Delafloxacin	0.094 mg/g	
Pine needles	Biochar	Caffeine	1.41 mg/g	Anastopoulos et al. (2020)
Rice hull	Biochar	Sodium diclofenac	97% at pH 2	Filipinas et al. (2021)
			80% at pH 7	
Oil palm fiber	Biochar	Acetaminophen	7.3 mg/g	Grisales-Cifuentes et al. (2021)
		Cephalexin	7.9 mg/g	
		Valsartan	23.85 mg/g	
Moringa seed powder	Biochar	Diclofenac	100.876 mg/g	Bagheri et al. (2020)
Walnut shell	Biochar	Salicyclic acid	683 mg/g	Anfar et al. (2020)
		Naproxen	533 mg/g	
		Ketoprofen	444 mg/g	
Bovine manure	Biochar	Tetracycline	52.95% at 500°C	Zhao et al. (2021)
			77.2% at 700°C	
Groundnut shell	Biochar	Paracetamol	3.02 mg/g	N'diaye et al. (2019)
Bamboo	Biochar	Sulfamethazine	65.74 mg/g	Ahmed et al. (2016)
		Sulfamethoxazole	88.1 mg/g	
		Sulfathiazole	237.71 mg/g	

Vine wood	Activated carbon	Amoxicillin, Cephalexin, Tetracyline, Penicillin G	74-88%	Pouretedal & Sadegh (2014)
Potato peel waste	Activated carbon	Sodium diclofenac	69 mg/g	Bernardo et al. (2016)
Hickory chips	Biochar	Sulfamethoxazole	25.7 mg/g	Huang et al. (2020)
		Sulfapyridine	58.6 mg/g	
Egg shell	Powder	Dexamethasone	0.097 mg/g at 35°C	Pavlović et al. (2017)
		Febantel	0.122 mg/g at 35°C	
		Praziquantel	0.044 mg/g at 25°C	
		Procaine	0.134 mg/g at 35°C	
		Tylosin	0.132 mg/g at 35°C	
Rabbit manure	Biochar	Ciprofloxacin	76.41% at 400°C (Dosage of 1.5g/L), 96.8% at 500°C (dosage of 0.8g/L), 92.5% at 600°C (Dosage of 0.3g/L), and 96.79% at 700°C (Dosage of 0.3g/L)	Huang et al. (2020)

2.7.2 Adsorbents from Microorganisms

Microorganisms have received increasing attention as potential adsorbents for the removal of pharmaceutical compounds (PCs) from wastewater due to their diverse surface properties and biological activities. The microorganisms investigated include bacteria,

fungi, and microalgae (Mayans et al., 2021; Roy et al., 2024; Zambrano et al., 2021). These organisms can remove pharmaceutical contaminants through different mechanisms, including adsorption, biosorption, and biodegradation.

Bacteria have been extensively studied because of their structural and functional characteristics that facilitate pollutant interactions. Bacterial cells consist of cytoplasm, a cell wall, a nucleoid region, and a cell membrane, which contain functional groups capable of interacting with contaminants (Rohde, 2019). Analytical techniques such as potentiometric titration, Fourier transform infrared spectroscopy (FTIR), and X-ray diffraction (XRD) have been employed to characterize bacterial surface properties and investigate adsorption mechanisms (Adewuyi, 2020). These approaches have improved the understanding of the type, nature, and abundance of binding sites responsible for contaminant removal.

Fungi have also attracted considerable interest due to their ability to remove PCs through both enzymatic degradation and adsorption onto fungal biomass (Mayans et al., 2021; Torres-Farradá et al., 2024). The fungal cell wall, composed of components such as chitin, chitosan, proteins, lipids, polyphosphates, and inorganic ions, provides functional groups that contribute to biosorption processes (Adewuyi, 2020; Latif et al., 2023). Among fungal species, white-rot fungi have been widely investigated because of their strong oxidative enzyme systems and ability to degrade a broad range of environmental contaminants, including pharmaceuticals, heavy metals, dyes, and persistent organic pollutants (Latif et al., 2023; Torres-Farradá et al., 2024).

White-rot fungi, particularly *Phanerochaete chrysosporium*, have been among the most extensively studied fungal species for pollutant removal (Latif et al., 2023; Torres-Farradá et al., 2024). Their pollutant adsorption capacity is mainly associated with ligninolytic enzymes, including laccase, lignin peroxidase, and manganese peroxidase, which facilitate the biodegradation of complex organic compounds. In addition to biodegradation, white-rot fungi can remove pollutants through adsorption-related

processes such as biosorption and bioprecipitation. For example, Zhang and Geißen (2012) reported 60–80% removal of carbamazepine using *Phanerochaete chrysosporium* in a bioreactor, while Rodarte-Morales et al. (2012) achieved 60–90% removal efficiencies for selected pharmaceuticals in reactor systems.

Although natural fungal biomass has demonstrated potential for pharmaceutical removal, most studies have focused on biodegradation rather than adsorption. Recently, biochar derived from fungal biomass has emerged as a promising alternative adsorbent due to its enhanced surface area, porosity, and surface functional groups. Studies by Grimm et al. (2022), Koji et al. (2022), and Wu et al. (2019) demonstrated effective pollutant removal using biochar produced from edible spent mushroom substrates. However, investigations into fungal-derived biochar for pharmaceutical adsorption remain limited, particularly for biochar produced from non-edible white-rot fungi. The use of non-edible fungal species avoids competition with food resources, making fungal-derived biochar a sustainable option for adsorption-based wastewater treatment.

Microalgae represent another group of microorganisms investigated for pharmaceutical removal from aqueous environments. Similar to bacteria and fungi, their cell walls provide adsorption sites due to the presence of components such as proteins, lignin, hemicellulose, cellulose, pectins, and extensin (Adewuyi, 2020). Several studies have demonstrated the ability of microalgae to remove pharmaceutical contaminants. For example, Hom-Diaz et al. (2017) investigated pharmaceutical removal using microalgae, while Wu et al. (2015) reported ciprofloxacin adsorption by *Enteromorpha prolifera* and Li et al. (2017) evaluated tetracycline removal using *Sargassum* sp.

A summary of microorganisms used as adsorbents for the removal of PCs from aqueous solutions, along with their corresponding removal efficiencies and adsorption capacities, is presented in Table 2.5.

Table 2.5: Microorganisms used as Adsorbents in the Removal of Pharmaceuticals from Wastewater

Adsorbent	Specific name	Pharmaceutical compounds	Removal efficiency (%)/Adsorption capacity (mg/g)	Reference(s)
Bacteria	Comamonas	Ciprofloxacin	80% under both nitrate and sulfate reducing conditions.	Martins et al. (2018)
	Arcobacter			
	Dysgonomonas			
	Macellibacteroides		84% under nitrate reducing conditions	
		17β-estradiol	0%	
		Sulfamethozole		
Fungi	Trametes versicolor (TV)	Endocrine disrupting chemicals	Within 6hours of exposure:	Becker et al. (2017)
	Myceliophthora thermophile (MT)		83% for TV	
			87% for MT	
Microalgae	Enteromorpha prolifera	Ciprofloxacin	21.7 mg/g at 293 K	Wu et al. (2015)
	Sargassum sp.	Tetracycline	73.8%	Li et al. (2017)
			278.4 mg/g	

2.8 Preparation of Biochar

Biochar is a carbon-rich solid material produced through the thermal conversion of biomass under limited or oxygen-free conditions (Chauhan et al., 2022). It is commonly prepared through three main methods: pyrolysis, hydrothermal carbonization, and microwave carbonization (Yang et al., 2019). Figure 2.3 presents a diagram summarizing these three biochar preparation methods. Biochar possesses physical and chemical properties that are important during its preparation and application. These properties largely determine the effectiveness and efficiency of biochar in pollutant removal. The physical properties of biochar include surface area, pore volume, and pore size distribution (Weber & Quicker, 2018). The chemical properties include elemental composition (carbon, nitrogen, hydrogen, sulfur, and oxygen), pH, total carbon (TC), ash content, fixed carbon, and volatile matter (Weber & Quicker, 2018; Yang et al., 2019). Therefore, a well-designed methodology for biochar preparation is essential to produce high-quality biochar with desirable properties.

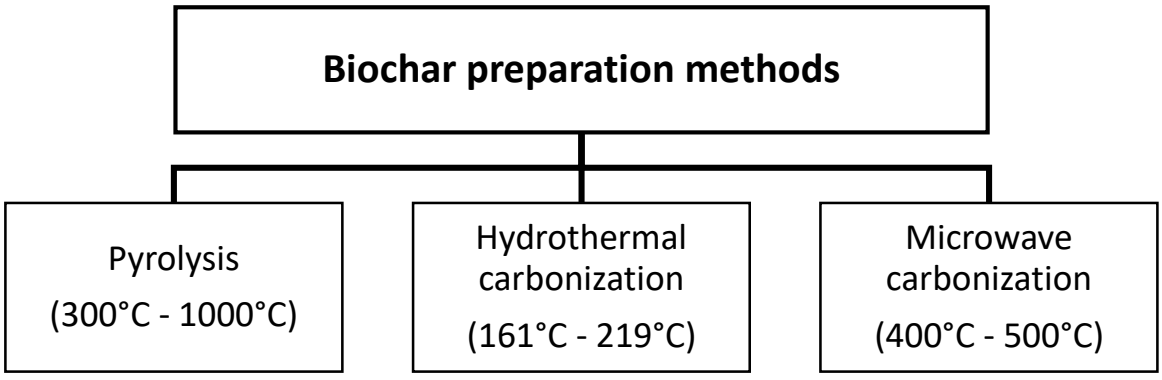

Figure 2.3: Summary of the Biochar Preparation Methods

2.8.1 Pyrolysis Method

Pyrolysis is widely considered one of the most effective methods for producing biochar for water treatment applications because it converts biomass into a stable, carbon-rich adsorbent with tunable surface properties (Kaudza et al., 2026). Biochar produced through pyrolysis generally contains a high proportion of stable aromatic carbon structures and fewer readily biodegradable organic compounds compared with the original biomass (Ravindiran et al., 2024). Consequently, pyrolysis-derived biochar is less likely to contribute significantly to the biological oxygen demand (BOD), chemical oxygen demand (COD), and total organic carbon (TOC) of treated wastewater, making it suitable for wastewater treatment applications.

Pyrolysis involves pre-drying biomass followed by thermal decomposition under oxygen-limited conditions at temperatures generally ranging from 300°C to 1000°C (Weber & Quicker, 2018). Based on operating conditions, including temperature, heating rate, and residence time, pyrolysis is commonly classified into slow, medium, fast, and flash pyrolysis (Zhang et al., 2014). Table 2.6 summarizes the different pyrolysis methods.

Slow pyrolysis is conducted at relatively low temperatures using slow heating rates (0.1–1 °C/s) and longer residence times ranging from minutes to hours, conditions that favor biochar formation. Medium pyrolysis operates under intermediate heating rates (10–200 °C/s) with residence times of approximately 10–20 seconds. Fast pyrolysis involves rapid heating (≈1000 °C/s) and short residence times ranging from milliseconds to seconds, whereas flash pyrolysis occurs at temperatures above 800°C with very high heating rates and residence times of less than 1 second (Weber & Quicker, 2018; Yang et al., 2019).

The selection of pyrolysis conditions depends on the desired end product. Slow and medium pyrolysis are generally preferred for biochar production because they maximize solid carbonaceous yields, whereas fast pyrolysis promotes bio-oil production and flash pyrolysis favors gas formation (Weber & Quicker, 2018). The distribution of pyrolysis products varies depending on process parameters, as summarized in Table 2.6.

Besides operating conditions, biomass composition significantly affects pyrolysis behavior and product yield. Most lignocellulosic biomass consists mainly of cellulose, hemicellulose, and lignin, which exhibit different thermal degradation patterns. Hemicellulose decomposes primarily between 220–315°C, cellulose between 280–400°C, and lignin undergoes gradual decomposition over a broader temperature range extending beyond 400°C (Weber & Quicker, 2018). Therefore, biomass with different lignin and cellulose contents may produce biochars with varying yields, ash contents, and structural characteristics.

Furthermore, pyrolysis parameters strongly influence the physicochemical properties of biochar, including surface area, pore structure, surface functional groups, and carbon content (Dang et al., 2020; Varela et al., 2024). Consequently, optimizing pyrolysis conditions is essential for producing biochar with properties suitable for specific applications.

Table 2.6: Summary of the Pyrolysis Methods

Pyrolysis method	Heating rate	Liquid products (Tar)	Gas products	Solid product (Biochar)
Slow	Low (0.1 to 1°C/s)	30%	35%	35%
Medium	Moderate (10 to 200°C/s)	50%	25%	25%
Fast	High (1000°C/s)	75%	13%	12%
Flash	High (1000°C/s)	5%	80%	10%

2.8.2 Hydrothermal Carbonization Method

Hydrothermal carbonization involves the reaction of biomass in aqueous environment; therefore, it does not require pre-drying of the biomass (Zhang et al., 2014). The biomass is carbonized at high pressure and high steam temperatures greater than 160°C but less than 220°C, which leads to a high yield of biochar as compared to the pyrolysis method. However, it is not ideal methods for preparing biochar for use in wastewater treatment since it contains high concentrations of organics (Yang et al., 2019). The high concentrations of organics can increase the biological oxygen demand (BOD), chemical oxygen demand (COD), and total organic carbon (TOC) of the wastewater (Adewuyi, 2020).

2.8.3 Microwave Carbonization Method

Microwave carbonization involves subjecting the biomass to temperatures between 400°C to 500°C in the absence of oxygen (Zhang et al., 2014). In microwave carbonization, the temperature at the center of the biomass is higher than at the surface, whereas for pyrolysis, the temperature at the surface of the biomass is higher than at the center.

Consequently, microwave carbonization saves more energy than pyrolysis (Yang et al., 2019; Zhang et al., 2014). Similar to hydrothermal carbonization, microwave carbonization is not an ideal methods for preparing biochar for use in wastewater treatment since it contains high concentrations of organics which can increase the biological oxygen demand (BOD), chemical oxygen demand (COD), and total organic carbon (TOC) of the wastewater (Adewuyi, 2020).

2.9 Factors Affecting the Adsorption Process

There are several factors that affect the efficiency of adsorption process. Some of the main factors include pH of the solution, temperature, contact time between adsorbent and solution, dosage of the adsorbent, and initial concentration of the adsorbate (Bernardo et al., 2016; Huang et al., 2020). Therefore, these factors should be considered for the optimization of the process parameters.

2.9.1 pH of Solution

Solution pH is a key parameter in adsorption, as it determines both the ionization state of the adsorbate and the surface charge of the adsorbent, thereby influencing their interactions (Bellahsen et al., 2021). For instance, sulfamethoxazole (SMX) has negative logarithmic acid dissociation constants (pKa_1 and pKa_2) of 1.7 and 5.6, respectively, while trimethoprim (TMP) has pKa_1 and pKa_2 values of 1.32 and 7.45, respectively (Esteki et al., 2020; Ngumba et al., 2016). Accordingly, SMX exists predominantly in a positively charged form at $pH < 1.7$ and in a negatively charged form at $pH > 5.6$ (Esteki et al., 2020; Fauziyen et al., 2024).

Although Fauziyen et al. (2024) reported that SMX is neutral between its pKa_1 and pKa_2 values, Esteki et al. (2020) argued that SMX is never entirely neutral. Specifically, Esteki et al. (2020) demonstrated that when the amine group become predominantly neutral at pH 4.7 ($pKa_1 + 3$), approximately 10% of the sulfonamide group is negatively charged. Similarly, when the sulfonamide group becomes predominantly neutral below pH 2.6

(pKa_1 - 3), approximately 10% of the amine group is positively charged. Therefore, SMX exist as a mixture of charged species across the entire pH range and is never fully neutral. In contrast, TMP is positively charged below pH 7.45 and becomes neutral above this value. Although many studies report a single pKa value (≈7), TMP has pKa_1 and pKa_2 values of 1.32 and 7.45 (Esteki et al., 2020; Liu et al. 2025; Ngumba et al. 2016). At pH values below pKa_1, both protonatable nitrogen rings are protonated, resulting in doubly charged species (TMP^{2+}). Between pKa_1 and pKa_2 one nitrogen ring is deprotonated, yielding a singly charged species (TMP^{+}). Above pKa_2, both nitrogen rings are deprotonated and TMP exist predominantly in a neutral form.

Adsorbents, in contrast, are characterized by the point of zero charge (pH_{pzc}), at which the surface carries no net charge (Cevallos-Mendoza et al., 2024; Hassaan et al., 2023; Hmamouchi et al., 2022). Consequently, the relationship between solution pH and pH_{pzc} governs the electrostatic interactions that influence adsorption.

2.9.2 Temperature of Solution

The temperature of the solution also plays a significant role in the adsorption process. Depending on the behavior of the adsorbate and adsorbent, the process can either be endothermic or exotherm reaction. Endothermic reactions are indicated by an increase in adsorption capacity with increasing temperature (Hasani et al., 2022; Lestari et al., 2022; Samimi et al., 2023; Yu et al., 2022). This is attributed to the easy opening of adsorbate pores, which promotes the adsorbates' binding to the adsorbent site (Lestari et al., 2022).

On the other hand, exothermic reactions are indicated by a decrease in adsorption capacity with increasing temperature (Aragaw & Alene, 2022; Khan et al., 2025). This is attributed to the expansion of the adsorbents' active sites, which tends to release back the adsorbates to the liquid phase (Aragaw & Alene, 2022).

2.9.3 Contact Time Between Adsorbent and Solution

The longer the contact time between the adsorbent and solution, the greater the opportunity for adsorbate molecules to bind to the surface of the adsorbent (Bernardo et al., 2016). According to Bellahsen et al. (2021), there are three phases in the adsorption process. The first phase involves rapid adsorption of the adsorbate on the surface of the adsorbent due to unbounded sites. The second phase involves slow adsorption because most sites are already bounded by the adsorbate. In the third phase, the adsorbent can no longer adsorb any adsorbate; thus, the equilibrium is reached. The time taken to reach equilibrium depends on the behavior of each adsorbate and adsorbent. Therefore, equilibrium time varies across different adsorbate and adsorbents.

For instance, Li et al. (2022) reports that SMX adsorption on corncob xylose residue-derived biochar reached equilibrium at 100 minutes. On the hand, tetracycline adsorption on biochar derived from antibiotic fermentation residue failed to reach equilibrium in 1400 minutes (Zhao et al., 2024). The data provided did not specify the equilibrium time, implying that it was after 1400 minutes.

2.9.4 Dosage of the Adsorbent

In most cases, an increase in adsorbent dosage leads to a higher removal of the adsorbate from the solution. This is so because, when the dosage increases, the surface area of the adsorbent, which serves as a bind site of the adsorbate increases (Huang et al., 2020). However, in some cases, an excess of biochar decreases the removal of the adsorbate (Huang et al., 2020). This phenomenon is attributed to particle agglomeration, which reduces the available surface area and limits access to adsorption sites (Alhothali et al., 2021; Mahmoud et al., 2025).

2.9.5 Initial Concentration of the Adsorbate

In most cases, the overall removal rate decreases with increasing initial concentration due to full occupation of the binding sites by the adsorbates (Aragaw & Alene, 2022; Bellahsen et al., 2021; Khan et al., 2025). Conversely, the adsorption capacity increases with increasing concentration due to the stronger driving force for mass transfer (Khan et al., 2025).

2.10 Adsorbent Removal Efficiency and Adsorption Capacity

Adsorbent removal efficiency is the ratio of the amount of adsorbate adsorbed by the adsorbent to the amount of the adsorbate in the solution before the adsorption process (Huang et al., 2020). Both the initial concentration of adsorbate (C_0) and concentration of adsorbate after adsorption (C_t) are measured using equipment such as a ultraviolet-visible spectrophotometer and Liquid Chromatography-Tandem Mass spectrometry (LC-MS/MS) (Jiao et al., 2024; Zhao et al., 2024). Equation 2.1 shows the formula for calculating the adsorbent removal efficiency (η).

$$\eta = \frac{C_0 - C_t}{C_0} \times 100\% \quad (2.1)$$

Where:

C_0 = initial adsorbate concentration (mg/L)

C_t = concentration of adsorbate remaining in solution at time t (mg/L)

Adsorbent adsorption capacity is the amount of adsorbate taken up by the adsorbent per unit mass of the adsorbent (Huang et al., 2020). Equilibrium adsorption capacity (q_e) is the adsorption capacity at equilibrium time (Cevallos-Mendoza et al., 2024; Zhao et al., 2024). According to Li et al. (2022), equilibrium time is the time at which the adsorption process reaches balanced and steady state. At this point, no significant changes in amount of adsorbate removed occur. Equation 2.2 shows the formula for calculating the adsorbent's adsorption capacity (q_t).

$$q_t = \frac{(C_0 - C_t)V}{m} \quad (2.2)$$

Where:

q_t = adsorption capacity at time t (mg/g)

C_0 = initial adsorbate concentration (mg/L)

C_t = equilibrium concentration of adsorbate at time t (mg/L)

V = volume of solution (L)

m = mass of adsorbent (g)

2.11 Adsorption Models

2.11.1 Kinetic Models

Kinetic models are used to determine the adsorption rate of an adsorbate (Kaudza et al., 2026). They describe the adsorption process over time and explain the transfer of the adsorbate from the solution to the adsorption sites on the adsorbent (Otieno, 2023). To study the adsorption kinetics of a particular adsorbate, data on its initial concentration and post-adsorption concentrations at different contact times are collected to determine the removal efficiency and adsorption capacity. The resulting data are then plotted as removal efficiency or adsorption capacity against time to generate a kinetic curve(Liu et al., 2022). The kinetic curve is subsequently used to fit appropriate kinetic models.

There are several kinetic models that have been developed. Some of the kinetic models used to fit pharmaceutical adsorption data include: pseudo-first-order, pseudo-second-order, intra-particle diffusion (IPD), and Elovich model (Chauhan et al., 2022). These models can either be linear regression models and non-linear regression models. However, the linear regression models are not accurate as compared to the non-linear regression models (Ehiomogue et al., 2021); therefore, non-linear regression is often preferred.

The selection of the best fitting model is determined by correlating theoretical models with experimental data assessed through the determination coefficient (R^2). R^2 values ranges between 0-1, with 1 indicating perfect fit (Foo & Hameed, 2010). The best fitting model is the one with the highest R^2 (Paredes-Laverde et al., 2018). Equation 2.3 is used to calculate R^2 (Foo & Hameed, 2010). Equations 2.4 to 2.7 present the pseudo-first-order, pseudo-second-order, intra-particle diffusion, and Elovich models, respectively.

$$R^2 = \frac{(q_{e,meas} - \overline{q_{e,calc}})^2}{\sum(q_{e,meas} - \overline{q_{e,calc}})^2 + (q_{e,meas} - q_{e,calc})^2}$$

(2.3)

Where:

$q_{e,meas}$ = measured equilibrium adsorption capacity (mg/g)

$q_{e,calc}$ = calculated equilibrium adsorption capacity (mg/g)

$$q_t = q_e[(1 - exp(-k_1 t)]$$

(2.4)

Where:

q_t = adsorption capacity at time t (mg/g)

q_e = adsorption capacity at equilibrium time (mg/g)

k_1 = pseudo-first order rate constant (1/minute)

t = time (minutes)

$$q_t = \frac{k_2 q_e^2 t}{1 + k_2 q_e t}$$

(2.5)

Where:

q_e = adsorption capacity at equilibrium time (mg/g)

q_t = adsorption capacity at time t (mg/g)

k_2 = pseudo-second-order rate constant (g/mg min)

t = time (minutes)

$$q_t = k_{ip}\sqrt{t} + C_{ip}$$

(2.6)

Where:

q_t = adsorption capacity at time t (mg/g)

k_{ip} = measure of the diffusion coefficient (mg/g/min$^{1/2}$)

C_{ip} = intra-particle diffusion constant (mg/g)

t = time (minutes)

$$q_t = \frac{1}{\beta}\ln(1 + \alpha\beta t) \quad (2.7)$$

Where:

q_t = adsorption capacity at time t (mg/g)

β = desorption constant (g/mg)

α = adsorption rate during the initial phase (mg/g/min)

t = time (minutes)

The pseudo-first-order model, also known as the Lagergren model, was first proposed in 1898 by Lagergren to describe the kinetics of liquid-solid phase adsorption of oxalic acid and malonic acid onto charcoal (Syafiuddi et al., 2018). It was also used by Ho and Mckay in 1998 to describe the kinetics of phosphate on tamarind nut shell activated carbon (Syafiuddi et al., 2018). The model has also been applied in the adsorption of pharmaceuticals on various adsorbents (Chauhan et al., 2022; Dang et al., 2021; Li et al., 2022; Varela et al., 2024). It assumes the involvement of physisorption in the system (Do et al., 2025; Syafiuddi et al., 2018). According to Al-Ghouti & Da'ana (2020), physisorption involves weak interactions such as London forces, dipole-dipole forces, and Van der Waals interactions.

The pseudo-second-order model was proposed by Ho and Mckay in 1998 to describe the kinetics of divalent metal ions onto peat (Syafiuddi et al., 2018). It has also been used to describe the kinetics of various PCs (Chauhan et al., 2022; Dang et al., 2021; Li et al., 2022; Varela et al., 2024). The model assumes chemisorption, which involves strong

interactions resulting from mechanisms such as hydrogen bonding and electrostatic interactions (Al-Ghouti & Da'ana, 2020; Dang et al., 2020). Chauhan et al. (2022) reported that, in most cases, the pseudo-second-order model best fits pharmaceutical adsorption data compared to the pseudo-first order, intraparticle diffusion, and Elovich models.

The IPD model has also been applied in the adsorption of pharmaceuticals on various adsorbents (Chauhan et al., 2022; Dang et al., 2021; Li et al., 2022; Varela et al., 2024). It is used to understand the kinetics of an adsorbate within the solid phase (adsorbent) (Kotabewatta & Priyantha, 2024). According to Kotabewatta & Priyantha (2024) and; Li et al. (2022), the model assumes an initial stage where adsorbate species bind to the outer surface of the adsorbent through boundary layer diffusion. This stage is followed by diffusion of the adsorbates into the macropores, mesopores, and micropores of the adsorbent (Kotabewatta & Priyantha, 2024; Li et al., 2022). Thereafter, the adsorbates move through the pores at a slower rate until the adsorption rate becomes equal to the desorption rate (Kotabewatta & Priyantha, 2024; Li et al., 2022). The model also assumes homogenous pore distribution, which may not be true for adsorbents with complex pore structures, such as activated carbon (Musah et al., 2023; Nayak & Pal, 2019; Zhu et al., 2016).

The Elovich model is associated with heterogenous adsorption systems, which assume that an adsorbent's active sites have varying adsorption energies (Do et al., 2025). It also assumes the involvement of both physisorption and chemisorption in the system (Do et al., 2025). The model has been applied in the adsorption of various pharmaceuticals, including sulfamethoxazole and paracetamol (Chauhan et al., 2022). Table 2.7 presents a summary of the discussed kinetic models. Table 2.8 shows a summary of the models applied for predicting kinetic data of adsorbent-mediated adsorption of pharmaceuticals.

Table 2.7: Summary of the discussed kinetic models

Kinetic model	Equation	Page number
Pseudo-first-order	$q_t = q_e[(1 - exp(-k_1 t)]$	32
Pseudo-second-order	$q_t = \frac{k_2 q_e^2 t}{1 + k_2 q_e t}$	33
Intra-particle diffusion	$q_t = k_{ip}\sqrt{t} + C_{ip}$	33
Elovich	$q_t = \frac{1}{\beta}\ln(1 + \alpha\beta t)$	33

Table 2.8: Summary of the Models Applied for Predicting Kinetic Data of Adsorbent-mediated Adsorption of Pharmaceuticals

Kinetic model	Adsorbent	Pharmaceutical	References
Pseudo-first-order	Giant reed	Amoxicillin	Chauhan et al. (2022)
	Pure glucose	Paracetamol	
	Corncob biochar	Flouroquinolones	Chauhan et al. (2022)
		Acetaminophen	Dang et al. (2021)
		Amoxicillin	Varela et al. (2024)
	Corncob xylose residue biochar		Varela et al. (2024)
		Sulfamethoxazole	Li et al. (2022)
Pseudo-second-order	Giant reed	Amoxicillin	Chauhan et al. (2022)
	Goose berry seed shells	Naproxen	
	Corncob xylose residue biochar		Chauhan et al. (2022)
	Corncob biochar	Sulfamethoxazole	
		Flouroquinolones	Li et al. (2022)
		Acetaminophen	Dang et al. (2021)

		Amoxicillin	Varela et al. (2024)
Intraparticle diffusion (IPD)	Textile effluent sludge		Varela et al. (2024)
	Cherry stalk	Levofloxacin	Chauhan et al. (2022)
		Ofloxacin	
	Corncob xylose residue biochar	Ciprofloxacin	Chauhan et al. (2022)
	Corncob biochar	Sulfamethoxazole	Chauhan et al. (2022)
		Acetaminophen	
		Amoxicillin	Li et al. (2022)
			Varela et al. (2024)
Elovich	Raw bamboo	Sulfamethoxazole	Varela et al. (2024) Chauhan et al. (2022)
	Pure glucose	Pracetamol	Chauhan et al. (2022)

2.11.2 Isotherm Models

Isotherm models are used to describe the interaction between an adsorbate and adsorbent at constant temperature (Ehiomogue et al., 2021). They relate the equilibrium adsorption

capacity to the equilibrium concentration of the adsorbate in the liquid phase. To obtain the isotherm curve, data of equilibrium adsorption capacity are plotted against the equilibrium concentration (Cevallos-Mendoza et al., 2024; Dang et al., 2020). The isotherm curve is then used to fit existing models (Cevallos-Mendoza et al., 2024; Dang et al., 2020).

There are six types of adsorption isotherm models based on their shape: Types I, II, III, IV, V and VI (Ehiomogue et al., 2021). The models are also classified according to the number of parameters: one-parameter models, two-parameter models, three-parameter models, four-parameter models, and five-parameter models (Ehiomogue et al., 2021). Similar to kinetics models, the best-fitting isotherm model is determined by correlating theoretical models with experimental data, assessed through the determination coefficient, R^2. Some of the isotherm models used in the adsorption of pharmaceuticals include Freundlich, Langmuir, Sips, Temkin, and Dubinin-Radushkevich models (Chauhan et al., 2022). Equation 2.8 to 2.12 shows the Freundlich, Langmuir, Sips, Temkin, and Dubinin-Radushkevich models, respectively.

$$q_e = K_F + C_e^{1/s} \quad (2.8)$$

Where:

q_e = adsorption capacity at equilibrium time (mg/g)

k_F = Freundlich constant ((mg/g(L/mg)$^{1/s}$)

s = adsorption intensity or surface heterogeneity

C_e = concentration of adsorbate at equilibrium time (mg/L)

$$q_e = \frac{q_{max} K_L C_e}{[1 + K_L C_e]}$$

(2.9)

Where:

q_e = adsorption capacity at equilibrium time (mg/g)

q_{max} = maximum adsorption capacity (mg/g)

K_L = Langmuir isotherm constant (L/mg)

C_e = concentration of adsorbate at equilibrium time (mg/L)

$$q_e = \left(\frac{q_{max}\, a_S\, C_e^{\beta S}}{1 + a_S\, C_e^{\beta S}} \right)$$

(2.10)

Where:

q_e = adsorption capacity at equilibrium time (mg/g)

q_{max} = maximum adsorption capacity (mg/g)

a_S = constant related to adsorption affinity

C_e = concentration of adsorbate at equilibrium time (mg/L)

β_S = parameter that indicates surface heterogeneity

$$q_e = B\ ln(AC_e) \quad (2.11)$$

Where:

q_e = adsorption capacity at equilibrium time (mg/g)

B = constant related to the heat of adsorption (mg/g)

A_T = Temkin isotherm constant (L/g)

C_e = concentration of adsorbate at equilibrium time (mg/L)

$$q_e = q_{max} exp - K\left(RT\ ln\left(1 + \left(\frac{1}{C_e}\right)\right)^2\right) \quad (2.12)$$

Where:

q_e = adsorption capacity at equilibrium time (mg/g)

q_{max} = maximum adsorption capacity (mg/g)

K = Dubinin-Radushkevich constant (mol^2/J^2)

R = gas constant (8.314 J/mol. K)

T = absolute temperature (K)

C_e = concentration of adsorbate at equilibrium time (mg/L)

The Freundlich model was originally developed for animal charcoal adsorption (Al-Ghouti & Da'ana, 2020). It assumes both monolayer and multilayer adsorption, with stronger binding sites occupied first, followed by a decline in adsorption energy (Ehiomogue et al., 2021; Musah et al., 2022). The model also assumes a heterogenous adsorbent surface, whose topography is patch-wise. This implies that one patch includes all sites with same adsorption energy and that patches do not interact with each other (Al-Ghouti & Da'ana, 2020). The type of Freundlich isotherm is indicated by the value of s. $1/s$ represents the intensity of the adsorption or surface heterogeneity(Chikri et al., 2020). When $1/s$ is greater than zero but less than 1, the adsorption is favorable; when $1/s$ is greater than 1, the adsorption process is unfavorable; and it is considered irreversible when $1/s$ is equal to 1 (Al-Ghouti & Da'ana, 2020).

The Langmuir model assumes that the thickness of adsorbed layer is one molecule (monolayer) (Chikri et al., 2020; Ehiomogue et al., 2021). According to Musah et al. (2022), once an adsorbate occupies a site, no further adsorption can occur on that site, and there are no interactions between adsorbates occupying different sites. The model also assumes a homogenous adsorbent surface, which might not be true for complex adsorbents such as activated carbon, whose surfaces are heterogenous (Chikri et al., 2020; Musah et al., 2022). The nature of adsorption is indicated by a separation factor (R_L). When R_L = 1,

the adsorption is linear; when R_L = 0, the adsorption is irreversible; when R_L > 1, the adsorption is unfavorable; and it is favorable when R_L is greater than zero but less than 1 (0 < R_L < 1) (Al-Ghouti & Da'ana, 2020; Chikri et al., 2020). Equation 2.14 shows the formula for R_L.

$$R_L = \frac{1}{1 + K_L + C_o} \quad (2.14)$$

Where:

R_L = separation factor

K_L = Langmuir isotherm constant (L/mg)

C_o = initial adsorbate concentration (mg/L)

The Sips model is a combination of the Langmuir and Freundlich models (Brião et al., 2023; Ehiomogue et al., 2021). It assumes a heterogeneous adsorbent surface and a monolayer adsorption at high adsorbate concentration (Ehiomogue et al., 2021). It was developed to address the problem of the continuous increase in the adsorbed amount with increasing concentration, which is typically observed in the Freundlich isotherm model (Al-Ghouti & Da'ana, 2020; Ehiomogue et al., 2021).

The Temkin model was originally used to describe hydrogen adsorption on platinum electrodes present in acidic solutions (Al-Ghouti & Da'ana, 2020). It is only valid within an intermediate concentration range. The model assumes chemical adsorption (Ehiomogue et al., 2021; Musah et al., 2022). It also assumes that the adsorption heat is a

function of temperature, with a linear decrease in the energy of all molecules in a layer as surface coverage increases (Ehiomogue et al., 2021; Musah et al., 2022). Although Al-Ghouti & Da'ana (2020) reported that the model is not appropriate for complex adsorption systems, including those involving aqueous phases, some studies have used it to analyze pharmaceutical adsorption data (Chauhan et al., 2022; Lach et al., 2018).

The Dubinin-Radushkevich model was originally developed for vapor and gas adsorption on microporous adsorbents such as activated carbon and zeolites (Al-Ghouti & Da'ana, 2020). Consequently, it may not provide an accurate mean free energy for distinguishing the type of adsorption process (physisorption/chemisorption) in a solid-liquid system (Al-Ghouti & Da'ana, 2020). The model assumes a heterogenous surface with a pore filling mechanism (Musah et al., 2022). It also assumes multilayer adsorption, involving Van der Waals forces; as such, it can be applied to physical adsorption processes.

Given the heterogeneous nature of activated biochar surfaces, the Freundlich, Sips and Dubinin-Radushkevich models are expected to provide better fits to the experimental data in this study than the Langmuir and Temkin models. However, this expectation does not hold for all activated biochar. For instance, cobalt iron oxide ($CoFe_2O_4$)-activated biochar derived from banana pseudostem fibers exhibited the best fit with the Langmuir model, suggesting a homogeneous adsorbent surface and monolayer interactions between the adsorbent and Amoxicillin (Chauhan et al., 2022). Table 2.9 presents a summary of the discussed adsorption isotherm models, while Table 2.10 summarizes the isotherm models applied for predicting pharmaceutical removal by various adsorbents.

Table 2.9: Summary of the Discussed Isotherm Models

Isotherm model	Equation	Page number
Freundlich	$q_e = K_F + C_e^{1/s}$	37
Langmuir	$q_e = \frac{q_{max} K_L C_e}{[1 + K_L C_e]}$	37
Sips	$q_e = \left(\frac{q_{max}\, a_S\, C_e^{\beta S}}{1 + a_S\, C_e^{\beta S}}\right)$	38
Temkin	$q_e = B\, ln(A_T C_e)$	38
Dubinin-Radushkevich	$q_e = q_{max} exp - K\left(RT\, ln\left(1 + \left(\frac{1}{C_e}\right)\right)^2\right)$	38

Table 2.10: Models Applied to Predict Isotherm Data for Adsorbent-mediated Pharmaceutical Adsorption

Isotherm model	Adsorbent	Pharmaceutical	References
Freundlich	Goose berry seed shells	Naproxen	Chauhan et al. (2022)
		Amoxicillin	
	Municipal solid waste	Tetracycline	Chauhan et al. (2022)
		Caffeine	
		Ciprofloxacin	
	Corncob biochar	Flouroquinolones	Dang et al. (2021)
		Acetaminophen	
		Amoxicillin	Varela et al. (2024)
Langmuir	Date stone seeds	Ibuprofen	Chauhan et al. (2022)
	Banana stem fibers	Amoxicillin	
	Pamelo peel	Carbamazepine	

	Corncob xylose residue biochar	Sulfamethoxazole	
		Flouroquinolones	Li et al. (2022)
	Corncob biochar		Dang et al. (2021)
		Acetaminophen	
		Amoxicillin	Varela et al. (2024)
Sips	Giant reed	Amoxicilin	Chauhan et al. (2022)
	Municipal solid waste	Ciprofloxacin	
	Pulp mill sludge biochar	Diclofenac	Coimbra et al. (2019)
		Salicylic acid	
		Ibuprofen	
		Acetaminophen	
Temkin	Corn husk	Lefloxacin	Chauhan et al. (2022)
		Tetracycline	

	Cherry stalk	Caffeine	
		Ciprofloxacin	Chauhan et al. (2022)
	Activated carbon	Salicylic acid	Chauhan et al. (2022)
		Ibuprofen sodium	Lach et al. (2018)
Dubinin-Radushkevich	Pamelo peel	Carbamazepine	Chauhan et al. (2022)
	Pure glucose	Pracetamol	
	Corncob biochar	Acetaminophen	Varela et al. (2024)
		Amoxicillin	

2.12 Data Analysis Methods

The adsorbent removal efficiency of PCs from aqueous solutions during the adsorption process is affected by factors such as the pH of solution, adsorbent dosage, and contact time (Bellahsen et al., 2021). To achieve the maximum removal efficiency, a systematic approach to designing and conducting the experiments, along with statistical analysis, is required (Asghar et al., 2014). This is accomplished through optimization techniques such

as computational fluid dynamics (CFD), response surface methodology (RSM), and the Taguchi method (Asghar et al., 2014; Maddodi et al., 2020).

2.12.1 Computational Fluid Dynamics

Computational Fluid Dynamics (CFD) offers numerical solutions to mathematical models such as the conservation equations of mass, momentum, and energy in fluid flow systems (Patil & Kadam, 2023). According to Wilberforce et al. (2021), CDF involves the simulation of a process using software such as COMSOL Multiphysics 3.4 and ANSYS FLUENT 18.0. The model is built in software such as SOLIDWORKS and then exported to the simulation software (Wilberforce et al., 2021). Prior to the simulation, critical factors affecting the process and their levels need to be identified in order to be used in the simulation (Amna et al., 2023; Wilberforce et al., 2021; Yekeen et al., 2023). Finally, the factor-level combination that yields the best response is validated using experimental results for that combination to assess the deviation between the simulation results and the experimental data (Amna et al., 2023; Bakhshandeh et al., 2022; Dehaghani et al., 2022; Yekeen et al., 2023).

For instance, Amna et al. (2023) conducted a study on the analysis of mercury adsorption by inverse-vulcanized porous sulfur copolymers using CFD. In the study, parameters such as mercy-ion concentration, the volumetric flow rate of wastewater, temperature, and thickness of the adsorbent material were analyzed. The simulation yielded a maximum adsorption capacity of 249μg/g, while the experimental validation yielded an adsorption capacity of 244μg/g (Amna et al., 2023). In addition, Yekeen et al. (2023) investigated the mechanisms of enhanced oil recovery via nanoparticle-surfactant solutions using CFD. Parameters such as design dimensions and porosity were analyzed. The authors reported that the simulation prediction results agreed with the experimental results, demonstrating that the lowest amount of oil (37.84%) was retained with the micromodel after multiwalled carbon nanotubes-SDBS flooding (Yekeen et al., 2023).

CFD offers a number of benefits. It helps reduce the number of experiments and thereby lowers costs (Bakhshandeh et al., 2022; Dehaghani et al., 2022). In addition, it allows evaluation of process parameters before their physical application, making it effective for scaling up lab processes to the industrial level (Amna et al., 2023). However, the accuracy of CFD models depends heavily on the quality of input data and assumptions made during the simulation (Amna et al., 2023; Bakhshandeh et al., 2022; Dehaghani et al., 2022; Yekeen et al., 2023).

2.12.2 Response Surface Methodology

Unlike the conventional method, which follows a one-factor-at-a-time approach (univariate approach), response surface methodology (RSM) follows a multivariate approach, where two or more factors are considered (Asghar et al., 2014). The multivariate approach has more advantages over univariate approach because interactions between factors and linear or nonlinear relationships with the responses can be studied using the multivariate approach. Additionally, the number of experiments required for process optimization is fewer in the multivariate approach than in the univariate approach (Asghar et al., 2014).

Optimizing a process using RSM as the optimization tool involves undertaking a series of steps. First, it requires designing experiments to measure the dependent variables (Otieno, 2023). Prior to designing the experiments, critical factors that affect the process are identified, along with their minimum and maximum levels (Bhattacharya, 2021). In most cases, central composite design (CCD) is used in the design of the experiments (Asghar et al., 2014; Otieno, 2023). Statistical software such as Design expert and Minitab are used for the design of the CCD (Bhattacharya, 2021; Maddodi et al., 2020). Equation 2.15 shows the formula for calculating the number of experiments designed by CCD.

$$N_E = k^2 + 2k + c$$

(2.15)

Where:

N_E = total number of experiments

k = number of studied factors

c = number of center point replicates

After obtaining the experimental design, the experiment can be conducted. The experimental results are analyzed using statistical software such as Design expert software and Minitab, which fit the dependent and independent variables to a second order polynomial equation to determine the relationship between the variables (Asghar et al., 2014; Otieno, 2023). Equation 2.16 presents the second order polynomial equation.

$$y = \alpha_0 + \sum_{i=1}^{v} \alpha_i x_i + \sum_{i=1}^{v} \alpha_{ii} x_i^2 + \sum_{i=1}^{v} \alpha_{ij} x_i x_j + \varepsilon$$

(2.16)

Where:

y = predicted response variable

α_0 = value of the fixed response at the center point of the design

α_i = linear effect regression term

α_{ii} = quadratic effect regression term

α_{ij} = interaction effect regression term

x_i = level of the independent variable

v = number of independent variables

ε = random error

The statistical software also offers adequacy measures such as the Analysis of Variance (ANOVA), lack-of-fit test, and F-test (Otieno, 2023). Additionally, the software provides surface plots of the experimental data and other diagnostic plots, such as predicted versus actual plot (Bhattacharya, 2021; Otieno, 2023). Finally, the process is optimized by setting the desired conditions (maximize, minimize or target) for the process (Otieno, 2023). RSM uses desirability function (D) to represent the closeness of the response to its ideal value (Otieno, 2023). D ranges from 0 – 1; when D = 0, the response is unacceptable, and when D = 1, the response is close to the target value (Otieno, 2023).

2.12.3 Taguchi Method

Taguchi method is a statistical approach used in engineering, biotechnology, and other fields to improve the quality of goods and processes. Similar to RSM, Taguchi also follows a multivariate approach, considering two or more factors (Asghar et al., 2014). However, the number of experiments required for the same number of factors and levels is fewer in Taguchi than in RSM (Asghar et al., 2014). Additionally, the Taguchi method incorporates the experimental design as part of the optimization process (Karna & Sahai, 2012). It also accounts for noise factors through the use of a Signal-to-Noise ratios (S/N), where the signal is the desired value and the noise is the undesired value (Karna & Sahai, 2012; Yusuff et al., 2021). The S/N ratio is classified into three categories: larger the better, smaller the better, and nominal the better (Karna & Sahai, 2012; Yusuff et al., 2021). The “larger the better” criterion is applied when maximum results are desired, such as increasing the removal efficiency of an adsorbent. The “smaller the better” criterion is used when minimum results are preferred, such as reducing carbon dioxide emissions. The “nominal the better” criterion is used when a target value is required. Equation 2.17 shows the formula for calculating the S/N in the “larger the better” condition.

$$S/_N = -10\log\left[\frac{1}{n}\sum_{i=1}^{o}\frac{1}{z_i^2}\right]$$

(2.17)

Where:

$S/_N$ = Signal to noise ratio

n = number of measurements

o = total number of observations

z_i= observed value

To apply the Taguchi method as an optimization tool, several steps need to be followed (Karna & Sahai, 2012). First, the main function, side effects, and failure modes must be identified. Second, noise factors, testing conditions, and quality characteristics are determined. Third, the objective function to be optimized is identified. Fourth, control factors and their levels are established, and then an orthogonal array matrix experiment is selected. The experiment is conducted based on this matrix, and the data are analyzed to predict the optimal levels and performance. Finally, a verification experiment is performed, and future actions are planned.

Taguchi uses Orthogonal Arrays in experiments, which help in determining the combinations of factors and levels to be considered in an experiment (Karna & Sahai, 2012). According to Agrawal et al. (2020), statistical software such as Minitab is used in the design of the orthogonal arrays. Equation 2.18 shows the orthogonal arrays design.

$$OA = L_a(b^f)$$

(2.18)

Where:

OA = Orthogonal array

L = Latin square

a = number of rows (runs)

b = number of levels

f = number of columns (factors)

Determining the factors affecting the process and their levels requires a thorough understanding of the process. This includes understanding the minimum and maximum values of the factors. If the minimum and maximum values are far apart, the levels can be spaced farther apart or more levels can be tested. Conversely, if the minimum and maximum values of the factors are close, the levels can be closer together or fewer levels can be used (Karna & Sahai, 2012). Analysis of Variance (ANOVA) or response graph methods are used to determine the significance of the factors (Karna & Sahai, 2012). The S/N ratio is used to identify the optimum values of the factors (Agrawal et al., 2020).

2.13 Evaluating the Suitability of the Kinetic and Isotherm Equations Using Experimental Data

The closeness between equilibrium adsorption capacity obtained from experimental data and that from isotherm models is evaluated using statistical tools such as the average relative error (% ARE), the determination coefficient (R^2), and Chi-square (x^2) (Abin-bazaine et al., 2022; Paredes-Laverde et al., 2018). Equation 2.3 presents the formula for the determination coefficient (R^2). Equation 2.19 and 2.20 shows the formula for average relative error (% ARE) and Chi-square (x^2), respectively.

$$\% \, ARE = \frac{100}{r} \sum_{i=1}^{n} \left| \frac{q_{e,calc} - q_{e,exp}}{q_{e,exp}} \right|$$

(2.19)

Where:

n = number of measurements

$q_{e,calc}$ = calculated equilibrium adsorption capacity (mg/g)

$q_{e,exp}$ = experimental equilibrium adsorption capacity (mg/g)

$$x^2 = \sum_{i=1}^{n} \frac{(q_{e,exp} - q_{e,calc})^2}{q_{e,calc}}$$

(2.20)

Where:

x^2 = Chi-square

n = number of measurements

$q_{i,calc}$ = calculated equilibrium adsorption capacity (mg/g)

$q_{i,exp}$ = experimental equilibrium adsorption capacity (mg/g)

In this study, these statistical metrics were used to assess the goodness-of-fit between experimental and model-predicted data and to determine the best-fitting kinetic and isotherm models. According to Abin-bazaine et al. (2022), the model is considered to adequately fit the experimental data when the average relative error is less than or equal to 5% and Chi-square (x^2) is less than or equal to 0.05.

2.14 Summary of Literature Review and Research Gap

Encroachment of pharmaceuticals into the aquatic environment is one of the major environmental concerns worldwide due to the adverse effects on human health and aquatic species. One pharmaceutical class of particular concern is antibiotics, specifically sulfamethoxazole and trimethoprim, because of their negative impacts such as the development of antibiotic resistance and antimicrobial resistance genes. Among the various methods to combat antibiotic resistance, wastewater treatment appears to be a promising approach, as it helps reduce the entry of pharmaceuticals into the aquatic environment.

There are numerous technologies for treating wastewater. Among these, adsorption using adsorbents such as agricultural waste has gained considerable interest among researchers because it is cost-effective, scalable, and environmentally friendly. White-rot fungi are natural adsorbents that have been studied extensively for their potential in removing pharmaceuticals from aqueous solutions. Most studies concerning pollutant removal using white-rot fungus focus on bioremediation. However, research on the removal of pharmaceutical or other pollutants using white-rot fungus biochar is limited. Furthermore, no studies have investigated the adsorption of sulfamethoxazole and trimethoprim using white-rot fungus biochar or its combination with corncob biochar.

Therefore, there is a need to explore and optimize adsorption-based systems utilizing these materials. In this study, the adsorption performance of white-rot fungus biochar and corncob biochar, both individually and in combination, was evaluated. To systematically investigate the effects of key operational parameters and determine optimal conditions for maximum removal efficiency, the Taguchi method was employed as an experimental design and optimization tool for the adsorption process involving a mixture of white-rot fungus biochar and corncob biochar. This approach enables efficient evaluation of multiple factors while minimizing the number of experimental runs, thereby providing a robust framework for optimizing the adsorption process.

2.15 Conceptual Framework of the Study

Figure 2.4 presents the conceptual framework of the study, illustrating the dependent, independent, and extraneous variables involved in biochar preparation and adsorption experiments.

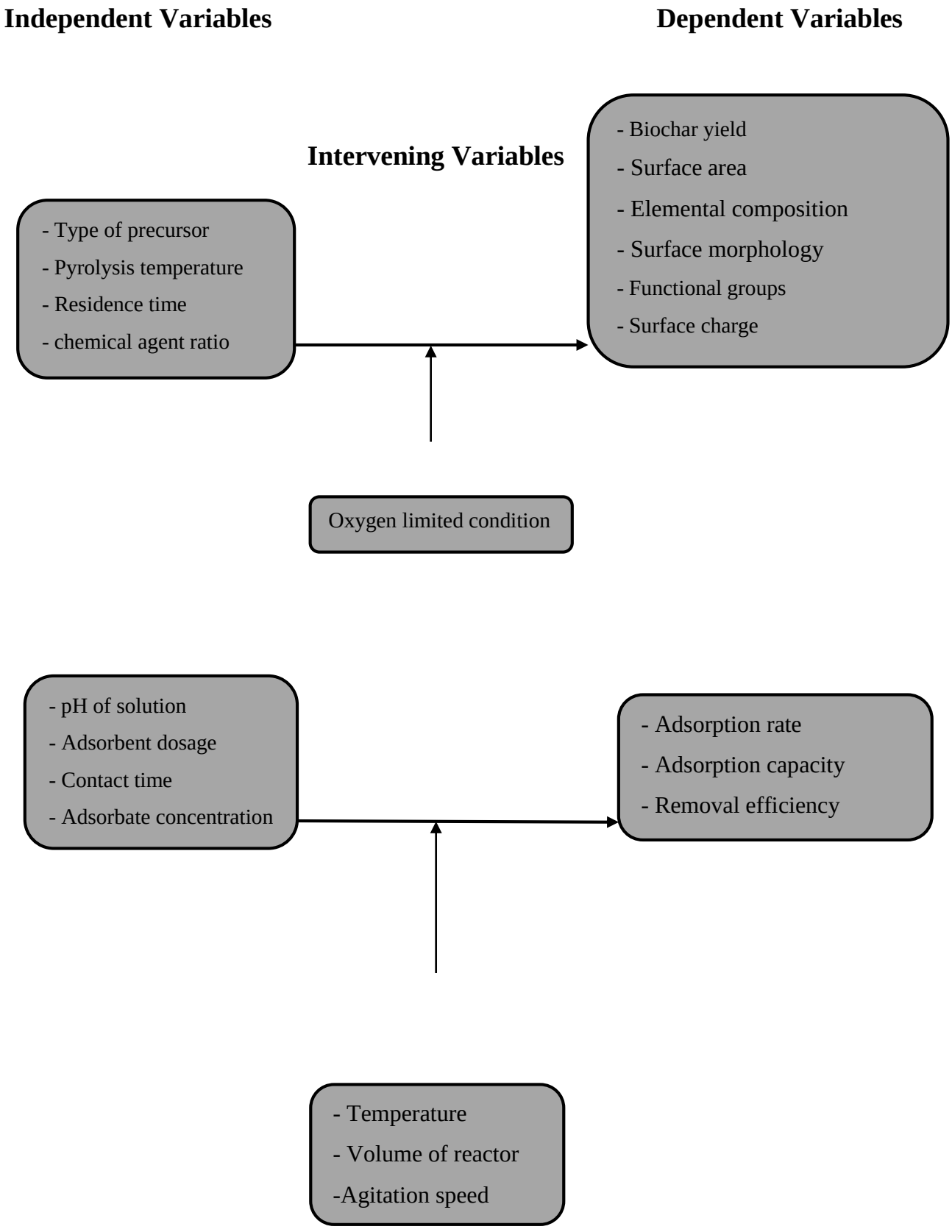
Independent Variables
Dependent Variables
Intervening Variables
- Biochar yield
- Surface area
- Elemental composition
- Surface morphology
- Functional groups
- Surface charge
- Type of precursor
- Pyrolysis temperature
- Residence time
- chemical agent ratio
Oxygen limited condition
- pH of solution
- Adsorbent dosage
- Contact time
- Adsorbate concentration
- Adsorption rate
- Adsorption capacity
- Removal efficiency
- Temperature
- Volume of reactor
-Agitation speed

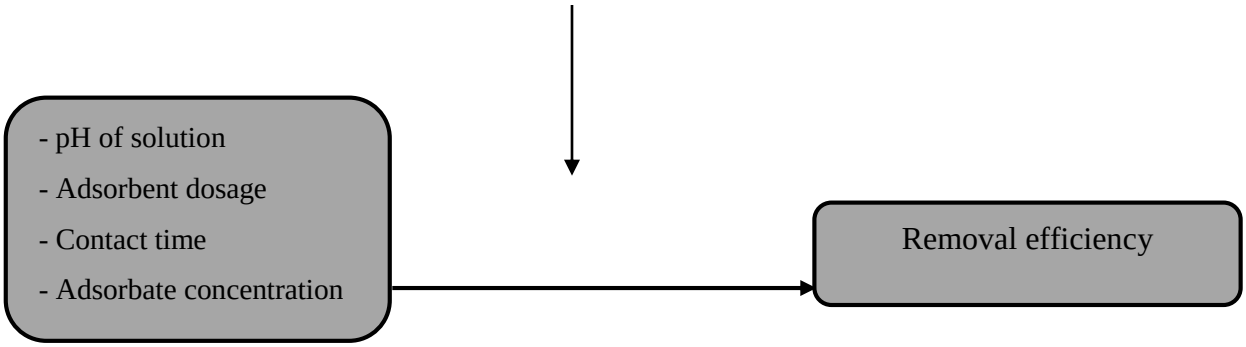

Figure 2.4: Conceptual Framework of the Study

CHAPTER THREE

MATERIALS AND METHODS

3.1 Preparation of White-Rot Fungus Biochar and Corncob Biochar and Characterization

The flow of experimental activities conducted to achieve the first objective of the study is illustrated in Figure 3.1. A summary of the characterization analyses performed on WR700, CB700, and their respective precursors is presented in Table 3.1.

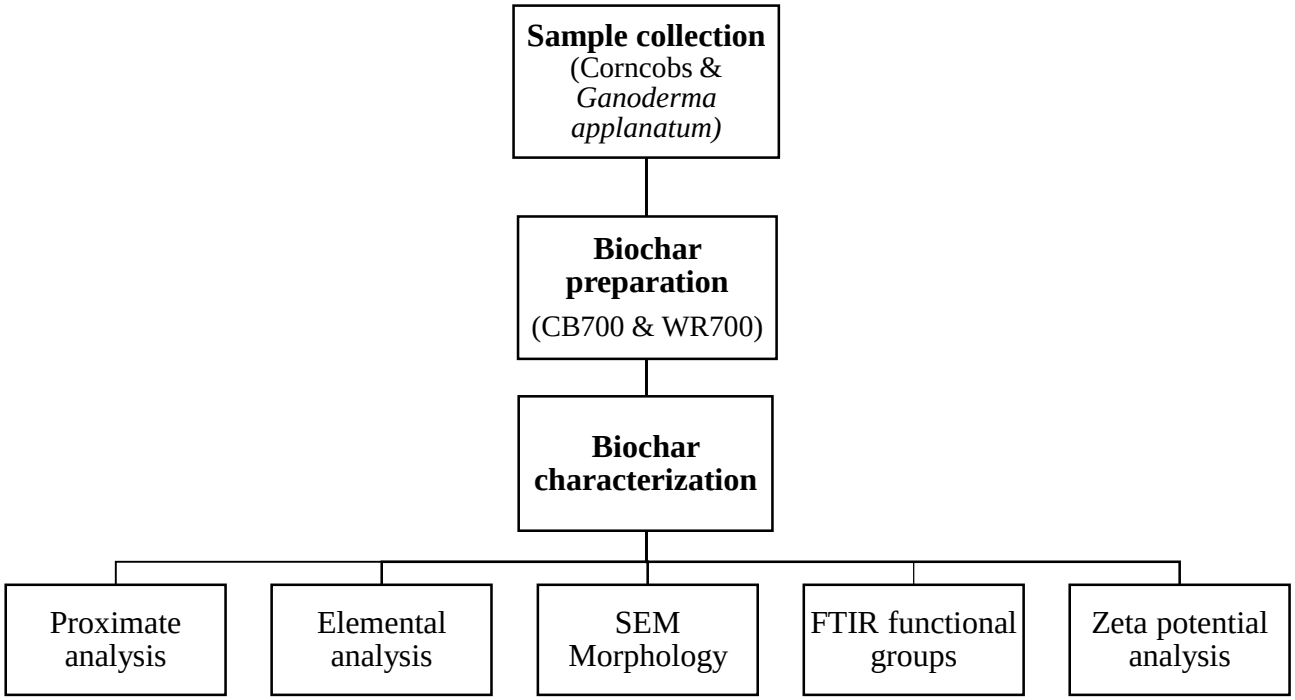

Figure 3.1: The Flow of Experimental Activities Conducted

Table 3.1: Summary of Characterization Analyses Conducted on WR700, CB700, and their Precursors

Analysis	Instrument	Model	Analyzed sample
Elemental composition	CHNS Elemental analyzer	Vario MACRO cube	WR700, CB700
Surface morphology	SEM	JCM-7000 NeoScope™ Benchtop SEM	WR700, CB700, white-rot fugus, corncob
Functional groups	FTIR	ALPHA FTIR Spectrometer	WR700, CB700, white-rot fugus, corncob
Surface charge	Zeta potential analyzer	Nano Zetasizer ZSPn	WR700, CB700
Moisture, ash, volatile matter, fixed carbon	Oven dryer Analytical balance		WR700, CB700

3.1.1 Study Area and Sample Collection

The study was conducted in laboratories at Jomo Kenyatta University of Agriculture and Technology (JKUAT), Kenya, specifically within the Department of Soil Water and Environmental Engineering. This work was complimented by additional tests carried out in the laboratories of the Department of Chemistry and the Department of Civil Engineering. Due to limited availability of a carbon, hydrogen, nitrogen, and sulfur (CHNS) analyzer, further analyses were conducted at an external laboratory within the Department of Biological and Chemical Engineering, Aarhus University, Denmark.

JKUAT is located in Juja, along Thika-Nairobi highway. Juja lies between latitude -1.102554 and longitude 37.013193, with an average altitude of 1519 m above sea level. The area has an average annual maximum temperature of 23.4°C and receives approximately 1024.2 mm of rainfall annually. The location and climatic characteristics of the study area, including mean annual temperature and rainfall, were obtained from Google Earth and historical meteorological records provided by the Kenya Meteorological Department (KMD)**,** respectively.

Corncobs were collected from JKUAT farm. Fresh *Ganoderma applanatum* (Pers.) Pat., belonging to the mushroom family *Polyporaceae*, was collected from Timboroa forest in Uasin Gishu County, Kenya (0.1086° N, 35.4910° E) in January 2025. The specimens were identified and authenticated at the Department of Botany, JKUAT. Voucher specimens' accepted name and author name were authenticated and verified from the Global Biodiversity Information Facility database. Voucher specimens were deposited in the JKUAT Botany Herbarium (JKUATBH) with accession number CK-JKUATBH/001GF/2025.

3.1.2 Preparation of Biochar

White-rot fungus (*Ganoderma applanatum*) and corncobs were dried under direct sunlight for three days and subsequently manually crushed into smaller particle sizes using a mortar and pestle. Precursor impregnation was carried out at a 2:1 weight-to-volume ratio by mixing 2 kg of the crushed precursor with 1 liter of H_3PO_4 (85% wt), followed by storage at room temperature for 24 hours. After impregnation, the precursor was oven-dried at 105 °C for 24 hours. Thereafter, 200 g of the dried precursor was weighed in triplicate, compacted, and wrapped in aluminum foil to minimize oxygen exposure. The samples were then subjected to pyrolysis under oxygen-limited conditions in an electric muffle furnace (Yamato Scientific Co., Ltd., FM-36, Tokyo, Japan) at 700°C with a residence time of 1 hour.

The selection of phosphoric acid (H_3PO_4) as the activating agent was based on its relatively low environmental impact, making it a safer alternative to other chemical activating agents (Jabar et al., 2022; Oginni et al., 2019; Putranto et al., 2022). Additionally, H_3PO_4 has been shown to enhance biochar porosity, surface area, and functional groups (Oginni et al., 2019; Sun & Webley, 2010). The pyrolysis temperature (700°C) was chosen based on previous studies by Magid et al. (2021), Varela et al. (2024), and Weber & Quicker (2018), which reported that higher pyrolysis temperatures increase surface area, pore volume, and pore size (Magid et al., 2021). However, temperatures exceeding 700°C were associated with excessive ash formation, particularly in biomass with low lignin content (Weber & Quicker, 2018).

Following pyrolysis, the muffle furnace was allowed to cool for 30 minutes. The biochar samples were then removed and left to cool at room temperature for an additional hour. The masses of the white-rot fungus biochar and corncob biochar were measured using an analytical balance, and biochar yield was calculated using Equation 3.1 (Sarfaraz et al., 2021).

$$\text{Biochar yield (\%)} = \frac{M_{Biochar}}{M_{Precursor}} \times 100 \quad (3.1)$$

Where:

Biochar yield (%) = Percentage biochar yield

$M_{Biochar}$ = mass of biochar (g)

$M_{Biomass}$ = mass of precursor (g)

After weighing, each biochar was washed with distilled water to remove residual H_3PO_4. The pH was subsequently adjusted to 7 using 1 M NaOH and dried in an HAS-T50 oven (Biobase Biodustry (Shandong) Co., Ltd., Jinan, China) at 105°C for 24 hours. The corncob biochar was then sieved to obtain particle sizes ranging from 2 mm to 2.9 mm, while white-rot fungus biochar was sieved to sizes between 0.42 mm and 1.3 mm. Finally, each biochar was neutralized using 0.1 M of NaOH and HCl, dried again at 105°C for 24 hours, and stored in air tight containers at room temperature. For identification, containers holding white-rot fungus biochar were labelled WR700, whereas those containing corncob biochar were labelled CB700. Each biochar was stored for eight months without any further treatment prior use.

It is important to note that the difference in particle size between WR700 and CB700 may contribute to variations in their adsorption capacities. In general, smaller particle sizes are associated with higher adsorption capacities (Manila et al., 2024; Musthofa et al., 2023). In addition to particle size, the adsorption performance is influenced by other factors, including surface chemistry, surface charge, and adsorbent dosage (Cevallos-Mendoza et al., 2024; Dang et al., 2021; Varela et al., 2024).

3.1.3. Determination of Proximate Composition

Proximate analysis was conducted using the gravimetric method. The moisture content of each biochar was determined by weighing 1.5g of each biochar in a crucible of known mass. Each biochar sample was weighted in triplicate. The crucibles were then placed in an oven at 105 °C for 1 hour. After 1 hour, the crucibles were removed from the oven and placed in a desiccator to cool. Once cooled, the crucibles were reweighed. This process was repeated until the weight after cooling became constant, and the final weight was recorded. The percentage moisture content was calculated using Equation 3.2 (Adekanye et al., 2022; Inegbedion, 2022).

The volatile matter was determined by placing a mass of biochar sample from the moisture determination experiment into crucibles of known mass, which were then closed with lids. The crucibles were subsequently placed in a muffle furnace at 550°C for 8 minutes. Afterward, the crucibles were removed from the muffle furnace and placed in a desiccator to cool. Once cooled, the weight of the crucibles was measured. The volatile matter was calculated using Equation 3.3 (Inegbedion, 2022).

The ash content was determined by placing the mass of biochar from the volatile matter experiment into open crucibles and heating them in a muffle furnace at 550°C for 13 hrs. The crucibles were then removed from the muffle furnace and placed in a desiccator to cool. After cooling, the mass of the ash produced was measured using an analytical balance. The ash content was calculated using Equation 3.4 (Inegbedion, 2022; Sarfaraz et al., 2021). Finally, fixed carbon content was calculated using Equation 3.5 (Inegbedion, 2022).

$$\text{Moisture Content (\%)} = \frac{M_1 - M_2}{M_2} \times 100 \quad (3.2)$$

Where:

M_1 = mass of wet biochar (g)

M_2 = mass of dry biochar (g)

$$\text{Volatile matter (\%)} = \frac{M_2 - M_3}{M_3} \times 100 \quad (3.3)$$

Where:

M_2 = mass of dry biochar (g)

M_3 = mass after heating at 550°C (g)

$$\text{Ash Content (\%)} = \frac{M_4}{M_2} \times 100 \quad (3.4)$$

Where:

M_2 = mass of dry biochar (g)

M_4 = mass after heating at 700°C (g)

$$\text{Fixed Carbon (\%)} = 100\% - (MC\ (\%) + VM\ (\%) + AC\ (\%)) \quad (3.5)$$

Where:

$MC\ (\%)$ = percentage moisture content

$VM\ (\%)$ = percentage volatile matter

$AC\ (\%)$ = percentage ash content

3.1.4 Determination of Elemental Composition

The elemental composition (Carbon, hydrogen, nitrogen, and sulfur) of WR700 and CB700 was analyzed in duplicate using vario MACRO cube CHNS elemental analyzer (Elementar Analysensysteme GmbH, Langenselbold, Germany) at the Department of Biological and Chemical Engineering, Aarhus University, Denmark. Oxygen was determined using Equation 3.6, as described by Ellison et al. (2023)

$$O = 100 - (C + N + H + S + A) \quad (3.6)$$

Where:

O = mass percentage of oxygen (%)

C = mass percentage of carbon (%)

N = mass percentage of nitrogen (%)

H = mass percentage of hydrogen (%)

S = mass percentage of sulfur (%)

A = mass percentage of ash (%)

3.1.5 Determination of Surface Morphology

The surface morphology of WR700, CB700, WR700 precursor (white-rot fungus), and CB700 precursor (corncob) were analyzed using a JCM-7000 NeoScope™ Benchtop Scanning Electron Microscope (Japan Electron Optics Laboratory (JEOL) Co., Ltd, Tokyo, Japan). To determine the surface morphology of each biochar, the samples were mounted onto aluminum stubs using double-sided conductive carbon tape. The Scanning Electron Microscope (SEM) instrument was switched on and allowed to stabilize under vacuum conditions. Thereafter, appropriate imaging parameters, such as accelerating voltage (5-15 kV), working distance, and magnification range, were selected. Each mounted sample was placed into the SEM chamber and scanned using a focused electron beam. Images were captured at different magnifications to observe surface texture, pore structure, and morphological features (Gu et al., 2025; Hussain et al., 2026).

3.1.6 Determination of Functional Groups

ALPHA Fourier Transform Infrared (FTIR) Spectrometer (Bruker Optics GmbH & Co. KG (Bruker Corporation), Ettlingen, Germany) was used to determine the functional groups of WR700 and CB700 before and after adsorption. Functional groups of WR700 precursor (white-rot fungus) and CB700 precursor (corncob) were also determined. The functional groups of each biochar were determined by mixing the samples with potassium bromide (KBr) and pressing them into pellets (Areti et al., 2024). To eliminate interference from CO_2, H_2O vapor, and instrument noise, a background spectrum was recorded using a clean KBr pellet prior to sample analysis. Thereafter, each sample was placed in the sample holder, and spectra were recorded over a range of 4000-400 cm^{-1}. The recorded spectra were then baseline-corrected. The resulting FTIR spectra data were plotted using Origin 2025b.

3.1.7 Determination of Point of Zero Charge

The point of zero charge of each biochar was determined using a Nano Zetasizer ZSP zeta potential analyzer (Malvern Panalytical Ltd., Malvern, United Kingdom). To determine the point of zero charge of each biochar, conical flasks containing 50 mL of 0.01M potassium nitrate (KNO_3) solution were prepared. Thereafter, 0.01g of biochar was added to each flask to form a suspension. The pH was then adjusted over a range of 2-11 using 0.1M NaOH and 0.1M HCl. Each pH value was prepared in triplicate. The suspensions were allowed to equilibrate for 24 hours. Prior to analysis, the pH was rechecked and adjusted where necessary. A portion of each suspension was transferred into a zeta potential cell, and the surface charge was measured using the zeta potential analyzer (Mortazavian et al., 2022).

3.2 Adsorption Kinetics, Equilibrium Isotherms, and Adsorption Mechanisms

The flow of experimental activities conducted to achieve the second objective of the study is illustrated in Figure 3.2.

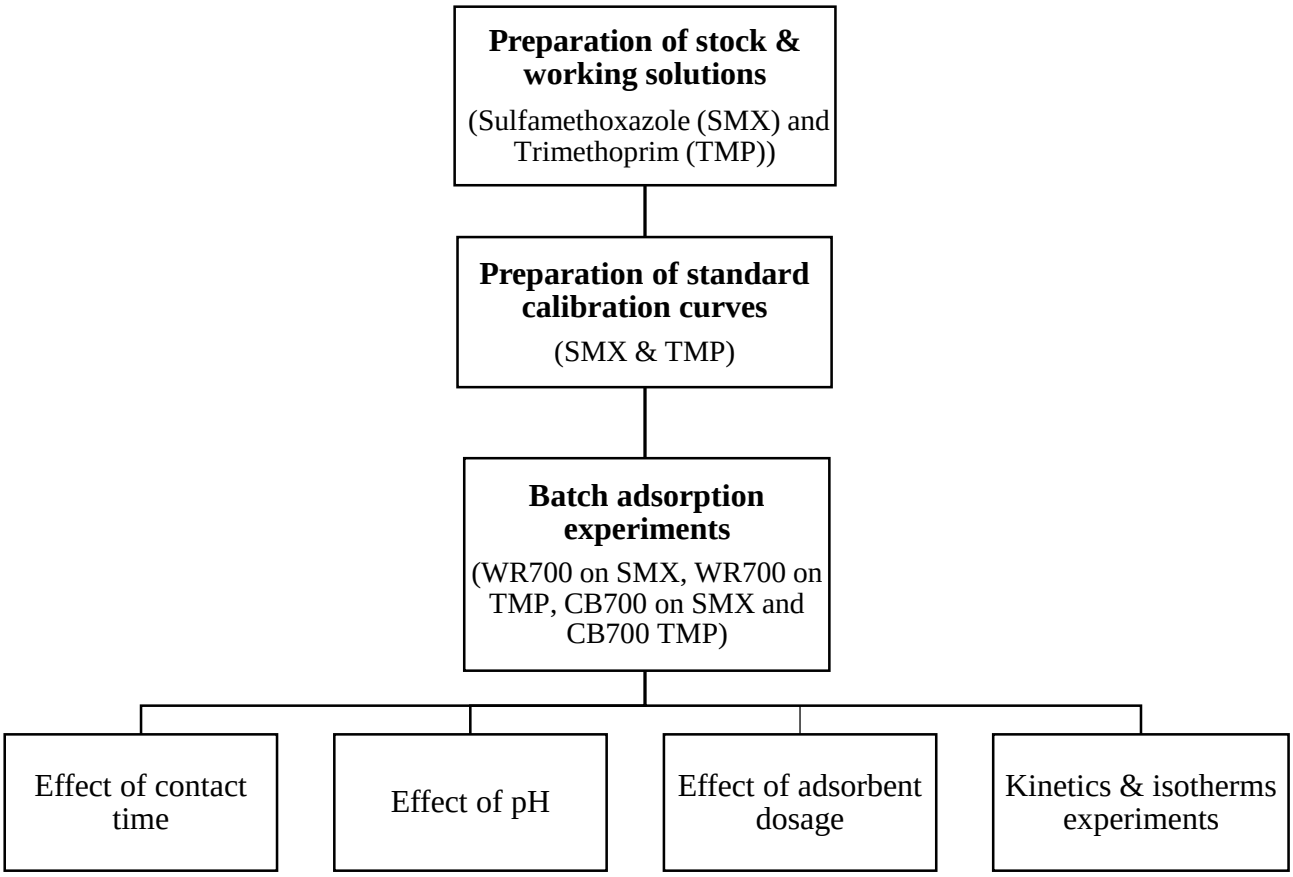

Figure 3.2: The Flow of Experimental Activities Conducted

3.2.1 Preparation of Stock Solution and Working Solutions

Stock solutions (1000 mg/L) for each antibiotic were prepared by dissolving 5 mg of each antibiotic in 5 mL of methanol, which served as the solubilizing agent. Working solutions were then prepared by diluting the stock solutions with distilled water. The required volume of stock solution for preparing a specific concentration of the working solution (0.5–6 mg/L) was calculated using Equation 3.7 (Nwabueze et al., 2024). The stock solutions were stored in the dark at 4°C.

$$V_1 = \frac{C_2 V_2}{C_1} \quad (3.7)$$

Where:

V_1 = volume of stock solution to be drawn (mL)

C_2 = concentration of working solution (mg/L)

V_2 = volume of working solution (mL)

C_1 = concentration of stock solution (mg/L)

3.2.2 Detection Method for Sulfamethoxazole and Trimethoprim using Ultraviolet (UV) Spectrophotometer

Standard calibration curves for sulfamethoxazole (SMX) and trimethoprim (TMP) were prepared using concentrations ranging from 0.2-6 mg/L. The analysis was carried out using a UV-1800 UV Spectrophotometer (Shimadzu, Canby, Oregon, USA) with 1 cm matched quartz cells. The maximum absorbance wavelengths (λ_{max}) were determined to be 265 nm and 275 nm for sulfamethoxazole and trimethoprim, respectively. The λ_{max} was

selected based on the peak absorbance recorded when the solution was scanned between 200 and 800 nm in spectrum mode, using distilled water as a blank. To control the shift in λ_{max} that occur due to changes in pH of the solution, the blank and working solutions were prepared at the same pH (Silva et al., 2017).

3.2.3 Adsorption Factor Experiments

Parallel experiments were conducted to assess the effect of contact time, pH, and adsorbent dosage on the adsorption of SMX and TMP on white-rot fungus biochar (WR700) and corncob biochar (CB700). All experiments were conducted in triplicate using synthetic water, and average values and standard deviations were reported.

To determine the effect of contact time, a WR700 dosage of 1 g/L and a CB700 dosage of 4 g/L were selected based on preliminary experiments. The solution volume was 250 ml, and the initial adsorbate concentration was 1 mg/L. The samples were collected at varying times (2, 4, 10, 20, 30, 40, 60, 80, and 100 minutes). The selected contact times were established based on preliminary trial experiments, which provided an indication of the adsorption behavior and the approximate time required to attain equilibrium.

To determine the effect of pH, WR700 dosage of 1 g/L, CB700 dosage of 4 g/L, solution volume of 20 ml, initial adsorbate concentration of 1 mg/L, and equilibrium time from the contact time experiments were used. The experiment was conducted at varying pH of solution (4, 5, 6, 7, 8, 9, and 10). The selected pH range was chosen to represent conditions normally encountered in wastewater systems and natural aquatic environments. Additionally, this range allowed for the evaluation of the influence of solution pH on adsorption behavior, as pH affects the surface charge of biochar, the ionization state of SMX and TMP, and the interactions between the adsorbates and adsorption sites.

To determine the effect of adsorbent dosage, solution volume of 20 ml, initial adsorbate concentration of 1 mg/L, equilibrium time from the contact time experiments, and optimum pH from the pH experiment were used. The experiment was conducted at varying adsorbent dosage (0.8, 1, 2, 4, and 6 g/L). The selected dosages were based on preliminary experiments, which identified the amount that provided effective adsorption performance while maintaining practical adsorbent utilization. The dosage range was selected to evaluate the influence of adsorbent quantity on adsorption efficiency, as the amount of adsorbent determines the availability of active adsorption sites and the extent of adsorbate–adsorbent interactions.

All experiments were conducted at an agitation speed of 150 rotations/ minute, at a temperature of 30°C using a BT 150 thermostatic water bath shaker (MRC Ltd., Holon, Israel). Control samples consisted of SMX and TMP at the identified conditions, with no adsorbent added.

3.2.4 Adsorption Kinetics and Isotherm Experiments

Each biochar (WR700 and CB700) was used in the study of the adsorption kinetics and isotherms of SMX and TMP. The experiments were conducted at constant shaking speed of 150 rotations/minute, a solution volume of 250 ml, and temperature of 30°C. The optimum pH of solution and adsorbent dosage were kept constant. Sulfamethoxazole and trimethoprim were spiked in 250 ml solution in separate beakers to obtain seven varying concentrations (0.5, 1, 2, 3, 4, 5, and 6 mg/L) of each compound using distilled water. Samples of the solution were collected at time intervals of 2, 4, 10, 20, 40, 30, 50, 60, 70, 90, 100, and 120 minutes. The supernatants were filtered using a 0.45 µm syringe filters to remove any adsorbent particles. Control samples consisted of SMX and TMP at the same conditions but without any adsorbent. The obtained data were fitted to models discussed in section 2.11.

To minimize adsorbent and antibiotic standard consumption, a reduced solution volume of 20 ml was used for the pH and dosage experiments. These experiments were performed while maintaining the same adsorbent dosage and initial adsorbate concentration as those used in the kinetic and isotherm experiments. Each experimental run involved a single sampling point to avoid volume-change effects. In contrast, contact time, kinetic, isotherm experiments employed a larger solution volume of 250 ml to accommodate multiple sampling intervals.

3.3 Removal Performance of White-Rot Fungus Biochar and Corncob Biochar Mixtures

The flow of experimental activities conducted to achieve the third objective of the study is illustrated in Figure 3.3

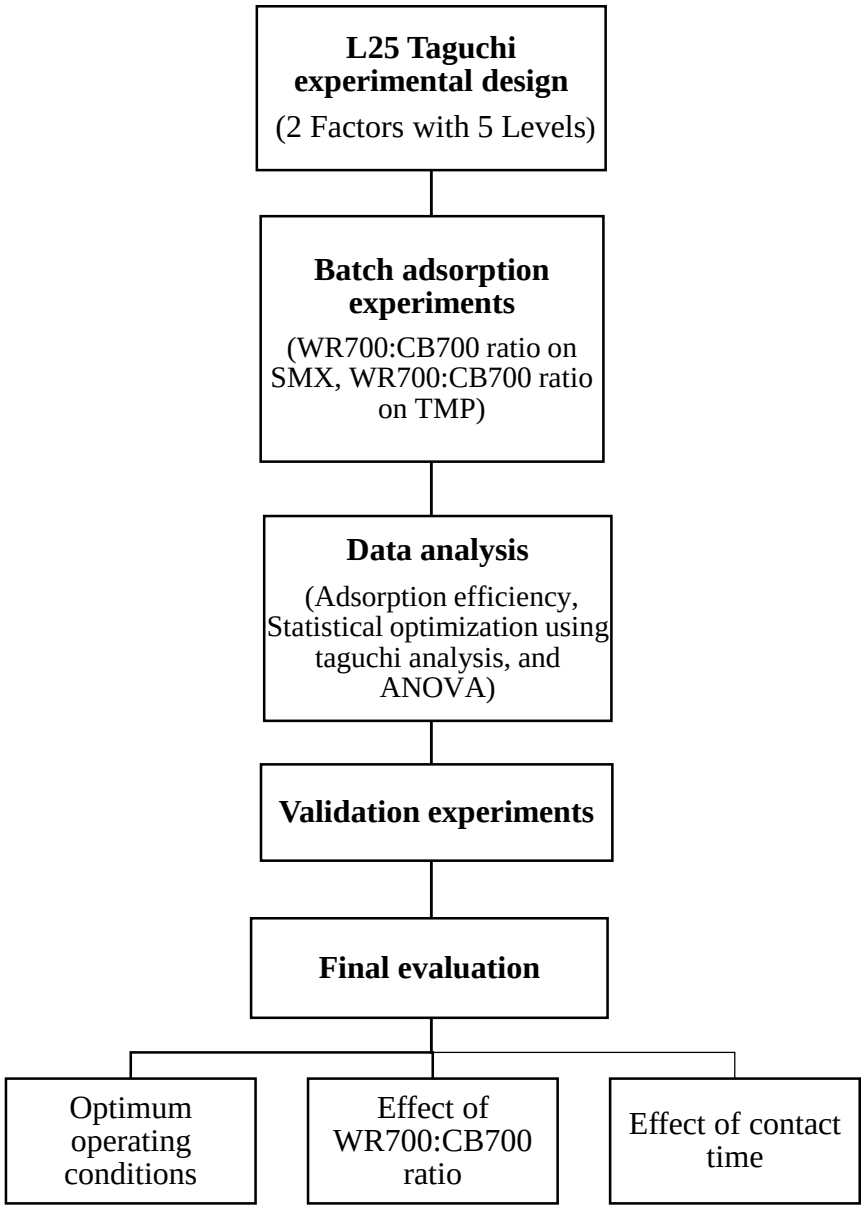

Figure 3.3: The Flow of Experimental Activities Conducted

The removal performance of the biochar mixtures was evaluated using batch adsorption experiments. A Taguchi L25 orthogonal array design was employed, considering two factors at five levels, resulting in 25 experimental runs. All experiments were conducted in triplicate. The two factors evaluated were the WR700:CB700 ratio and contact time.

Table 3.2 presents the factors and their corresponding levels in the L25 orthogonal array. The experiments were performed under constant conditions of shaking speed (150 rotations/min), reactor volume (250 mL), pH (6 for SMX and 8 for TMP), adsorbent dosage (4 g/L), initial adsorbate concentration (1 mg/L), and temperature (30 °C). Minitab statistical software was used to design the Taguchi L25 orthogonal array experiment. The L25 Taguchi orthogonal array designs for the optimization of sulfamethoxazole and trimethoprim adsorption are presented in Tables 3.3 and 3.4, respectively. The optimum level of each factor was determined based on the highest signal-to-noise (S/N) ratio (Equation 2.17), while the significance of each factor was evaluated using analysis of variance (ANOVA). Minitab statistical software was used to calculate the S/N ratios and generate the ANOVA tables.

The selected WR700:CB700 ratio levels were chosen to represent a broad and balanced distribution of biochar compositions within the adsorption system. Ratios of 80:20 and 20:80 represented extreme compositions, allowing evaluation of system behavior under highly dominant proportions of either biochar. Ratios of 65:35 and 35:65 represented intermediate compositions, whereas a ratio of 50:50 represented an equal mixture of both biochars. The selected contact time levels were based on the adsorption duration observed during the contact time experiments for each biochar.

The optimum conditions obtained from the Taguchi analysis were validated through triplicate experiments. The removal efficiency for each factor combination was calculated using Equation 2.1.

Table 3.2: L25 Orthogonal Array with 2 Factors Checked at 5 Levels

Factor	Parameter	Level 1	Level 2	Level 3	Level 4	Level 5
A	WR700:CB700 ratio	80:20	65:35	50:50	35:65	20:80
B	Contact time (minutes)	20	30	40	60	80

Table 3.3: L25 Taguchi Orthogonal Array Design for Optimization of Sulfamethoxazole Adsorption Using Mixtures of White-Rot Fungus Biochar and Corncob Biochar

Run	A: WR700:CB700 ratio	B: Time (minutes)
1	20:80	20
2	20:80	30
3	20:80	40
4	20:80	60
5	20:80	80
6	35:65	20
7	35:65	30
8	35:65	40
9	35:65	60
10	35:65	80
11	50:50	20
12	50:50	30
13	50:50	40
14	50:50	60
15	50:50	80
16	65:35	20
17	65:35	30
18	65:35	40
19	65:35	60
20	65:35	80
21	80:20	20
22	80:20	30
23	80:20	40
24	80:20	60
25	80:20	80

Table 3.4: L25 Taguchi Orthogonal Array Design for Optimization of Trimethoprim Adsorption Using Mixtures of White-Rot Fungus Biochar and Corncob Biochar

Run	A: WR700:CB700 Ratio	B: Time (Minutes)
1	20:80	20
2	20:80	30
3	20:80	40
4	20:80	60
5	20:80	80
6	35:65	20
7	35:65	30
8	35:65	40
9	35:65	60
10	35:65	80
11	50:50	20
12	50:50	30
13	50:50	40
14	50:50	60
15	50:50	80
16	65:35	20
17	65:35	30
18	65:35	40
19	65:35	60
20	65:35	80
21	80:20	20
22	80:20	30
23	80:20	40
24	80:20	60
25	80:20	80

CHAPTER FOUR

RESULTS AND DISCUSSION

4.1 Preparation of White-Rot Fungus Biochar and Corncob Biochar and Characterization

4.1.1 Biochar Yield

There were variations in the triplicate measurements of each biochar, likely due to random experimental errors (Christodoulides & Christodoulides, 2017; Wha et al., 2022). Therefore, average values and standard deviations were calculated.

The average dry-basis biochar yields obtained at an H_3PO_4 activating agent ratio of 2:1 (w/v), pyrolysis temperature of 700°C, and residence time of 1 hour were 52.61 ± 5.01% and 63.41 ± 6.02% for WR700 and CB700, respectively. The higher yield of CB700 compared with WR700 is likely attributable to differences in the physicochemical composition of the feedstocks. The higher biochar yield of CB700 compared with WR700 indicates that the two feedstocks responded differently to the same H_3PO_4 activation and pyrolysis conditions. This difference is likely attributable to inherent differences in the physicochemical properties of the feedstocks, which influence the extent of thermal decomposition and carbon retention during pyrolysis (Hassan et al., 2020).

The biochar yields obtained in the present study are within the range reported in the literature for H_3PO_4-activated biochars produced under different pyrolysis conditions. For example, Tsarpali et al. (2024) reported biochar yields ranging from 28% to 52%, while Daniel et al. (2023) obtained a higher yield of 77.22% using biomass impregnated with 10% H_3PO_4 and pyrolyzed at 500°C for 1 hour under a nitrogen atmosphere. The higher yield reported by Daniel et al. (2023) is likely due to the lower pyrolysis temperature, which reduces thermal decomposition and the loss of volatile matter compared with the 700°C pyrolysis temperature used in the present study.

Overall, the yields obtained for WR700 and CB700 are consistent with previous studies demonstrating that higher pyrolysis temperatures promote greater devolatilization and thermal decomposition of biomass, resulting in reduced biochar yields (Putranto et al., 2022; Tsarpali et al., 2024). Consequently, the lower yield of WR700 and the comparatively higher yield of CB700 can be attributed to the combined effects of feedstock composition and the pyrolysis conditions employed in this study.

4.1.2 Determination of Proximate Composition

Proximate analysis results of WR700 and CB700 are presented in Table 4.1.

Table 4.1: Proximate Analysis Results for WR700 and CB700

Proximate analysis	Sample	
	WR700	**CB700**
Moisture content (%)	6.44 ± 1.42	10.26 ± 2.03
Volatile matter (%)	5.25 ± 1.12	9.1 ± 0.05
Ash (%)	18.15 ± 1.05	8.9 ± 0.11
Fixed carbon (%)	70.16 ± 2.94	71.74 ± 2.88

WR700 and CB700 were stored at moisture contents of 6.44 ± 1.42% and 10.26 ± 2.03%, respectively. Both biochar exhibited a strong fixed carbon retention of 70.16 ± 2.94% and 71.74 ± 2.88% for WR700 and CB700, respectively. Fixed carbon excludes all gases lost via volatile matter emissions (Xu et al., 2019). As such, fixed carbon usually forms a porous skeletal structure that enhances adsorption capacity (Das et al., 2021). WR700 contain a higher ash content (18.15 ± 1.05%) compared to CB700 (8.9 ± 0.11%). Depending on the nature of adsorbate-adsorbent interaction, high ash content can either hinder or enhance the adsorption process. For instance, Li et al. (2017) reported that ash content may block the pores of the adsorbent, thereby hindering the adsorbate's access to

the pores. Conversely, Yang et al. (2023) reported that ash on the surface of ash-biochar composite enhanced methylene blue removal by providing alkaline adsorption environment and more oxygen-based n-π interaction sites.

4.1.3 Determination of Elemental Composition

Elemental analysis results of WR700 and CB700 are presented in Table 4.2.

Table 4.2: Elemental Analysis Results for WR700 and CB700

Biochars	Mass composition					Atomic ratio			
	C (%)	H (%)	N (%)	S (%)	O (%)	C/N	H/C	O/C	(O+N)/C
WR700	71.73 ± 0.06	2.09 ± 0.04	1.94	3.28 ± 4.51	2.82 ± 4.42	36.98	0.03	0.04	0.07
CB700	78.03 ± 1.05	2.12 ± 0.08	0.41 ± 0.03	0.02 ± 0.001	10.53 ± 1.16	190.26	0.03	0.14	0.14

The analysis was conducted in duplicate. WR700 and CB700 exhibited high total carbon content of 71.73 ± 0.06% and 78.03 ± 1.05%, respectively, indicating strong carbon retention. Conversely, the contents of H, N, S, and O were relatively low for both biochar, likely due to volatilization and gas release during pyrolysis (Xu et al., 2019). However, the oxygen content of CB700 (10.53 ± 1.16%) was higher compared to WR700 (2.82 ± 4.42%). This suggests the presence of more oxygen-containing functional groups, such as hydroxyl and carbonyl groups, on the surface of CB700 than on WR700 (Figueredo et al., 2017; Mukome et al., 2013). These functional groups can increase the biochar's polarity, thus enhancing its ability to interact with polar contaminants through mechanisms like hydrogen bonding and electrostatic attraction (Buczek et al., 2025; Huang et al., 2020).

WR700 had C/N, H/C, O/C, and (O+N)/C ratios of 36.98, 0.03, 0.04, and 0.07, respectively. CB700 had C/N, H/C, O/C, and (O+N)/C ratios of 190.26, 0.03, 0.14, and 0.14, respectively. The high C/N ratio indicated a high amount of carbon compared to hydrogen (Figueredo et al., 2017; Mukome et al., 2013). Low ratios of H/C suggests the absence of organic residues on the biochar (Ippolito et al., 2020; Xu et al., 2019). Low O/C, and (O+N)/C ratios indicated an increase in aromacity and decrease in polarity of the biochar (Xu et al., 2019).

4.1.4 Determination of Surface Morphology

The scanning electron micrographs of the white-rot fungus (precursor) at a magnification of 60× (200 μm scale) and the activated sample (WR700) at a magnification of 55× (200 μm scale) are shown in Figure 4.1(a) and (b), respectively. Figure 4.1(c) and (d) show the scanning electron micrographs of the corncob (precursor) at a magnification of 120× (100 μm scale) and the activated sample (CB700) at a magnification of 200× (100 μm scale), respectively.

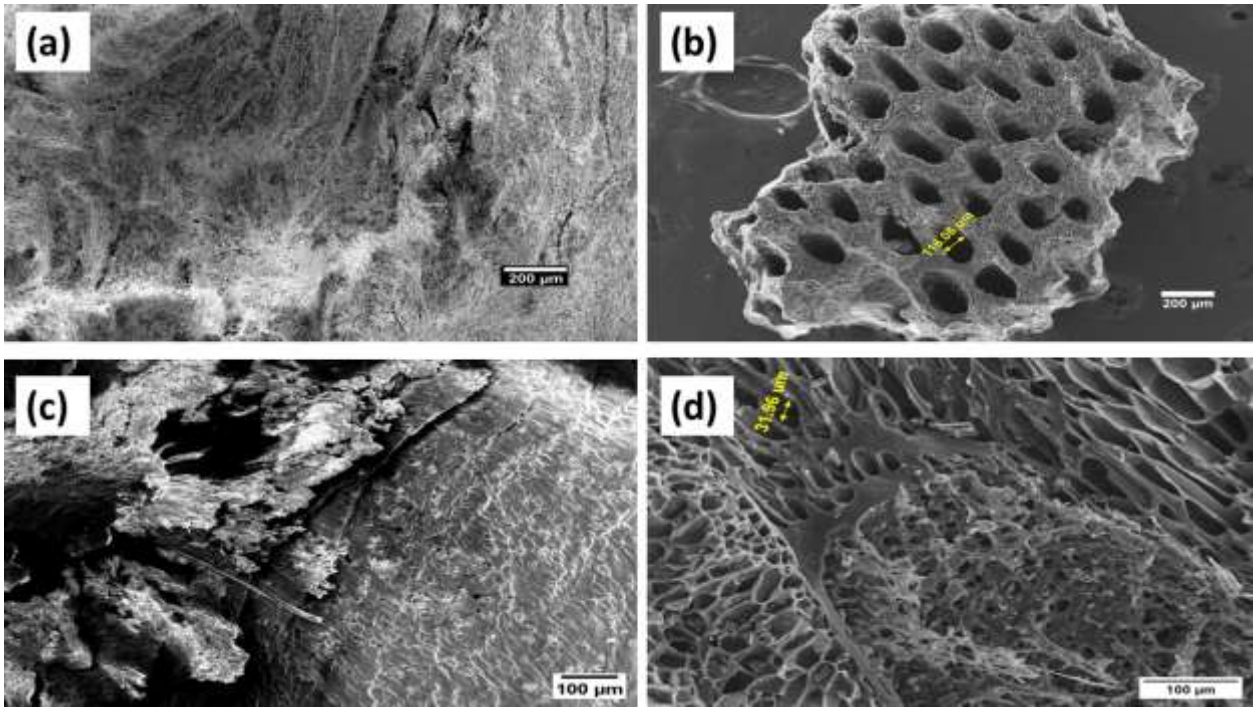

Figure 4.1: Scanning Electron Micrographs: (a) White-rot Fungus (Precursor) at a Scale of 200 µm; (b) WR700 at a Scale of 200 µm; (c) Corncob (Precursor) at a Scale 100 µm; (d) CB700 at a Scale of 100 µm

White-rot fungus (Figure 4.1(a)) exhibited a rough surface characterized by intertwined and overlapping fibers. In contrast, the activated sample (WR700) (Figure 4.1(b)) revealed well-developed pores and cavities. Corncob (Figure 4.1(c)) displayed a highly fractured and rough surface with irregular topography. Similarly, the activated sample (CB700) (Figure 4.1(d)) showed the presence of well-formed pores and cavities.

The development of visible cavities and pores in the activated biochar samples indicates the effect of H_3PO_4 activation on the surface morphology of the precursors. The formation of these cavities and pores can be attributed to the impregnation of white-rot fungus and corncob precursors with H_3PO_4, which facilitated acid diffusion into the precursor structure. This enhanced the interaction between the chemical activator and precursor through acid hydrolysis, resulting in improved pore development (Oginni et al., 2019; Sun

& Webley, 2010). The exterior pores observed in WR700 exhibited tunnel-like structures with varying sizes, whereas those in CB700 displayed honeycomb-like structures with irregular dimensions. During adsorption, these exterior pores serve as primary pathways that facilitate the transport of adsorbate molecules to the micropores located within the internal surface of the activated carbon (Oginni et al., 2019).

4.1.5 Determination of Functional Groups

The FTIR spectra of the WR700 precursor (white-rot fungus), WR700, and WR700 after single adsorption of SMX and TMP are presented in Figure 4.2(a). Similarly, the FTIR spectra of the CB700 precursor (corncob), CB700, and CB700 after single adsorption of SMX and TMP are presented in Figure 4.2(b).

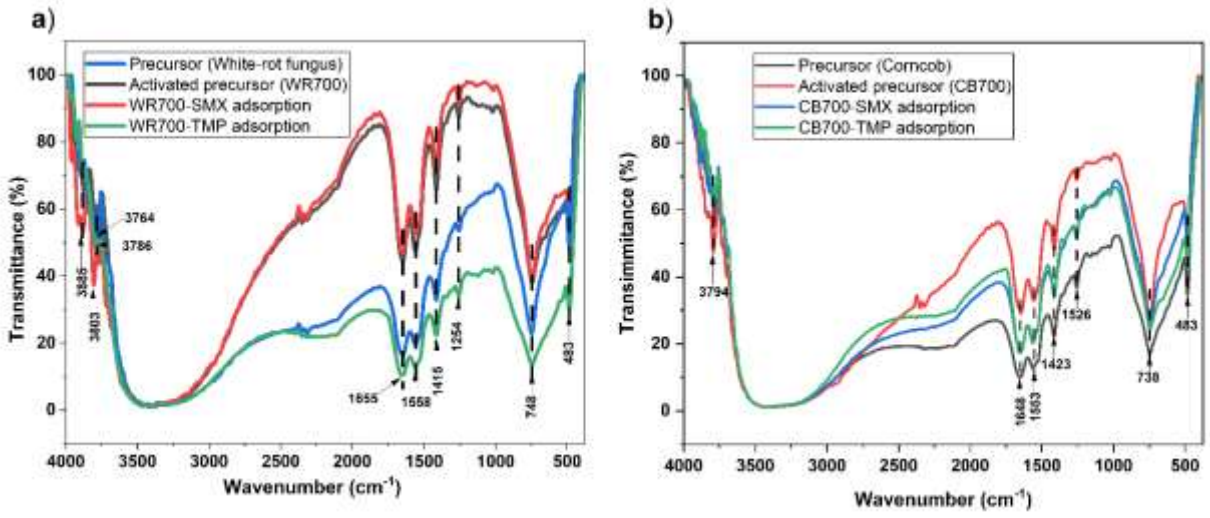

Figure 4.2: FTIR Spectra: (a) WR700 and Precursor; (b) CB700 and Precursor

All spectra illustrate significant changes in the functional groups. WR700's precursor exhibited characteristic peaks at 3885 and 3785 cm^{-1}, corresponding to O–H stretching vibrations, and additional peaks at 1655, 1558, and 1415 cm^{-1}, attributed to C=O, C=C, and C–O groups, respectively (Rudakiya & Gupte, 2019; Varela et al., 2024). Upon

activation (WR700), these functional groups remained present, with increased intensity, suggesting enhanced surface functionality.

Following SMX adsorption, the spectrum showed both amplification and attenuation of peak intensities, indicating moderate interaction with surface groups. In contrast, TMP adsorption led to a pronounced reduction in peak intensities, implying a stronger binding affinity (Varela et al., 2024). While most peak positions remained unchanged, a slight shift in the O–H stretching band was observed from 3764 cm^{-1} to 3803 cm^{-1} (SMX) and 3786 cm^{-1} (TMP), confirming the continued presence of hydroxyl groups post-adsorption (Zhao et al., 2024). These spectral changes suggest that O–H, C=O, C=C, and C–O groups actively participated in the adsorption of both SMX and TMP (Rudakiya & Gupte, 2019; Varela et al., 2024; Zhao et al., 2024).

For corncob and its activated biochar (CB700), all spectra displayed a peak at 3794 cm^{-1}, which is linked to OH groups (Zhao et al., 2024). Additional peaks appeared at 1648, 1553, and 1423 cm^{-1} corresponding to C=O, C=C, and C-O groups (Rudakiya & Gupte, 2019; Varela et al., 2024). After activation of the precursor, a significant increase in the intensity of these peaks was observed. This can be attributed to the thermal decomposition of the precursor, which increased the presence of the functional groups (Adekanye et al., 2022). Following the adsorption of both antibiotics, an increase and decrease in the intensity of the peaks was observed. However, there was no change in the peak position of these groups. This suggested that the OH, C=O, C=C, and C-O groups were involved in the adsorption of SMX and TMP on CB700 (Adekanye et al., 2022; Varela et al., 2024; Vuong et al., 2023).

All observed functional groups play an important role in adsorption process. They facilitate mechanisms such as π–π electron donor-acceptor interactions, complexation, ion exchange hydrogen bonding, and electrostatic interactions (Ambaye et al., 2020; Dang et al., 2021; Jha et al., 2023; Li et al., 2020).

4.1.5.1 Spectral Deconvolution and Quantification of Hydrogen Bonding Interactions

Spectral deconvolution of the biochar's FTIR spectra post-adsorption was performed to evaluate the contribution of hydrogen bonding to the adsorption of SMX and TMP. O–H, C–O, and C=O functional groups were identified as key participants in the interaction with both antibiotics (Buczek et al., 2025; Wei et al., 2024). Deconvolution of each functional group region was performed using band fitting in OriginPro 2025, as described by Geminiani et al. (2023). The spectrum was divided into three distinct regions: 3800–2700 cm^{-1} for O–H, 1507–1264 cm^{-1} for C–O, and 1743–1648 cm^{-1} for C=O (Bouramdane et al., 2024; Buczek et al., 2025; Mendes et al., 2023). Baseline for each spectrum region was corrected using a linear function anchored at the endpoints of each interval. Thereafter, Gaussian fitting was performed iteratively until convergence was achieved at a Chi-square tolerance of 10^{-9}. However, it should be noted that Gaussian peak fitting assumes ideal peak shapes and may introduce uncertainties in cases of overlapping bands, potentially affecting the accuracy of peak positions, widths, and area contributions (Dubrovkin, 2016; Zhang et al., 2026).

The deconvoluted spectra of WR700 and CB700 are shown in Figure 4.3 and 4.4, respectively.

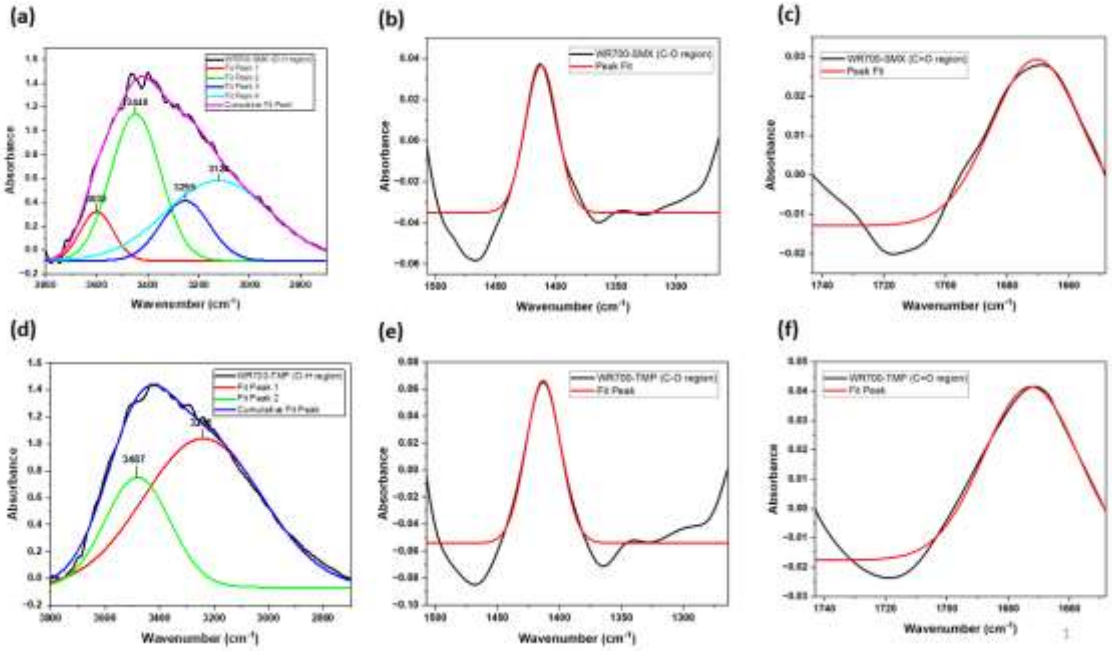

Figure 4.3: Deconvoluted FTIR Spectra of WR700 after Antibiotic Adsorption: (a) O–H Region (SMX), (b) C–O Region (SMX), (c) C=O Region (SMX), (d) O–H Region (TMP), (e) C–O Region (TMP), and (f) C=O Region (TMP)

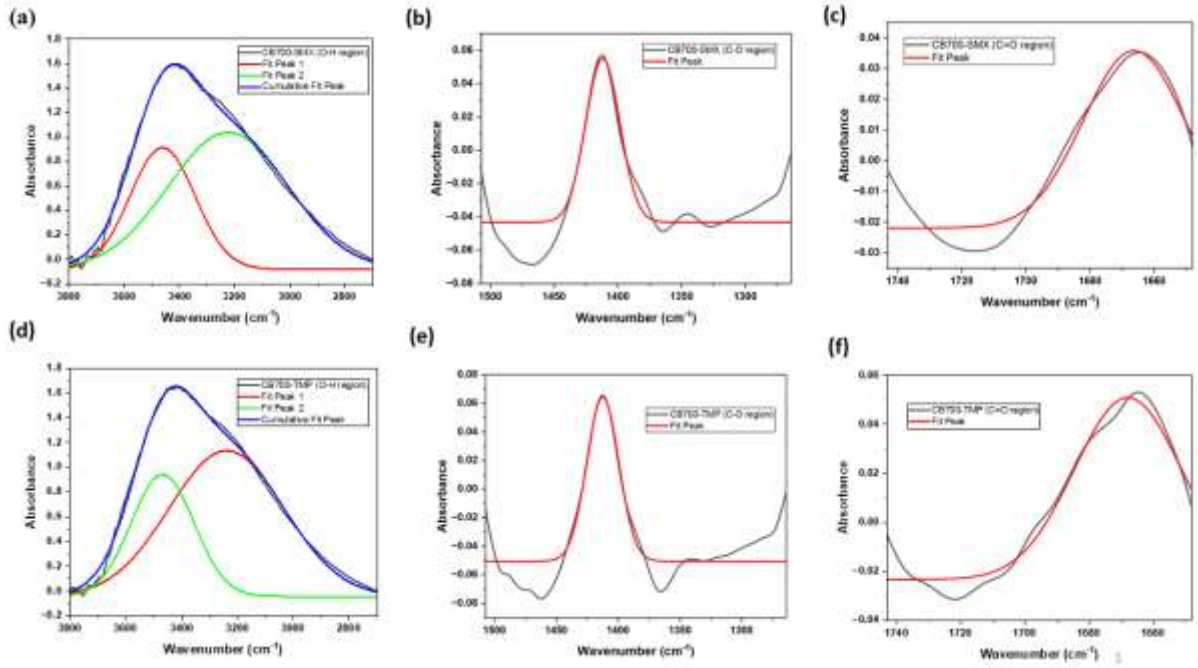

Figure 4.4: Deconvoluted FTIR Spectra of CB700 after Antibiotic Adsorption: (a) O–H Region (SMX), (b) C–O Region (SMX), (c) C=O Region (SMX), (d) O–H Region (TMP), (e) C–O Region (TMP), and (f) C=O Region (TMP)

These spectral modifications confirm the involvement of hydrogen bonding in the adsorption mechanism, with O–H and C=O groups acting as hydrogen donors and acceptors in interactions with both antibiotics. Figure 4.5 (a) and (b) presents the peak areas in the O–H region for WR700 after SMX and TMP adsorption, respectively.

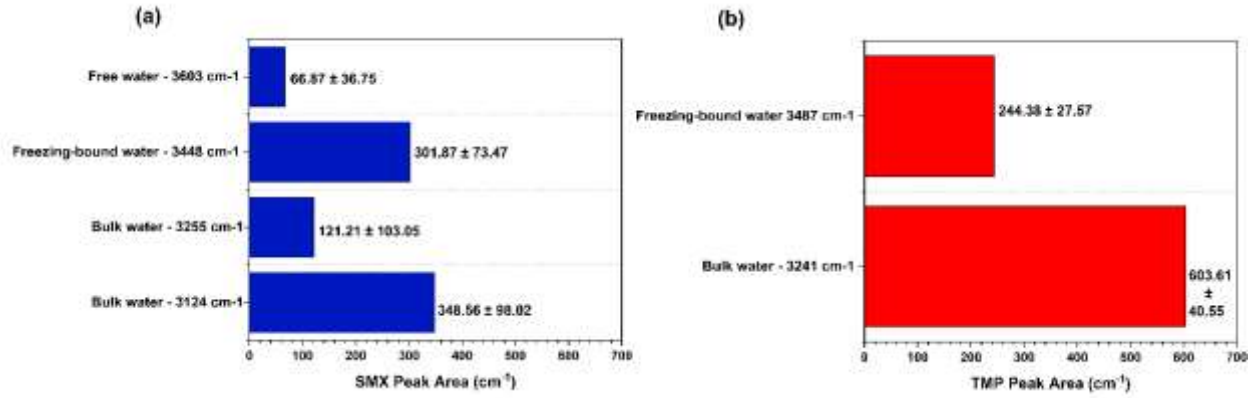

Figure 4.5: WR700's Peak Areas in the 3800-2700 cm-1 Region: (a) SMX, (b) TMP

The peak areas were obtained from single spectrum deconvolution. For SMX, the peak at 3603 cm^{-1} corresponds to non-hydrogen bonded O–H species (Buczek et al., 2025; Geminiani et al., 2023), while peaks at 3448, 3255, and 3124 cm^{-1} indicate hydrogen-bonded O–H groups (Buczek et al., 2025; Geminiani et al., 2023). The total area of hydrogen-bonded O–H species was 771.64 ± 274.54 cm^{-1}. In contrast, the O–H region of WR700 after TMP adsorption contained only hydrogen-bonded species, with peaks at 3487 and 3241 cm^{-1}, yielding a total area of 847.99 ± 68.12 cm^{-1}. For both antibiotics, the C=O region exhibited a single hydrogen-bonded peak, with areas of 1.55 ± 0.09 cm^{-1} (SMX) and 2.28 ± 0.09 cm^{-1} (TMP), indicating a minor contribution from C=O groups (Buczek et al., 2025). The C–O region showed non-hydrogen bonded peaks in both cases (Bouramdane et al., 2024; Mendes et al., 2023). Summing the contributions from all functional group regions, the total hydrogen-bonded peak area was 773.19 ± 274.63 cm^{-1} for SMX and 850.27 ± 68.21 cm^{-1} for TMP. These results suggest that TMP forms stronger hydrogen bonding interactions with WR700 than SMX, supporting the observed differences in adsorption efficiency.

Figures 4.6 (a) and (b) presents the peak areas in the O–H region of CB700 after SMX and TMP adsorption, respectively.

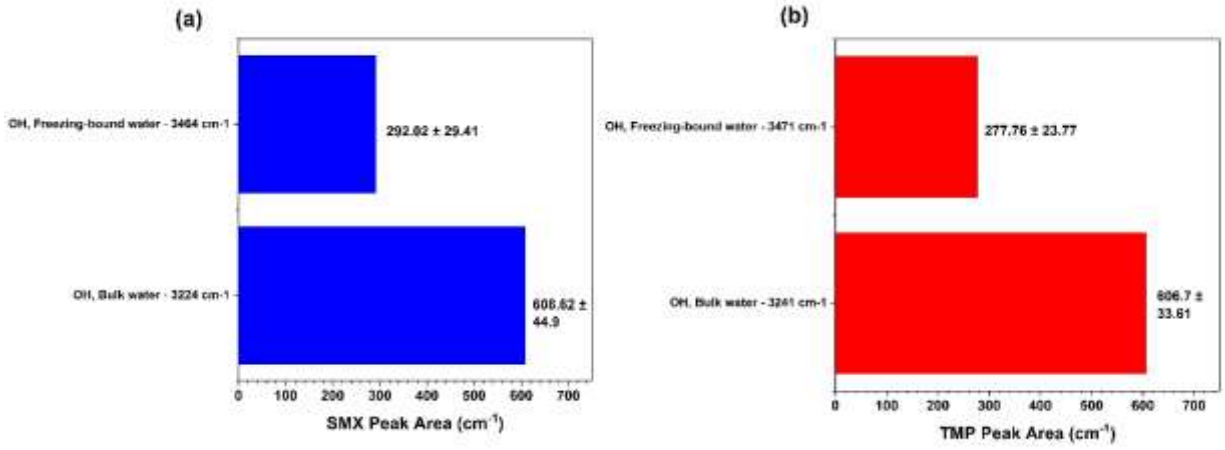

Figure 4.6: CB700's Peak Areas in the 3800-2700 cm-1 Region: (a) SMX, (b) TMP

SMX peaks at 3464, and 3224 cm^{-1} corresponds to hydrogen-bonded O–H groups (Buczek et al., 2025; Geminiani et al., 2023). The total area of hydrogen-bonded O–H species was 900.64 ± 74.31 cm^{-1}. Conversely, the O–H region of CB700 after TMP adsorption contained hydrogen-bonded species, with peaks at 3471 and 3241 cm^{-1}, yielding a total area of 884.46 ± 57.38 cm^{-1}. The O-H region of both antibiotics did not contain non-hydrogen bonded species. These results suggest that SMX forms stronger hydrogen bonding interactions with WR700 than TMP.

In the C=O region, both antibiotics showed a single hydrogen-bonded peak, with areas of 2.3 ± 0.13 cm^{-1} (SMX) and 3.11 ± 0.13 cm^{-1} (TMP), indicating a minor contribution from C=O groups (Buczek et al., 2025). In the C–O region, both antibiotics exhibited non-hydrogen bonded groups (Bouramdane et al., 2024; Mendes et al., 2023). Summing the contributions from all functional group regions, the total hydrogen-bonded peak area for SMX and TMP was 902.94 ± 74.44 cm^{-1} and 887.57 ± 57.51 cm^{-1}, respectively. Table 4.3 provides a summary of the peak areas for each biochar and antibiotic.

Table 4.3: Summary of the Peak Areas for Each Biochar and Antibiotic

Biochar	Antibiotic	Functional Group	Peak Positions (cm^{-1})	Type	Peak Area (cm^{-1})
WR700	SMX	O-H	3603	Non-H-bounded	66.87 ± 36.75
		O-H	3448, 3255, 3124	H-bounded	771.64 ± 274.54
		C=O	1670	H-bounded	1.55 ± 0.09
		C-O	1413	Non-H-bounded	2.39 ± 0.13
	TMP	O-H	3487, 3241	H-bounded	847.99 ± 68.12
		C=O	1684	H-bounded	2.28 ± 0.09
		C-O	1414	Non-H-bounded	4.16 ± 0.2
CB700	SMX	O-H	3464, 3224	H-bounded	900.64 ± 74.31
		C=O	1666	H-bounded	2.3 ± 0.13
		C-O	1413	Non-H-bounded	3.31 ± 0.16
	TMP	O-H	3471, 3241	H-bounded	884.46 ± 57.38
		C=O	1671	H-bounded	3.11 ± 0.13
		C-O	1414	Non-H-bounded	3.31 ± 0.16

4.1.7 Determination of Point of Zero Charge

The zeta potential analysis results are depicted in Figure 4.7. The analysis was conducted to determine the pH at which the surface of WR700 and CB700 has a net charge of zero (pH_{pzc}).

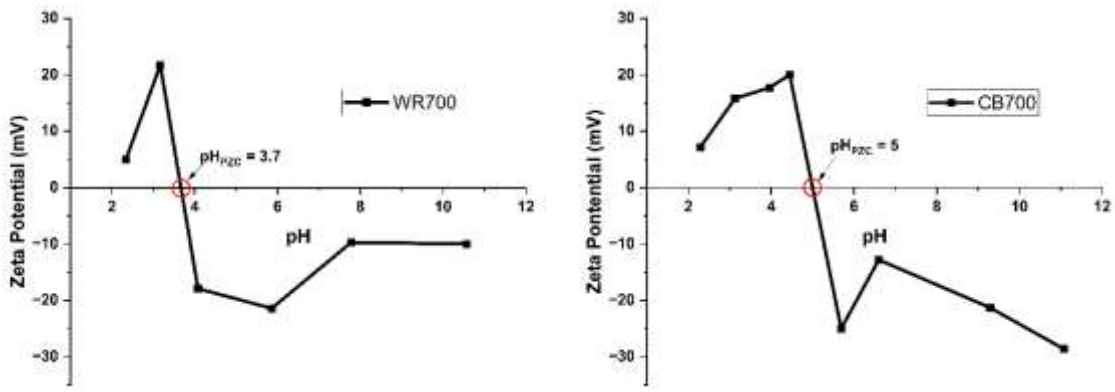

Figure 4.7:Point of Zero Charge (pH_{PZC}) of WR700 and CB700

As shown in Figure 4.7, the pH_{pzc} values of WR700 and CB700 are 3.7 and 5, respectively. This indicates that when WR700 is in a solution with a pH lower than 3.7 and CB700 is in a solution with a pH lower than 5, their surface will predominantly bear a positive charge due to the protonation of their surface functional groups (Cevallos-Mendoza et al., 2024; Hassaan et al., 2023). Conversely, when WR700 is in a solution with a pH higher than 3.7 and CB700 is in a solution with a pH higher than 5, their surface will predominantly bear a negative charge due to the deprotonation of their surface functional groups (Cevallos-Mendoza et al., 2024; Ezeuko et al., 2022; Hassaan et al., 2023; Hmamouchi et al., 2022). These findings, coupled with physicochemical characteristics of SMX and TMP, help to explain the charge interaction between the antibiotic molecules and each biochar.

4.2 Adsorption Kinetics, Equilibrium Isotherms, and Adsorption Mechanisms

4.2.1 Standard Calibration Curves

Sulfamethoxazole (SMX) and trimethoprim (TMP) standard calibration curves used during the adsorption experiments are presented in Figure 4.8.

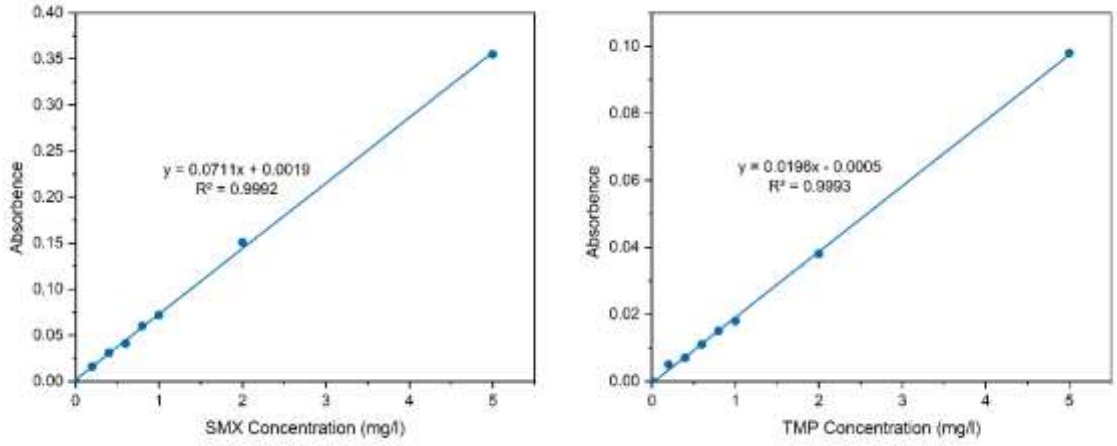

Figure 4.8: Standard Calibration Curves for SMX and TMP

As shown in Figure 4.11, linear equations were used to calculate the concentration of SMX (y = 0.0711x + 0.0019) and TMP (y = 0.0196x – 0.0005). According to Hadadare & Salunkhe (2013) and Sumbe et al. (2021), y represents absorbance of the analyte, while x represents concentration of the analyte. The coefficient of determination (R^2) of SMX and TMP was 0.9992 and 0.9993, respectively. This means that the data from the standard solutions followed the Beer-Lambert law, which states that absorbance is directly proportional to concentration and the path length of the light beam through the solution (Hardesty & Attili, 2010; Nandiyanto et al., 2023). However, the path length of the light beam through the solution was kept constant by maintaining the same cell and cuvette throughout the experiments.

4.2.2 Effect of Contact Time

To determine the equilibrium time for adsorption, the removal efficiencies of SMX and TMP by WR700 and CB700 were monitored over time (Figure 4.9).

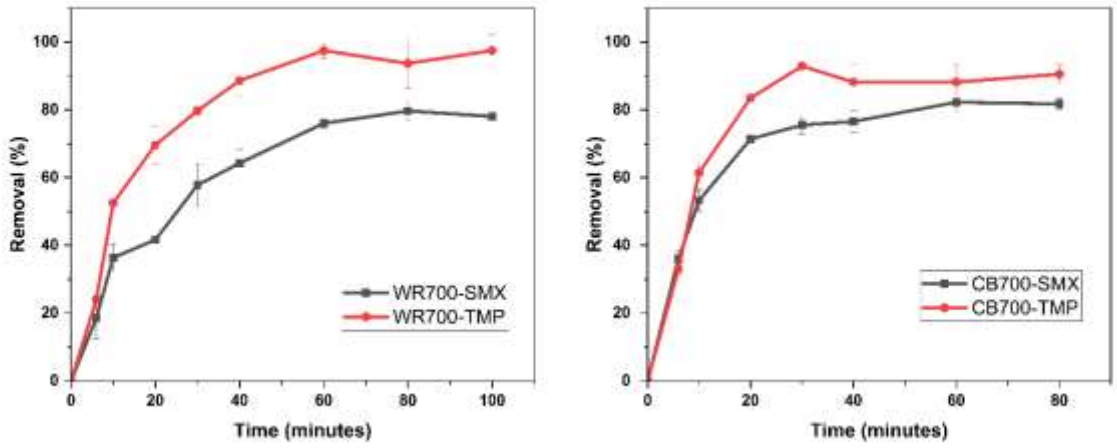

Figure 4.9: Effect of Contact Time on the Adsorption of SMX and TMP on WR700 and CB700

Adsorption on both materials was rapid during the initial stage, occurring within the first 30 minutes for WR700 and 20 minutes for CB700. During this period, WR700 achieved removal efficiencies of 57.8% (SMX) and 79.7% (TMP), while CB700 reached 71.4% and 83.5%, respectively.

Equilibrium was attained after 60 minutes for WR700, with adsorption capacities of 0.19 mg/g (SMX) and 0.21 mg/g (TMP). In contrast, CB700 reached equilibrium faster, at 20 minutes for SMX and 40 minutes for TMP, with corresponding capacities of 0.18 mg/g and 0.06 mg/g. The shorter equilibrium time for SMX on CB700 is consistent with its lower adsorption capacity compared to TMP, as shown in Figure 4.12.

The initial rapid adsorption is attributed to the abundance of available active sites and the strong concentration gradient driving mass transfer of SMX and TMP to the adsorbent surface (Cevallos-Mendoza et al., 2024). As adsorption progressed, the rate decreased due to site saturation, increased competition among adsorbate molecules, and slower intraparticle diffusion into the pores (Cevallos-Mendoza et al., 2024; Hambisa et al., 2023;

Zhao et al., 2024). Electrostatic repulsion between adsorbed and free molecules may have further contributed to the reduced uptake at later stages (Cevallos-Mendoza et al., 2024).

Overall, CB700 exhibited faster adsorption kinetics than WR700, while WR700 demonstrated slightly higher adsorption capacity for TMP and comparable capacity for SMX. The improved adsorption performance of the activated biochars compared with the unactivated white-rot fungus biochar and corncob biochar (which showed SMX removal efficiencies of only 0–30% during preliminary experiments) suggests that H_3PO_4 activation enhanced the adsorption properties of the biochars. This improvement may be attributed to the development of a more porous structure during activation.

4.2.3 Effect of pH

The effect of pH on the adsorption of SMX and TMP onto WR700 and CB700 is illustrated in Figure 4.10.

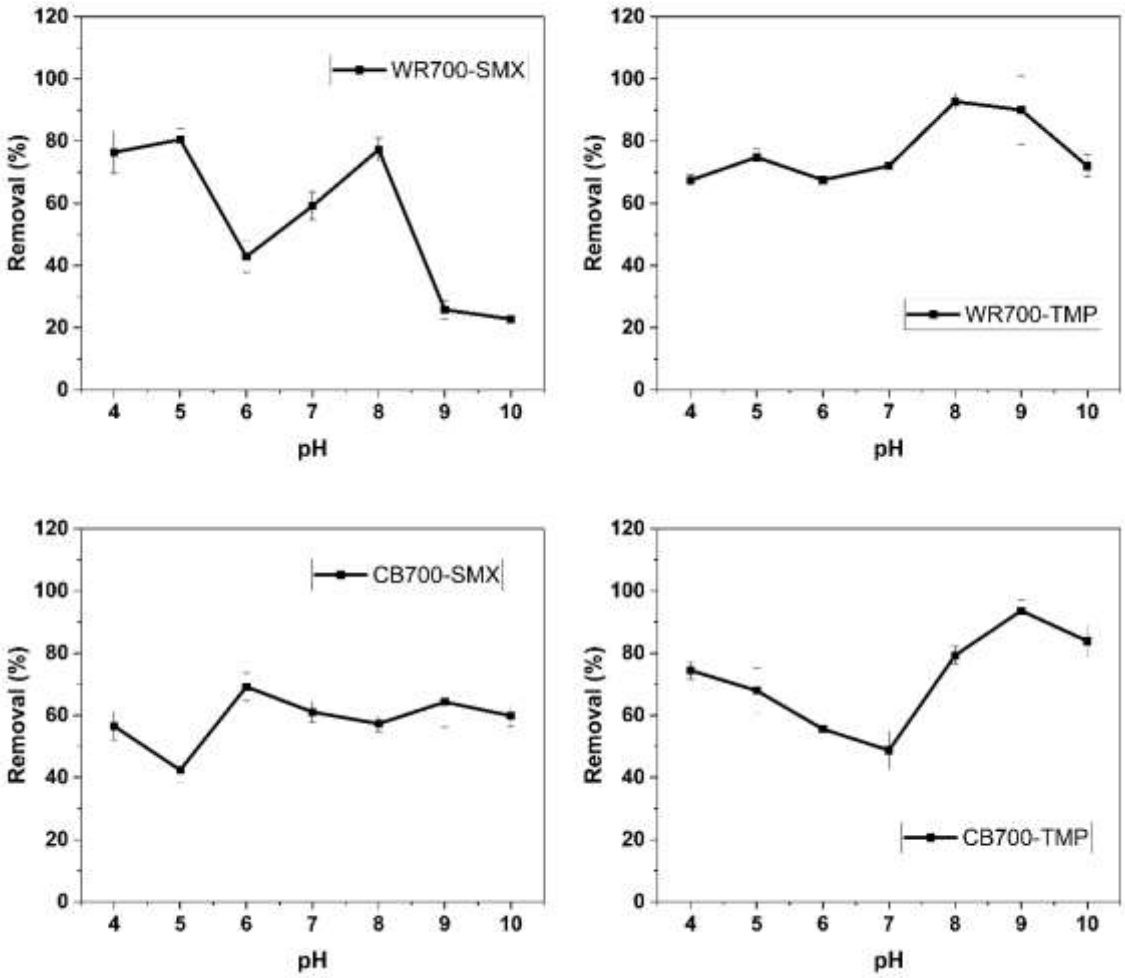

Figure 4.10: Effect of pH on the Adsorption of SMX and TMP on WR700 and CB700

The results show a significant dependence on pH ($P < 0.05$), with P-values of 6.13×10^{-7} (SMX-WR700), 2.4×10^{-4} (TMP-WR700), 1.46×10^{-3} (SMX–CB700), and 1.08×10^{-6} (TMP–CB700), as determined by ANOVA. While SMX did not exhibit a clear removal trend, TMP removal increased with increasing pH.

The pH-dependent behavior can be explained by the ionization states of the antibiotics. SMX has pKa_1 and pKa_2 values of 1.7 and 5.6, respectively, while TMP has pKa_1 and pKa_2 values of 1.32 and 7.45 (Esteki et al., 2020). Accordingly, SMX is predominantly cationic at pH < 1.7, anionic at pH > 5.6, and neutral at 1.7 < pH < 5.6 (Esteki et al., 2020; Fauziyen et al., 2024). In contrast, TMP is positively charged below pH 7.45 and becomes predominantly neutral above this value, with doubly and singly protonated species present below pKa_1 and between pKa_1 and pKa_2, respectively (Esteki et al., 2020; Liu et al., 2025; Ngumba et al., 2016). Tables 4 and 5 show summaries of SMX and TMP speciation, respectively.

Table 4.4: Summary of Sulfamethoxazole Speciation

pH Range	Dominant Species	Charge	Description
pH < 1.32	Protonated	SMX^+	Amine group protonated; molecule predominantly cationic
1.32 < pH <5.6	Neutral	SMX^0	Molecule predominantly neutral
pH > 5.6	Deprotonated	SMX^-	Sulfonamide group deprotonated; molecule predominantly anionic

Table 4.5: Summary of Ttimethoprim Speciation

pH Range	Dominant Species	Charge	Description
pH < 1.7	Protonated	TMP^{2+}	Both protonatable nitrogen rings are protonated (doubly charged)
1.7 < pH <7.45	Protonated	TMP^+	One nitrogen ring is deprotonated (singly charged)
pH > 7.45	Deprotonated	TMP^0	Both nitrogen rings are deprotonated (neutral)

Given the pH_{pzc} of WR700 (3.7), its surface is positively charged below this pH and negatively charged above it. Electrostatic interactions therefore do not consistently favor SMX adsorption, suggesting that non-electrostatic mechanisms, particularly hydrogen bonding (Ambaye et al., 2020; Jha et al., 2023; Li et al., 2020), play a dominant role across the experimental pH range (4-10). For TMP, adsorption on WR700 is primarily governed by electrostatic interactions. Below pH 7.2, attraction occurs between TMP cations and the negatively charged surface (Grimm et al., 2022; Saucier et al., 2017). Above this pH, TMP becomes neutral, and interactions between neutral TMP and negatively charged WR700 shift toward charge-induced dipole forces, with hydrogen bonding also contributing.

A similar trend is observed for CB700. SMX adsorption involves both electrostatic interactions and hydrogen bonding, with electrostatic forces contributing at pH 4–4.9 and hydrogen bonding becoming more significant above pH 5. TMP adsorption is largely driven by electrostatic attraction below pH 7.2 and charge-induced dipole interactions above 7.2, with additional contribution from hydrogen bonding.

4.2.4 Effect of Dosage

The effect of WR700 and CB700 dosage on the adsorption of SMX and TMP is illustrated in Figure 4.11.

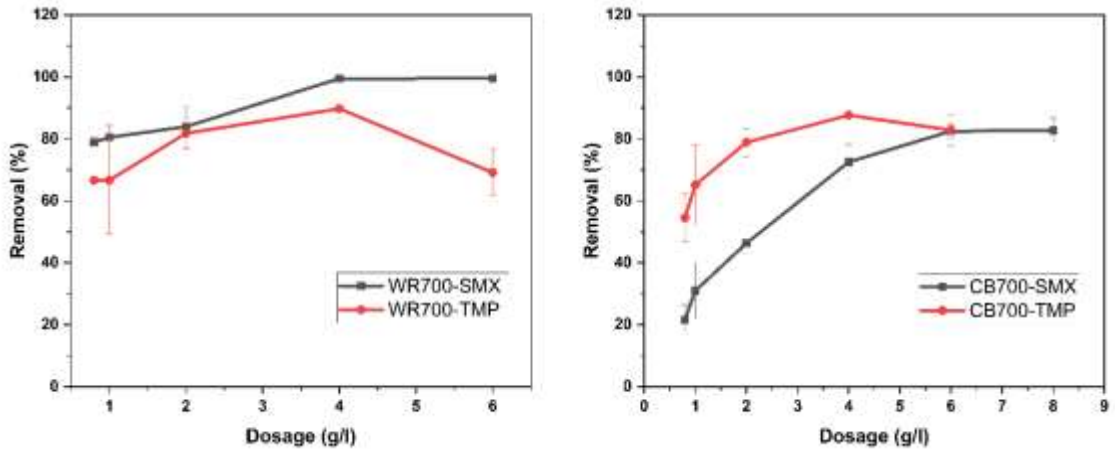

Figure 4.11: Effect of Dosage on the Adsorption of SMX and TMP on WR700 and CB700

The removal efficiency of both antibiotics increased with an increase in the adsorbent dosage. This could be attributed to the greater number of active sites available at higher dosages (Cevallos-Mendoza et al., 2024; Loh et al., 2024; Qais et al., 2023). However, increasing the dosage of WR700 and CB700 for SMX beyond 4 g/L and 6 g/L, respectively, resulted in only marginal improvements. Conversely, TMP adsorption on WR700 decreased from 89.78% at 4 g/L to 69.14% at 6 g/L, while TMP adsorption on CB700 decreased from 87.66% at 4 g/L to 82.84% at 6 g/L. This decline is likely due to site-site interactions, reduced suspension homogeneity, or particle aggregation, which reduces the effective surface area of the adsorbent (Alhothali et al. 2021; Mahmoud et al. 2025).

Thus, 4 g/l of WR700 was determined to be the optimal amount of adsorbent for achieving the highest adsorption of SMX and TMP, with adsorption capacities of 0.22 mg/g for each antibiotic. For CB700, 6 g/L and 4 g/L were identified as the optimal amounts of adsorbent for maximum adsorption of SMX and TMP, respectively. Their respective adsorption capacities were 0.12 mg/g and 0.15 mg/g.

Identifying the optimal dosage of adsorbents helps minimize waste while maximizing pollutant removal efficiency. As a result, an efficient and cost-effective adsorption process can be achieved (Mahmoud et al., 2025; Nugraha et al., 2025).

Both adsorbents exhibit lower adsorption capacities compared to other studies because the experiments were conducted in relatively low antibiotic concentrations (0 – 6 mg/L) to reflect the actual environmental levels. For instance, Dang et al. (2021) reported that corncob-derived biochar exhibited maximum adsorption capacities of 0.094 mg/g, 0.4 mg/g, and 0.306 mg/g for delafloxacin, ciprofloxacin, and ofloxacin. The solution concentrations used in that study ranged from 0 – 1.2 mg/L. On the other hand, Varela et al. (2024) reported that zinc chloride-activated corncob biochar exhibited maximum adsorption capacities of 332.08 mg/g and 175.86 mg/g for acetaminophen and amoxicillin, respectively. The solution concentrations used in that study ranged from 0 – 500 mg/L.

4.2.5 Adsorption Kinetics of Sulfamethoxazole and Trimethoprim

The kinetics of sulfamethoxazole (SMX) and trimethoprim (TMP) adsorption on WR700 and CB700 are illustrated in Figure 4.12.

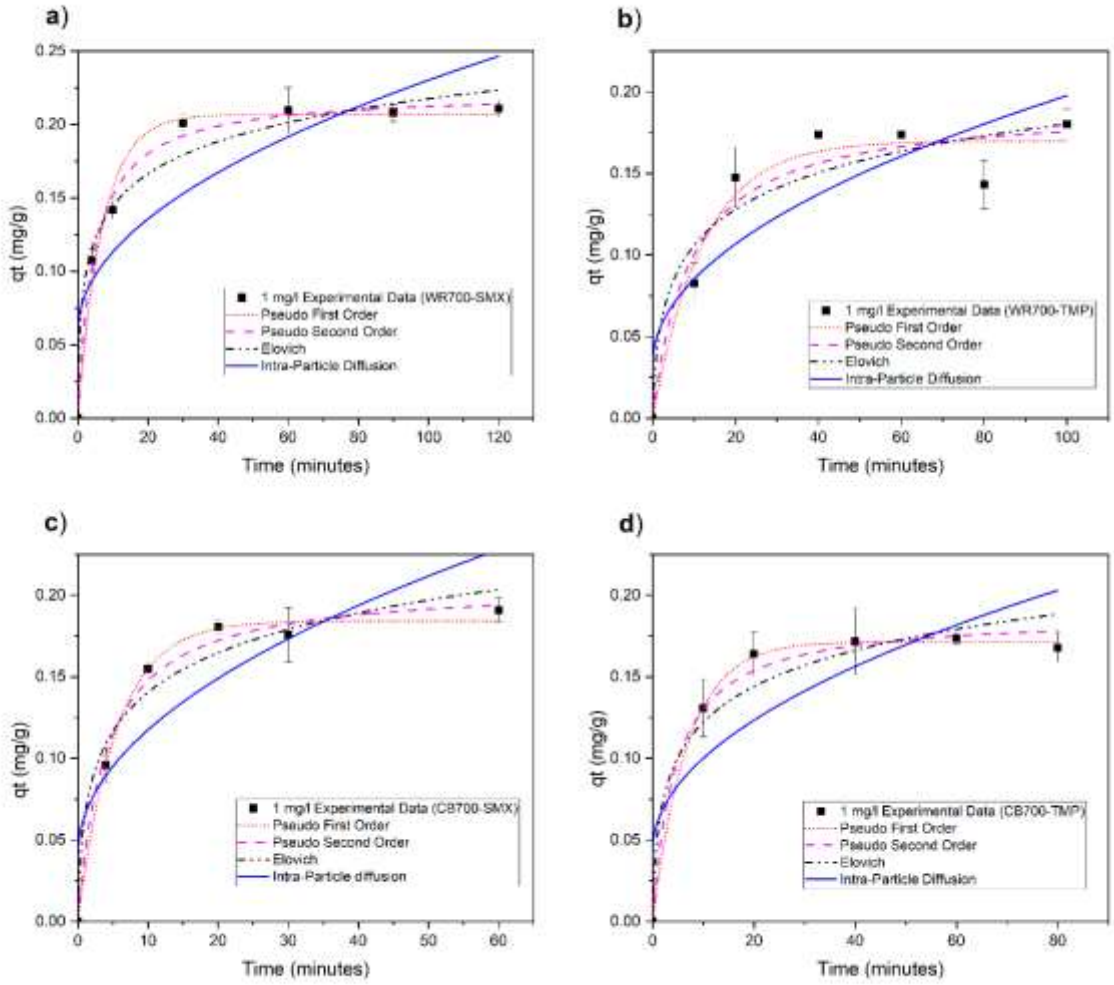

Figure 4.12: Kinetic Models of SMX and TMP Adsorption on WR700 and CB700: a) SMX Adsorption on WR700; b) TMP Adsorption on WR700; c) SMX Adsorption on CB700; and TMP Adsorption on CB700

As shown in Figure 4.12, the experimental data were analyzed using four kinetic models: pseudo-first-order (PFO), pseudo-second-order (PSO), Elovich, and intra-particle diffusion (IPD). The parameters for each model are presented in Table 4.6.

Table 4.6: Kinetic Models Parameters Concerning the Adsorption of SMX and TMP on WR700 and CB700

Kinetic model	Value of parameter			
	WR700-SMX	**WR700-TMP**	**CB700-SMX**	**CB700-TMP**
Pseudo first order				
$q_{e,exp}$ (mg/g)	0.21 ± 0.02	0.17	0.18	0.17
$q_{e,calc}$ (mg/g)	0.21 ± 0.01	0.17 ± 0.01	0.18 ± 0.003	0.17 ± 0.001
k_1 (1/min)	0.14 ± 0.02	0.08 ± 0.02	0.18 ± 0.01	0.15 ± 0.006
R^2	0.98	0.94	0.99	0.998
x^2	0.0001	0.0002	0.00003	5.6×10^{-6}
Pseudo second order				
$q_{e,calc}$ (mg/g)	0.22 ± 0.005	0.19 ± 0.02	0.21 ± 0.01	0.18 ± 0.01
k_2 (g/mg·min)	0.97 ± 0.13	0.58 ± 0.31	1.2 ± 0.24	1.16 ± 0.43
R^2	0.99	0.92	0.98	0.99
x^2	0.00005	0.0004	0.00006	4×10^{-5}
Elovich				
β	31.35 ± 4.45	30.45 ± 11.44	28.21 ± 0.22	56.7 ± 18.1
α	0.29 ± 0.19	0.08 ± 0.11	0.18 ± 0.01	5.1 ± 13.3
R^2	0.97	0.89	0.96	0.98
x^2	0.0002	0.0005	0.00005	8.9×10^{-5}
Intra-particle diffusion				
k_{ip}	0.02 ± 0.004	0.016 ± 0.004	0.02 ± 0.01	0.02 ± 0.01
C_{ip}	0.06 ± 0.03	0.03 ± 0.03	0.04 ± 0.03	0.04 ± 0.03
R^2	0.72	0.72	0.75	0.67
x^2	0.002	0.001	0.001	0.002

The results provide valuable insights on the adsorption rates of each antibiotic on WR700 and CB700, as well as the applicability of each model in describing the adsorption process. The experimental equilibrium adsorption capacities ($q_{e,exp}$) for WR700 were 0.21 ± 0.02 mg/g (SMX) and 0.17 mg/g (TMP), while those for CB700 were slightly lower but

comparable, at 0.18 mg/g (SMX) and 0.17 mg/g (TMP). These values are generally consistent with those obtained in the dosage experiments, with minor deviations likely attributable to experimental variability (Christodoulides & Christodoulides, 2017; Wha et al., 2022). Across both adsorbents, the calculated adsorption capacities ($q_{e,calc}$) from PFO and PSO models closely matched experimental values, although PSO tended to slightly overestimate q_e compared to PFO, particularly for CB700.

Model fitting based on R^2 values show subtle but informative trends. For WR700, SMX adsorption is marginally better described by the PSO model (R^2 = 0.99) compared to PFO (R^2 = 0.98), whereas TMP shows a slightly better fit to PFO (R^2 = 0.94 vs. 0.92 for PSO). In contrast, adsorption on CB700 is consistently better described by the PFO model for both SMX (R^2 = 0.99) and TMP (R^2 = 0.998), with PSO and Elovich models also providing strong but slightly lower fits. The Elovich model demonstrates reasonably good agreement for all systems ($R^2 \approx$ 0.89–0.98), indicating heterogeneous adsorption energies and the presence of multiple adsorption mechanisms. Meanwhile, the IPD model shows the poorest fit for both adsorbents ($R^2 \approx$ 0.67–0.75), suggesting that intra-particle diffusion is not the sole rate-limiting step. This deviation likely arises from the coexistence of multiple rate-controlling processes, including film diffusion, surface diffusion, and the heterogeneous pore structures of both WR700 and CB700 (Musah et al., 2023; Nayak & Pal, 2019; Zhu et al., 2016).

Further insight is obtained from the IPD intercept (C_{ip}) values for WR700 (59.15 ± 27.97 mg/g for SMX and 33.17 ± 26.7 mg/g for TMP) and for CB700 (0.04 ± 0.03 mg/g for both SMX and TMP), which indicate a large and minor contribution of film diffusion, respectively (Dharmarathna & Priyantha, 2024). This further reinforces that adsorption is governed by multiple mechanisms rather than a single diffusion process.

Although slight differences in R^2 values suggest preferred models (PSO for SMX on WR700 and PFO for most other cases), these differences are minimal and should not be overinterpreted. The close agreement between PFO and PSO fits across both adsorbents indicates that adsorption cannot be attributed exclusively to either physisorption or chemisorption. Instead, both mechanisms contribute simultaneously. This interpretation is strongly supported by complementary characterization data. FTIR deconvolution (Figures 4.3 and 4.4) reveals the presence of hydrogen bonding for both antibiotics. Additionally, zeta potential and surface functional group analyses confirm the involvement of electrostatic interactions alongside hydrogen bonding for both adsorbents.

Overall, the adsorption of SMX and TMP onto both WR700 and CB700 is best described by a combination of PFO, PSO, and Elovich models, reflecting the coexistence of physisorption and chemisorption processes. The initial stages of adsorption are likely governed by mass transfer and site accessibility, which can give rise to apparent PFO behavior, while chemical interactions such as hydrogen bonding contribute significantly to the overall adsorption mechanism. However, a clear distinction between physisorption and chemisorption cannot be established based on kinetic modeling alone and would require additional thermodynamic or spectroscopic evidence. The Elovich model further supports the presence of heterogeneous surfaces and multiple adsorption pathways. Therefore, adsorption on both WR700 and CB700 is governed by a complex interplay of physical and chemical interactions rather than a single dominant mechanism.

4.2.6 Adsorption Isotherms of Sulfamethoxazole and Trimethoprim

The adsorption behaviors of WR700 and CB700 toward SMX and TMP are presented in Figures 4.13 and 4.14, respectively, with the corresponding isotherm parameters summarized in Table 4.7. For WR700, the adsorption data were analyzed using five isotherm models: Freundlich, Sips, Langmuir, Temkin, and Dubinin-Radushkevich (D-R), whereas for CB700, only Freundlich, Temkin, and D-R models were applied, as the Sips and Langmuir models failed to converge for CB700 data.

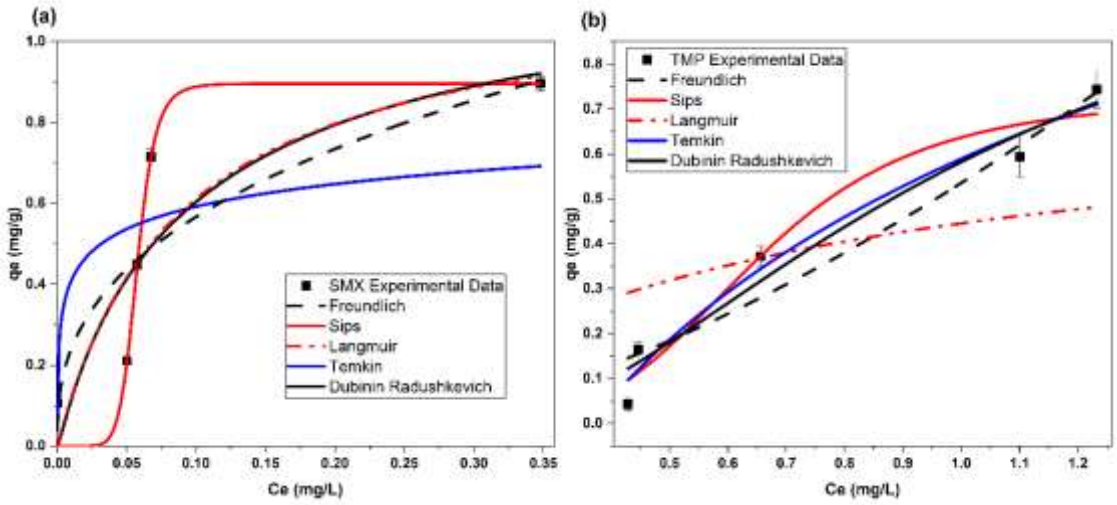

Figure 4.13: Isotherm Models of SMX and TMP Adsorption on WR700: a) SMX Adsorption on WR700; b) TMP Adsorption on WR700

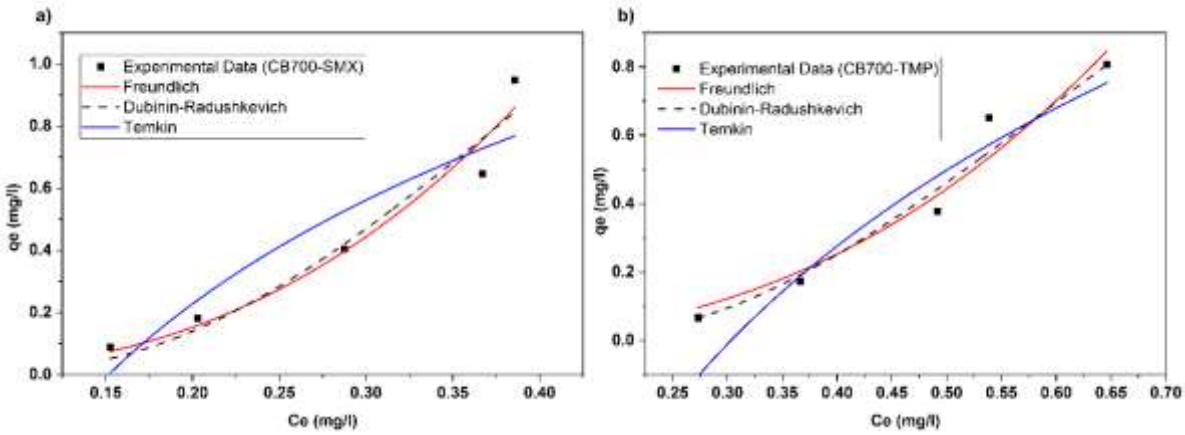

Figure 4.14: Isotherm Models of SMX and TMP Adsorption on CB700: a) SMX Adsorption on CB700; b) TMP Adsorption on CB700

Table 4.7: Isotherm Models Parameters Concerning the Adsorption of SMX and TMP on WR700 and CB700

Isotherm model	Value of parameter			
	WR700-SMX	WR700-TMP	CB700-SMX	CB700-TMP
Langmuir				
q_{max} (mg/g)	1.14 ± 0.37	0.74 ± 0.041		
K_L (L/mg)	11.47 ± 8.85	1.51 ± 0.78		
R^2	0.69	0.51		
x^2	0.03	0.04		
Freundlich				
K_F (mg/g(L/mg)1/s)	1.34 ± 0.47	0.54 ± 0.04	4.34 ± 1.6	2.03 ± 0.26
s	0.37 ± 0.17	1.53 ± 0.13	1.78 ± 0.35	2.35 ± 0.22
R^2	0.68	0.92	0.83	0.95
x^2	0.04	0.01	523.4	65.2
Sips				
q_{max} (mg/g)	0.9 ± 0.071	0.73 ± 0.18		
a_S	5.31×10^{10} ± 1.29×10^{12}	6.98 ± 10.69		
β_S	8.66 ± 8.5	4.49 ± 1.91		
R^2	0.95	0.86		
x^2	0.01	14.47		
Temkin				
B (mg/g)	0.08 ± 0.04	0.58 ± 0.00	1 ± 0.1	0.91 ± 0.13
A_T (L/g)	16161 ± 52525	2.76 ± 0.21	3.29 ± 0.13	6.6 ± 0.49
R^2	0.44	0.96	0.89	0.94
x^2	0.06	0.003	337.07	73.97

Dubinin				
q_{max} (mg/g)	1.12 ± 0.3	1.26 ± 0.19	3.88 ± 0.93	3.5 ± 0.33
K (mol²/J²)	0.11 ± 0.05	1.61 ± 0.29	0.91 ± 0.13	1.73 ± 0.09
R	1	0.43 ± 0.011	1	1
T	1	1	1	1
R^2	0.69	0.95	0.93	0.99
x^2	0.03	0.004	206.14	16.44

For TMP adsorption on WR700, the Langmuir model required modification due to the limited equilibrium concentration range (C_e = 1.233 mg/L) and the absence of a clear saturation plateau, which initially prevented convergence (Figure 4.13 (b)). Therefore, the maximum adsorption capacity (q_{max}) was fixed at the experimentally observed maximum value (0.744 mg/g), and only the Langmuir equilibrium constant (K_L) was optimized.

In the case of SMX adsorption on WR700, the Sips model provided the best fit (R^2 = 0.95, x^2= 0.01), indicating adsorption on a heterogeneous surface with cooperative interactions (Al-Ghouti & Da'ana, 2020). The high Sips exponent (β_S = 8.66 ± 8.5) suggests strong cooperativity, while the large affinity constant (a_S = 5.31 × 10^{10} ± 1.29 × 10^{12}) indicates highly favorable adsorption conditions, consistent with chemisorption interactions (Abubakar et al., 2025; Brião et al., 2023). In contrast, the Langmuir, Freundlich, Temkin, and D-R models showed poorer fits, with R^2 values of 0.69, 0.68, 0.44, and 0.69, respectively.

For TMP adsorption on WR700, the Temkin model yielded the best fit (R^2 = 0.96), followed by the D-R model (R^2 = 0.95) and the Freundlich model (R^2 = 0.92). The Sips model showed moderate agreement (R^2 = 0.86), whereas the Langmuir model exhibited the lowest fit (R^2 = 0.51). The Temkin model suggests adsorption involving significant chemisorption, where adsorption energy decreases linearly with surface coverage. Similarly, the D-R model indicates a pore-filling mechanism associated with strong adsorbate–adsorbent interactions (Al-Ghouti & Da'ana, 2020). The Freundlich model

further supports chemisorption behavior on a heterogeneous surface (Al-Ghouti & Da'ana, 2020). Collectively, these findings indicate that TMP adsorption is predominantly chemical rather than purely physical, with diffusion limitations or site accessibility potentially influencing the observed kinetics, consistent with the pseudo-first-order behavior identified earlier.

Integrating the kinetic, isotherm, and surface characterization data provides a unified mechanistic interpretation for WR700. SMX adsorption appears strongly cooperative on a heterogeneous, hydrophobic, and partially functionalized surface, with chemisorption dominating the process. TMP adsorption, while also governed by chemisorption, appears to be influenced by secondary factors such as diffusion resistance or site heterogeneity, resulting in distinct kinetic and isotherm characteristics. Thus, although adsorption of both SMX and TMP is largely driven by chemisorption, differences in molecular structure and interaction dynamics give rise to distinct adsorption behaviors.

For CB700, the D-R model provided the best fit for both antibiotics, with R^2 values of 0.93 for SMX and 0.99 for TMP. This was followed by the Temkin model (R^2 = 0.89 for SMX and 0.94 for TMP) and the Freundlich model (R^2 = 0.83 for SMX and 0.95 for TMP). However, the x^2 values for all models in both SMX and TMP adsorption are relatively large (Table 4.7), indicating deviations between predicted and experimental adsorption capacities, particularly at higher concentrations.

According to Al-Ghouti & Da'ana, (2020), Musah et al., (2022), and Syafiuddi et al., (2018), the D-R model reflects adsorption on a heterogeneous surface and suggests a pore-filling mechanism for antibiotics. This interpretation is consistent with the present findings for CB700. Similarly, the Temkin and Freundlich models also indicate surface heterogeneity. In the Freundlich model, the $1/s$ values for SMX (0.56) and TMP (0.43) are less than 1, indicating favorable adsorption of the antibiotics onto CB700 (Al-Ghouti & Da'ana, 2020). Favorable adsorption implies that CB700 exhibits strong affinity and bonding toward the antibiotics, even at low concentrations (Amaechi et al., 2024).

Overall, the adsorption behavior of CB700 for both SMX and TMP is best described by the D-R, Freundlich, and Temkin models, all of which consistently indicate a heterogeneous surface and strong interaction mechanisms. Compared to WR700, CB700 adsorption appears to rely more on pore-filling and heterogeneous surface interactions, whereas WR700 shows stronger evidence of cooperative chemisorption, particularly for SMX.

4.3 Removal Performance of White-Rot Fungus Biochar and Corncob Biochar Mixtures

The five-level, two-factor orthogonal matrix for the adsorption of sulfamethoxazole (SMX), along with the corresponding experimental values and the calculated S/N ratio for each run are shown in Table 4.8. Similarly, Table 4.9 presents the five-level, two-factor orthogonal matrix for trimethoprim (TMP) adsorption, including the experimental values and the calculated S/N ratios. The S/N ratios were calculated using Equation 2.17.

Table 4.8: SMX Experimental Design Matrix and Response Values

	SMX Adsorption variables		SMX Adsorption efficiency	
Run No.	**WR700:CB700**	**Time (minutes)**	**Experimental value (%)**	**S/N ratio**
1	20:80	20	47.22	34.27
2	20:80	30	53.69	34.63
3	20:80	40	58.21	34.92
4	20:80	60	55.63	34.97
5	20:80	80	60.80	35.29
6	35:65	20	48.86	34.48
7	35:65	30	57.11	34.85
8	35:65	40	60.28	35.13
9	35:65	60	60.28	35.18
10	35:65	80	62.82	35.51
11	50:50	20	57.94	34.83
12	50:50	30	63.15	35.20
13	50:50	40	64.45	35.49
14	50:50	60	61.20	35.53
15	50:50	80	66.41	35.86
16	65:35	20	51.02	34.35
17	65:35	30	54.62	34.71
18	65:35	40	54.02	35.00
19	65:35	60	57.62	35.04
20	65:35	80	63.03	35.37
21	80:20	20	39.97	33.53
22	80:20	30	39.30	33.89
23	80:20	40	47.43	34.18
24	80:20	60	51.49	34.23
25	80:20	80	55.56	34.55

Table 4.9: TMP Experimental Design Matrix and Response Values

Run No.	TMP Adsorption variables		TMP Adsorption efficiency	
	WR700:CB700	Time (minutes)	Experimental value (%)	S/N ratio
1	20:80	20	36.07	28.23
2	20:80	30	38.77	26.11
3	20:80	40	38.32	27.90
4	20:80	60	39.68	29.09
5	20:80	80	36.97	27.29
6	35:65	20	13.88	24.60
7	35:65	30	9.91	22.48
8	35:65	40	27.75	24.27
9	35:65	60	22.79	25.45
10	35:65	80	16.85	23.66
11	50:50	20	12.66	20.76
12	50:50	30	1.00	18.63
13	50:50	40	5.75	20.43
14	50:50	60	14.96	21.61
15	50:50	80	16.11	19.82
16	65:35	20	14.66	22.75
17	65:35	30	13.69	20.62
18	65:35	40	10.75	22.42
19	65:35	60	13.69	23.60
20	65:35	80	5.87	21.80
21	80:20	20	14.66	23.85
22	80:20	30	22.48	21.73
23	80:20	40	13.69	23.52
24	80:20	60	17.60	24.71
25	80:20	80	7.82	22.91

Figure 4.15 shows the main effect plot, in terms of S/N ratio, for the removal percentages of SMX and TMP against the WR700: CB700 ratio and contact time. From the plots, the optimal level of each factor was identified.

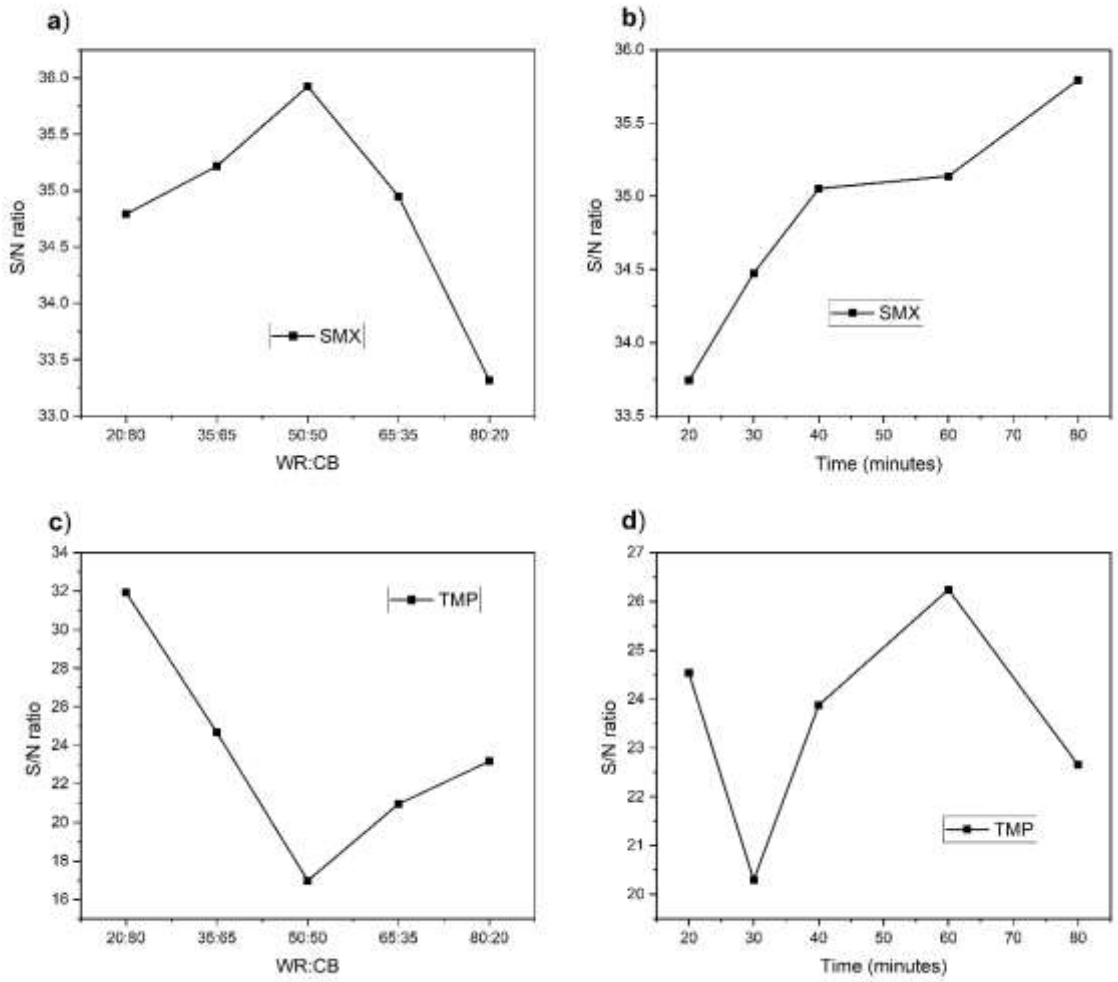

Figure 4.15: The Main Effect of Parameter by S/N ratios for Different Factors a) WR: CB Ratio on SMX, b) Contact Time on SMX, c) WR: CB Ratio on TMP, and d) Contact Time on TMP

The optimal levels for maximum SMX removal efficiency were a WR700: CB700 ratio of 50:50 and contact time of 80 minutes (Figure 4.15). For TMP, the optimal levels for maximum removal efficiency were a WR700: CB700 of 20:80 ratio and contact time of 60 minutes. Under these optimum conditions, the removal efficiency for SMX was 66.41% (S/N ratio = 35.86), while for TMP it was 39.68% (S/N ratio = 28.82). Upon validating these conditions, the maximum removal efficiencies for SMX and TMP were 65.56% (S/N ratio = 35.84) and 27.37% (S/N ratio = 28.17), respectively. The observed difference in TMP removal between the initial experiments (39.68%) and the validation experiments (27.37%) can be attributed to experimental variability, including slight fluctuations in pH, temperature, or adsorbent dosage, which can influence adsorption performance (Christodoulides & Christodoulides, 2017; Wha et al., 2022).

The combined use of WR700 and CB700 exhibited relatively low adsorption performance, with maximum removal efficiencies of 66.41% for SMX and 39.68% for TMP (Tables 4.8 and 4.9), compared to their individual adsorption capacities (82.51% for SMX and 87.7% for TMP on CB700, and 99.5% for SMX and 89.8% for TMP on WR700). From Figure 4.15, it was observed that the removal rates of both antibiotics decreased as the proportion of WR700 increased relative to CB700. Specifically, the S/N ratio decreased from 35.9 to 33.38 as the WR700:CB700 ratio changed from 50:50 to 80:20, suggesting that WR700 exerts an antagonistic effect on the adsorption process. Additionally, the maximum adsorption of SMX was attained at higher contact times, whereas TMP did not exhibit a clear pattern with respect to contact time. This difference is likely due to variations in their interaction mechanisms, as SMX and TMP have distinct physicochemical characteristics that influence their adsorption kinetics on WR700:CB700 biochar (Fauziyen et al., 2024; Liu et al., 2025).

The antagonistic effect of WR700 can be attributed to differences in the surface chemistry of WR700 and CB700, pore blockage, and the formation of a composite with reduced active sites. Although both WR700 and CB700 exhibited similar functional groups (–OH, C=O, C=C, and C–O) and individually achieved high removal efficiencies, their surface

chemistry can still vary depending on the precursor, which may affect their performance when combined (Rudakiya & Gupte, 2019; Varela et al., 2024; Zhao et al., 2024). In addition, the particle sizes of WR700 and CB700 ranged from 0.42–1.3 mm and 2–2.9 mm, respectively. The smaller particles of WR700 may have blocked the pores of CB700, thereby reducing its available surface area and active sites (Alhothali et al., 2021; Mahmoud et al., 2025).

The Analysis of Variance (ANOVA) results for SMX and TMP adsorption efficiency are shown in Tables 4.10 and 4.11, respectively.

Table 4.10: ANOVA Table for the Factors Affecting SMX Adsorption

Source	df	Sum of square	Mean square	F-Value	P-Value
WR700:CB700	4	666.6	166.643	25.69	0.000
Time	4	447.2	111.803	17.24	0.000
Error	16	103.8	6.486		
Total	24	1217.6			

Table 4.11: ANOVA Table for the Factors Affecting TMP Adsorption

Source	df	Sum of square	Mean square	F-Value	P-Value
WR700:CB700	4	2528.7	632.14	21.72	0.000
Time	4	79.92	19.88	0.68	0.614
Error	16	465.62	29.10		
Total	24	3073.72			

As illustrated in Table 4.10, both the WR700:CB700 ratio and contact time had a significant effect on SMX adsorption. This is supported by the P-values of 0.000 for both factors, which are less than the significance threshold of 0.05 (Yusuff et al., 2021). In contrast, for TMP adsorption (Table 4.11), only the WR700:CB700 ratio had a significant effect (P-value = 0.000 < 0.05), while contact time did not show a significant effect (P-value = 0.614 > 0.05), likely due to lower interaction of TMP with the combined adsorbent

(Table 4.9). However, because the Taguchi L25 design was primarily intended to estimate main effects, potential interactions between contact time and the WR700:CB700 ratio were not explicitly evaluated and, therefore, cannot be ruled out.

CHAPTER FIVE

CONCLUSIONS AND RECOMMENDATIONS

This study evaluated the removal of sulfamethoxazole and trimethoprim from aqueous solutions using white-rot fungus biochar, corncob biochar, and their mixtures. The key conclusions and recommendations arising from this study are summarized as follows:

5.1 Conclusions

Based on the results and findings presented in this thesis, the following conclusions can be drawn:

i. WR700 and CB700 possess desirable characteristics of activated biochar. Scanning electron microscopy (SEM) revealed well-developed pores, FTIR spectra confirmed the presence of key functional groups involved in the adsorption process such as C=O, C=C, and hydroxyl (–OH), and proximate and elemental analysis confirmed high carbon percentage in both biochars.

ii. The adsorption kinetics of both antibiotics were adequately described by the pseudo-first-order, pseudo-second-order, and Elovich models, suggesting the involvement of both physical and chemical adsorption processes. Equilibrium studies showed that SMX adsorption on WR700 was best described by the Sips model, whereas TMP adsorption on WR700 was better represented by the Temkin and Dubinin–Radushkevich models. For CB700, the Dubinin–Radushkevich, Freundlich, and Temkin models provided the best description of adsorption behavior, indicating adsorption on heterogeneous surfaces. When combined with biochar characterization results, these findings demonstrate that SMX and TMP adsorption on WR700 and CB700 occurred through multiple mechanisms involving surface heterogeneity, hydrogen bonding, electrostatic interactions, and pore filling.

iii. The combined WR700 and CB700 system exhibited lower removal efficiencies compared with the individual biochars. WR700 achieved removal efficiencies of 99.5% for SMX and 89.8% for TMP, while CB700 achieved 82.51% for SMX and 87.7% for TMP. In contrast, the combined biochar system achieved removal efficiencies of 65.56% and 27.37% for SMX and TMP, respectively, indicating that mixing WR700 and CB700 did not result in synergistic enhancement of antibiotic removal under the investigated conditions.

5.2 Recommendations for Future Work

The following recommendations are proposed:

i. Further research should investigate the effect of temperature on SMX and TMP adsorption using WR700 and CB700 to better understand the thermodynamic behavior of the adsorption process.
ii. Further studies should evaluate the regeneration and reusability of WR700 and CB700 to determine their long-term applicability and economic feasibility.
iii. Pilot-scale and field studies should be conducted to evaluate the practical applicability of WR700 and CB700 for antibiotic removal in complex wastewater matrices.

REFERENCES

Abdel-raouf, M. E., Maysour, N. E., Farag, R. K., & Abdul- Raheim, A.-R. M. (2019). Wastewater treatment methodologies: Review article. *International Journal of Environment & Agricultural Science*, *3*(1), 1–25. https://www.researchgate.net/publication/332183222_Wastewater_Treatment_Methodologies_Review_Article

Abdoul Magid, A. S. I., Islam, M. S., Chen, Y., Weng, L., Li, J., Ma, J., & Li, Y. (2021). Enhanced adsorption of polystyrene nanoplastics (PSNPs) onto oxidized corncob biochar with high pyrolysis temperature. *Science of the Total Environment*, *784*(147115), 1–11. https://doi.org/10.1016/j.scitotenv.2021.147115

Abin-bazaine, A., Trujillo, A. C., & Olmos-marquez, M. (2022). Adsorption isotherms : Enlightenment of the phenomenon of adsorption. In *Wastewater Treatment* (pp. 1–15). IntechOpen. https://doi.org/http://dx.doi.org/10.5772/intechopen.104260

Abubakar, A. M., Arowo, M. N., Selele, M. I., Houndedjihou, D., & Nayem, Z. (2025). Jovanovic and sips isotherm parameters of mango seed shell cadmium ion sorption from aqueous solution. *Sustainable Chemical Engineering*, *6*(1), 35–55. http://ojs.wiserpub.com/index.php/SCE/

Adekanye, T., Dada, O., & Kolapo, J. (2022). Pyrolysis of maize cob at different temperatures for biochar production : Proximate , ultimate and spectroscopic characterisation. *Research in Agricultural Engineering*, *68*(1), 27–34. https://doi.org/10.17221/106/2020-RAE

Adeoye, J. B., Tan, Y. H., Lau, S. Y., Tan, Y. Y., Chiong, T., Mubarak, N. M., & Khalid, M. (2024). Advanced oxidation and biological integrated processes for pharmaceutical wastewater treatment : A review. *Journal of Environmental Management*, *353*(120170), 1–28. https://doi.org/10.1016/j.jenvman.2024.120170

Adewuyi, A. (2020). Chemically modified biosorbents and their role in the removal of emerging pharmaceutical waste in the water system. *Water*, *12*, 1–31. https://www.mdpi.com/2073-4441/12/6/1551

Agrawal, T., Gautam, R., Agrawal, S., Singh, V., Kumar, M., & Kumar, S. (2020). Optimization of engine performance parameters and exhaust emissions in compression ignition engine fueled with biodiesel-alcohol blends using taguchi method , multiple regression and artificial neural network. *Sustainable Futures*, *2*, 1–12. https://doi.org/10.1016/j.sftr.2020.100039

Ahmed, M. B., Zhou, J. L., Ngo, H. H., Guo, W., Johir, M. A. H., & Sornalingam, K. (2016). Single and competitive sorption properties and mechanism of functionalized biochar for removing sulfonamide antibiotics from water. *Chemical Engineering Journal*. https://doi.org/10.1016/j.cej.2016.11.106

Ahmed, M., Mavukkandy, M. O., Giwa, A., Elektorowicz, M., Katsou, E., Khelifi, O., Naddeo, V., & Hasan, S. W. (2022). Recent developments in hazardous pollutants removal from wastewater and water reuse within a circular economy. *Clean Water*, *5*(12), 1–25. https://doi.org/10.1038/s41545-022-00154-5

Al-Ghouti, M. A., & Da'ana, D. A. (2020). Guidelines for the use and interpretation of adsorption isotherm models : A review. *Journal of Hazardous Materials*, *393*(122383), 1–22. https://doi.org/10.1016/j.jhazmat.2020.122383

Alhothali, A., Haneef, T., Mustafa, M. R. U., Moria, K. M., Rashid, U., Rasool, K., & Bamasag, O. O. (2021). Optimization of micro-pollutants' removal from wastewater using agricultural waste-derived sustainable adsorbent. *International Journal of Environmental Research and Public Health*, *18*(21), 1–18. https://doi.org/10.3390/ijerph182111506

Ali, A. F., & Gujiba, U. K. (2024). Household wastewater management in sub - saharan

africa : A review. *Discover Water*, *4*(6). https://doi.org/10.1007/s43832-024-00060-6

Amaechi, P. ., Elenwo, C. ., & Dimkpa, S. O. N. (2024). Langmuir and freundlich isotherm models' description of P. adsorption capacity of wetland and upland soil in rivers state. *Global Journal of Agricultural Research*, *12*(3), 14–29. https://doi.org/10.37745/gjar.2013/vol12n31429

Ambaye, T. G., Vaccari, M., van Hullebusch, E. D., Amrane, A., & Rtimi, S. (2020). Mechanisms and adsorption capacities of biochar for the removal of organic and inorganic pollutants from industrial wastewater. *International Journal of Environmental Science and Technology*, *18*(10), 3273–3294. https://doi.org/10.1007/s13762-020-03060-w

Amna, R., Ali, K., & Alhassan, S. M. (2023). Computational fluid dynamics analysis of mercury adsorption by inverse-vulcanized porous sulfur copolymers. *Industrial and Engineering Chemistry Research*, *62*(31), 12277–12290. https://doi.org/10.1021/acs.iecr.3c01674

Anand, U., Adelodun, B., Cabreros, C., Kumar, P., Suresh, S., Dey, A., Ballesteros Jr, F., & Bontempi, E. (2022). Occurrence , transformation , bioaccumulation , risk and analysis of pharmaceutical and personal care products from wastewater : A review. *Environmental Chemistry Letters*, *20*(6), 3883–3904. https://doi.org/10.1007/s10311-022-01498-7

Anastopoulos, I., Katsouromalli, A., & Pashalidis, I. (2020). Oxidized biochar obtained from pine needles as a novel adsorbent to remove caffeine from aqueous solutions. *Journal of Molecular Liquids*, *304*. https://doi.org/https://doi.org/10.1016/j.molliq.2020.112661

Anfar, Z., Zbair, M., Ahsiane, H. A., Jada, A., & Alem, N. El. (2020). Microwave assisted

green synthesis of Fe 2 O 3 / biochar for ultrasonic removal of nonsteroidal anti-inflammatory pharmaceuticals. *RSC Advances*, *10*, 11371–11380. https://doi.org/10.1039/d0ra00617c

Aragaw, T. A., & Alene, A. N. (2022). A comparative study of acidic, basic, and reactive dyes adsorption from aqueous solution onto kaolin adsorbent: Effect of operating parameters, isotherms, kinetics, and thermodynamics. *Emerging Contaminants*, *8*, 59–74. https://doi.org/10.1016/j.emcon.2022.01.002

Areti, H. A., Jabesa, A., Muleta, M. D., & Nemera, A. (2024). Adsorptive performances and valorization of green synthesized biochar–based activated carbon from banana peel and corn cob composites for the abatement of Cr (VI) from synthetic solutions : Parameters, isotherms, and remediation studies. *Heliyon*, *10*(e33811), 1–16. https://doi.org/10.1016/j.heliyon.2024.e33811

Asghar, A., Raman, A. A. A., & Daud, W. M. A. W. (2014). A comparison of central composite design and Taguchi method for optimizing fenton process. *Scientific World Journal*, *2014*, 1–14. https://doi.org/10.1155/2014/869120

Bagheri, A., Abu-Danso, E., Iqbal, J., & Bhatnagar, A. (2020). Modified biochar from moringa seed powder for the removal of diclofenac from aqueous solution. *Environmental Science and Pollution Research*, *27*(7), 7318–7327. https://doi.org/10.1007/s11356-019-06844-x

Bai, X., & Acharya, K. (2016). Removal of trimethoprim, sulfamethoxazole, and triclosan by the green alga Nannochloris sp. *Journal of Hazardous Materials*, *315*, 70–75. https://doi.org/https://doi.org/10.1016/j.jhazmat.2016.04.067

Bakhshandeh, M. H., Zarei, T., & Khorshidi, J. (2022). Chemical process design CFD study on beds of an adsorption desalination system in order to improve bed performance. *Chemical Process Design*, *1*(2), 59–73.

https://doi.org/10.22111/CPD.2023.44116.1015

Barasa, S. S., Ntie-kang, F., & Consortium, S. (2024). Sustainably addressing africa's antimicrobial pollution crisis. *Naure Reviews Earth & Environment*, *5*, 837–838. https://doi.org/10.1038/s43017-024-00618-x

Barros, A. R. M., Argenta, T. S., de Amorim de Carvalho, C., da Silva Oliveira, F., Milen Firmino, P. I., & Bezerra dos Santos, A. (2021). Effects of the antibiotics trimethoprim (TMP) and sulfamethoxazole (SMX) on granulation, microbiology, and performance of aerobic granular sludge systems. *Chemosphere*, *262*(127840), 1–11. https://doi.org/10.1016/j.chemosphere.2020.127840

Becker, D., Rodriguez-Mozaz, S., Insa, S., Schoevaart, R., Barceló, D., de Cazes, M., Belleville, M., Sanchez-Marcano, J., Misovic, A., Oehlmann, J., & Wagner, M. (2017). Removal of endocrine disrupting chemicals in wastewater by enzymatic treatment with fungal laccases. *Organic Process Research & Development*, *21*(4), 480–491. https://doi.org/10.1021/acs.oprd.6b00361

Bellahsen, N., Varga, G., Halyag, N., Kertész, S., Tombácz, E., & Hodúr, C. (2021). Pomegranate peel as a new low-cost adsorbent for ammonium removal. *International Journal of Environmental Science and Technology*, *18*(3), 711–722. https://doi.org/10.1007/s13762-020-02863-1

Bernardo, M., Rodrigues, S., Lapa, N., Matos, I., Lemos, F., Batista, M. K. S., Carvalho, A. P., & Fonseca, I. (2016). High efficacy on diclofenac removal by activated carbon produced from potato peel waste. *International Journal of Environment Science and Technology*, *13*, 1989–2000. https://doi.org/10.1007/s13762-016-1030-3

Bhattacharya, S. (2021). Central composite design for response surface methodology and its application in pharmacy. In *IntechOpen* (pp. 1–19). http://dx.doi.org/10.5772/intechopen.95835

Blandino, M., Fabbri, C., Soldano, M., Ferrero, C., Reyneri, A., Sciences, F., To, G., & Cereali, C. A. P. A. C. (2016). The use of cobs , a by-product of maize grain , for energy production in anaerobic digestion. *Italian Journal of Agronomy*, *11*(3), 754. https://doi.org/10.4081/ija.2016.754

Boeckel, T. P. Van, Brower, C., Gilbert, M., Grenfell, B. T., Levin, S. A., Robinson, T. P., Teillant, A., & Laxminarayan, R. (2015). Global trends in antimicrobial use in food animals. *PNAS*, *112*(18), 5649–5654. https://doi.org/10.1073/pnas.1503141112

Bouramdane, Y., Haddad, M., Mazar, A., Aît Lyazidi, S., Oudghiri Hassani, H., & Boukir, A. (2024). Aged lignocellulose fibers of cedar wood (9th and 12th century): Structural investigation using FTIR-deconvolution spectroscopy, x-ray diffraction (XRD), crystallinity indices, and morphological SEM analyses. *Polymers*, *16*(23), 1–19. https://doi.org/10.3390/polym16233334

Brião, G. D. V., Hashim, M. A., & Chu, K. H. (2023). The Sips isotherm equation : Often used and sometimes misused. *Separation Science and Technology*, *58*(5), 884–892. https://doi.org/10.1080/01496395.2023.2167662

Buczek, A., Rzepiela, K., Kupka, T., & Broda, M. A. (2025). Impact of O-H···π hydrogen bond on IR and NMR parameters of cannabidiol: Theoretical and experimental study. *Molecules*, *30*(12), 1–15. https://doi.org/10.3390/molecules30122591

Burdová, H., Brázová, V., Kwoczynski, Z., Snow, J., Trögl, J., & Kříženecká, S. (2024). Miscanthus x giganteus biochar: Effective adsorption of pharmaceuticals from model solution and hospital wastewater. *Journal of Cleaner Production*, *460*(142545), 1–12. https://doi.org/10.1016/j.jclepro.2024.142545

Cevallos-Mendoza, J. E., Cedeño-Muñoz, J. S., Navia-Mendoza, J. M., Figueira, F., Amorim, C. G., Rodríguez-díaz, J. M., & Montenegro, M. C. B. S. . (2024). Development of hybrid MIL-53 (Al)@ CBS for ternary adsorption of tetracyclines

antibiotics in water : Physical interpretation of the adsorption mechanism. *Bioresource Technology*, *396*(130453), 1–18. https://doi.org/10.1016/j.biortech.2024.130453

Chauhan, S., Shafi, T., Dubey, B. K., & Chowdhury, S. (2022). Biochar-mediated removal of pharmaceutical compounds from aqueous matrices via adsorption. *Waste Disposal and Sustainable Energy*, *5*(1), 37–62. https://doi.org/10.1007/s42768-022-00118-y

Chikri, R., Elhadiri, N., Benchanaa, M., & El maguana, Y. (2020). Efficiency of sawdust as low-cost adsorbent for dyes removal. *Journal of Chemistry*, *2020*, 1–17. https://doi.org/10.1155/2020/8813420

Chmielewski, J., Bąk-Badowska, J., Dietrich, G. J., Wójtowicz, B., Żeber-Dzikowska, I., Kordyzon, M., Król, H., Littva, V., & Gworek, B. (2023). Presence of pharmaceuticals in the aquatic environment: An underestimated threat to environmental health and a challenge for education. *Journal of Elementology*, *28*(3), 687–703. https://doi.org/10.5601/jelem.2023.28.3.2422

Christodoulides, C., & Christodoulides, G. (2017). *Measurement Errors* (pp. 39–56). https://doi.org/10.1007/978-3-319-53345-2_2

Coimbra, R. N., Calisto, V., Ferreira, C. I. A., Esteves, V. I., & Otero, M. (2019). Removal of pharmaceuticals from municipal wastewater by adsorption onto pyrolyzed pulp mill sludge. *Arabian Journal of Chemistry*, *12*(8), 3611–3620. https://doi.org/https://doi.org/10.1016/j.arabjc.2015.12.001

Dang, B. T., Gotore, O., Ramaraj, R., Unpaprom, Y., Whangchai, N., Bui, X. T., Maseda, H., & Itayama, T. (2020). Sustainability and application of corncob-derived biochar for removal of fluoroquinolones. *Biomass Conversion and Biorefinery*, *12*(3), 913–923. https://doi.org/10.1007/s13399-020-01222-x

Daniel, S. L., Rahman, A., Hamushembe, N. M., Kapolo, P., Uahengo, V., & Jonnalagadda, B. S. (2023). The production of activated carbon from acacia erioloba seedpods via phosphoric acid activation method for the removal of methylene blue from water. *Bioresource Technology Reports*, *23*(101568), 1–14. https://doi.org/10.1016/j.biteb.2023.101568

Das, S. K., Ghosh, G. K., Avasthe, R. K., & Sinha, K. (2021). Compositional heterogeneity of different biochar: Effect of pyrolysis temperature and feedstocks. *Journal of Environmental Management*, *278*(111501), 1–12. https://doi.org/10.1016/j.jenvman.2020.111501

Dehaghani, A. H. S., Soleimani, R., & Mohammadi, A. H. (2022). Simulation of chromium(III) ions biosorption from aqueous environment by olive stone biomass in a fixed-bed column and analysis of effective parameters using computational fluid dynamics method. *Desalination and Water Treatment*, *264*, 196–204. https://doi.org/10.5004/dwt.2022.28586

Diogo, B. S., Rodrigues, S., & Antunes, S. C. (2025). Mixture matters: Exploring the overlooked toxicity of sulfamethoxazole and trimethoprim in aquatic environments. *Environmental Toxicology*, 1–17. https://doi.org/10.1002/tox.24528

Diogo, B. S., Rodrigues, S., Golovko, O., & Antunes, S. C. (2024). From bacteria to fish: ecotoxicological insights into sulfamethoxazole and trimethoprim. *Environmental Science and Pollution Research*, *31*(39), 52233–52252. https://doi.org/10.1007/s11356-024-34659-y

Do, T., Van, H., Nguyen, T., Nguyen, T., & Nguyen, X. (2025). Development and application of coffee husk-based polyaniline composite (CF@ PANi) for enhanced ammonium removal from aqueous solutions. *RSC Advances*, *15*, 13882–13895. https://doi.org/10.1039/d5ra00949a

Dubrovkin, J. (2016). Evaluation of undetectable perturbations of peak parameters estimated by the least square curve fitting of analytical signal consisting of overlapping peaks. *Chemometrics and Intelligent Laboratory Systems*, *153*, 9–21. https://doi.org/https://doi.org/10.1016/j.chemolab.2016.02.004

Ehiomogue, P., Ahuchaogu, I. I., & Ahaneku, I. E. (2021). Review of adsorption isotherms models. *Acta Technica Corviniensis – Bulletin of Engineering*, *4*, 87–96. https://acta.fih.upt.ro/pdf/2021-4/ACTA-2021-4-16.pdf

Ellison, C., Abdelsayed, V., & Smith, M. W. (2023). Analysis of char structure and composition from microwave and conventional pyrolysis / gasification of low and middle rank coals. *Fuel*, *354*(129301), 1–12. https://doi.org/10.1016/j.fuel.2023.129301

Esteki, M., Dashtaki, E., Heyden, Y. Vander, & Simal-gandara, J. (2020). Application of rank annihilation factor analysis for antibacterial drugs determination by means of pH gradual change-UV spectral data. *Antibiotics*, *383*(9), 1–18. https://www.mdpi.com/2079-6382/9/7/383

Ezeuko, A. S., Ojemaye, M. O., Okoh, O. O., & Okoh, A. I. (2022). The effectiveness of silver nanoparticles as a clean-up material for water polluted with bacteria DNA conveying antibiotics resistance genes: Effect of different molar concentrations and competing ions. *OpenNano*, *7*(100060), 1–17. https://doi.org/10.1016/j.onano.2022.100060

FAO. (2015). *Sustainable development goals: 17 goals to transform our world*.

Fauziyen, S. P., Saputera, W. H., & Sasongko, D. (2024). Advancement and prospects in photocatalytic degradation of sulfamethoxazole (SMX) pharmaceutical waste. *South African Journal of Chemical Engineering*, *48*, 375–394. https://hdl.handle.net/10520/ejc-chemeng-v48-n1-a36

Figueredo, N. A., da Costa, L. M., Melo, L. C. A., Siebeneichlerd, E. A., & Tronto, J. (2017). Characterization of biochars from different sources and evaluation of release of nutrients and contaminants. *Revista Ciencia Agronomica*, *48*(3), 395–403. https://doi.org/10.5935/1806-6690.20170046

Filipinas, J. Q., Rivera, K. K. P., Ong, D. C., Pingul-Ong, S. M. B., Abarca, R. R. M., & de Luna, M. D. G. (2021). Removal of sodium diclofenac from aqueous solutions by rice hull biochar. *Biochar*, *3*(2), 189–200. https://doi.org/10.1007/s42773-020-00079-7

Foo, K. Y., & Hameed, B. H. (2010). Insights into the modeling of adsorption isotherm systems. *Chemical Engineering Journal*, *156*, 2–10. https://doi.org/10.1016/j.cej.2009.09.013

Gandam, P. K., Chinta, M. L., Gandham, A. P., Pabbathi, N. P. P., Konakanchi, S., Bhavanam, A., Atchuta, S. R., Baadhe, R. R., & Bhatia, R. K. (2022). A new insight into the composition and physical characteristics of corncob: substantiating its potential for tailored biorefinery objectives. *Fermentation*, *8*(12), 1–24. https://doi.org/10.3390/fermentation8120704

Geminiani, L., Campione, F. P., Canevali, C., Corti, C., Giussani, B., Gorla, G., Luraschi, M., Recchia, S., & Rampazzi, L. (2023). Historical silk: A novel method to evaluate degumming with non-invasive infrared spectroscopy and spectral deconvolution. *Materials*, *16*(5), 1–24. https://doi.org/10.3390/ma16051819

Ghazal, H., Koumaki, E., Hoslett, J., Malamis, S., Katsou, E., Barcelo, D., & Jouhara, H. (2022). Insights into current physical , chemical and hybrid technologies used for the treatment of wastewater contaminated with pharmaceuticals. *Journal of Cleaner Production*, *361*(132079), 1–22. https://doi.org/10.1016/j.jclepro.2022.132079

Göbel, A., McArdell, C. S., Joss, A., Siegrist, H., & Giger, W. (2007). Fate of

sulfonamides, macrolides, and trimethoprim in different wastewater treatment technologies. *Science of the Total Environment*, *372*(2–3), 361–371. https://doi.org/10.1016/j.scitotenv.2006.07.039

Gorito, A. M., Ribeiro, A. R. L., Rodrigues, P., Pereira, M. F. R., Guimarães, L., Almeida, C. M. R., & Silva, A. M. T. (2022). Antibiotics removal from aquaculture effluents by ozonation: Chemical and toxicity descriptors. *Water Research*, *218*(118497), 1–10. https://doi.org/10.1016/j.watres.2022.118497

Grimm, A., dos Reis, G. S., Dinh, V. M., Larsson, S. H., Mikkola, J. P., Lima, E. C., & Xiong, S. (2022). Hardwood spent mushroom substrate–based activated biochar as a sustainable bioresource for removal of emerging pollutants from wastewater. *Biomass Conversion and Biorefinery*, *14*(2), 2293–2309. https://doi.org/10.1007/s13399-022-02618-7

Grisales-Cifuentes, C. M., Serna Galvis, E. A., Porras, J., Flórez, E., Torres-Palma, R. A., & Acelas, N. (2021). Kinetics, isotherms, effect of structure, and computational analysis during the removal of three representative pharmaceuticals from water by adsorption using a biochar obtained from oil palm fiber. *Bioresource Technology*, *326*. https://doi.org/https://doi.org/10.1016/j.biortech.2021.124753

Gu, S., Li, Q., Kou, W., Sun, Z., Li, X., Wang, Y., Zhao, H., & Gao, P. (2025). Steam-assisted semi-carbonization pretreatment of corn stalks : Effects on physicochemical properties for enhanced biomass utilization. *Sustainability*, *17*(9091), 1–23.

Hadadare, M., & Salunkhe, V. (2013). Simultaneous estimation of beta sitosterol and palmitic acid from methanolic extract of caralluma adscedens var fimbriata by UV spectrophotometry. *Research Journal of Pharmaceutical, Biological and Chemical Sciences*, *4*(3), 225–232. https://www.rjpbcs.com/pdf/2013_4(3)/[26].pdf

Hardesty, J. H., & Attili, B. (2010). Spectrophotometry and the Beer-Lambert Law: An important analytical technique in chemistry. *Collin College, Department of Chemistry*, 1-6.

Hasani, N., Selimi, T., Mele, A., Thaçi, V., Halili, J., Berisha, A., & Sadiku, M. (2022). Theoretical, equilibrium, kinetics and thermodynamic investigations of methylene blue adsorption onto lignite coal. *Molecules*, *27*(6), 1–19. https://doi.org/10.3390/molecules27061856

Hassaan, M. A., Yılmaz, M., Helal, M., El-Nemr, M. A., Ragab, S., & El Nemr, A. (2023). Improved methylene blue adsorption from an aqueous medium by ozone-triethylenetetramine modification of sawdust-based biochar. *Scientific Reports*, *13*(1), 1–20. https://doi.org/10.1038/s41598-023-39495-7

Hassan, M., Liu, Y., Naidu, R., Parikh, S. J., Du, J., Qi, F., & Willett, I. R. (2020). Influences of feedstock sources and pyrolysis temperature on the properties of biochar and functionality as adsorbents: A meta-analysis. *Science of The Total Environment*, *744*(140714). https://doi.org/https://doi.org/10.1016/j.scitotenv.2020.140714

Hmamouchi, S., El Yacoubi, A., & El Idrissi, B. C. (2022). Using egg ovalbumin to synthesize pure α-Fe2O3 and cobalt doped α-Fe2O3: Structural, morphological, optical and photocatalytic properties. *Heliyon*, *8*(2), 1–11. https://doi.org/10.1016/j.heliyon.2022.e08953

Hom-Diaz, A., Jaén-Gil, A., Bello-Laserna, I., Rodríguez-Mozaz, S., Vicent, T., Barceló, D., & Blánquez, P. (2017). Performance of a microalgal photobioreactor treating toilet wastewater: Pharmaceutically active compound removal and biomass harvesting. *Science of The Total Environment*, *592*, 1–11. https://doi.org/https://doi.org/10.1016/j.scitotenv.2017.02.224

Hoogendijk, K., Myburgh, P. A., Howell, C. L., & Hoffman, J. E. (2023). Irrigation of agricultural crops with municipal wastewater: A review. *S. Afr. J. Enol. Vitic*, *44*(1), 31–54. https://doi.org/10.21548/44-1-5718

Huang, H.-B., Zhu, Y., & Yu, D. (2024). Low-dose trimethoprim-sulfamethoxazole treatment for pneumocystis pneumonia: A systematic review and meta-analysis. *Frontiers in Pharmacology*, *15*, 1–10. https://doi.org/10.3389/fphar.2024.1422490

Huang, J., Zimmerman, A. R., Chen, H., & Gao, B. (2020). Ball milled biochar effectively removes sulfamethoxazole and sulfapyridine antibiotics from water and wastewater. *Environmental Pollution*, *258*. https://doi.org/https://doi.org/10.1016/j.envpol.2019.113809

Huang, W., Chen, J., & Zhang, J. (2020). Removal of ciprofloxacin from aqueous solution by rabbit manure biochar. *Environmental Technology*, *41*(11), 1380–1390. https://doi.org/10.1080/09593330.2018.1535628

Hussain, S., Gajbhiye, P., Chandrakant, S., Vedpathak, A., Kit, C. C., Dixit, S., & Siddiqui, M. I. H. (2026). Characterization of biochar from prunus armeniaca shells collected in cold desert kargil , ladakh , as a soil enhancer. *Scientific Reports*, *16*(21221), 1–18. https://doi.org/10.3390/ma15176055

Inegbedion, F. (2022). Estimation of the moisture content, volatile matter, ash content, fixed carbon and calorific values of saw dust briquettes. *MANAS Journal of Engineering*, *10*(1), 17–20. https://doi.org/10.51354/mjen. 940760%0AEstimation

Ippolito, J. A., Cui, L., Kammann, C., Wrage-Mönnig, N., Estavillo, J. M., Fuertes-Mendizabal, T., Cayuela, M. L., Sigua, G., Novak, J., Spokas, K., & Borchard, N. (2020). Feedstock choice, pyrolysis temperature and type influence biochar characteristics: A comprehensive meta-data analysis review. *Biochar*, *2*(4), 421–438. https://doi.org/10.1007/s42773-020-00067-x

Jabar, J. M., Odusote, Y. A., Ayide, Y. T., & Yılmaz, M. (2022). African almond (terminalia catappa L) leaves biochar prepared through pyrolysis using H_3PO_4 as chemical activator for sequestration of methylene blue dye. *Results in Engineering*, *14*(100385), 1–9. https://doi.org/10.1016/j.rineng.2022.100385

Jha, S., Gaur, R., Shahabuddin, S., & Tyagi, I. (2023). Biochar as sustainable alternative and green adsorbent for the remediation of noxious pollutants: A comprehensive review. *Toxics*, *11*(117), 1–23. https://doi.org/10.3390/toxics11020117

Jiao, R., Liu, Z., Jin, O., Zhao, H., Di, S., Wang, Z., Dai, X., Ma, D., Qi, P., & Wang, X. (2024). The single adsorbent nano-TiO2 modified QuEChERS for simultaneous determination of 18 pyrrolizidine alkaloids in ginseng samples via LC-MS/MS. *Microchemical Journal*, *203*(110804), 1–10. https://doi.org/10.1016/j.microc.2024.110804

Jin, H., Yang, D., Wu, P., & Zhao, M. (2022). Environmental occurrence and ecological risks of psychoactive substances. *Environment International*, *158*(106970). https://doi.org/10.1016/j.envint.2021.106970

Karna, S. K., & Sahai, R. (2012). An overview on Taguchi method. *International Journal of Engineering and Mathematical Science*, *1*, 11–18. https://www.researchgate.net/profile/Shyam_Karna/publication/265282800_An_Overview_on_Taguchi_Method/links/550274ff0cf24cee39fc02cc/An-Overview-on-Taguchi-Method.pdf

Kasimanickam, V., Kasimanickam, M., & Kasimanickam, R. (2021). Antibiotics use in food animal production : Escalation of antimicrobial resistance : Where are we now in combating AMR ? *Medical Sciences*, *9*(14), 1–13. https://doi.org/10.3390/medsci9010014

Kaudza, C., Raude, J. M., & Ngumba, E. (2026). Removal of sulfamethoxazole and

trimethoprim from water using phosphoric acid-activated corncob biochar. *Environmental Science and Pollution Research*. https://doi.org/10.1007/s11356-026-37564-8

Kaudza, C., Raude, J. M., Ngumba, E., & Nyang, J. O. (2026). Adsorption mechanisms of sulfamethoxazole and trimethoprim using phosphoric acid activated white-rot fungus biochar. *Next Research*, *11*, 101991. https://doi.org/10.1016/j.nexres.2026.101991

Khan, M. I., Sufian, S., Hassan, F., Shamsuddin, R., & Farooq, M. (2025). Phosphoric acid based geopolymer foam-activated carbon composite for methylene blue adsorption: isotherm, kinetics, thermodynamics, and machine learning studies. *RSC Advances*, *15*(3), 1989–2010. https://doi.org/10.1039/d4ra05782a

Khasawneh, O. F. S., & Palaniandy, P. (2021). Occurrence and removal of pharmaceuticals in wastewater treatment plants. *Process Safety and Environmental Protection*, *150*, 532–556. https://doi.org/10.1016/j.psep.2021.04.045

Kneis, D., Lemay-St-Denis, C., Cellier-Goetghebeur, S., Elena, A. X., Berendonk, T. U., Pelletier, J. N., & Heß, S. (2023). Trimethoprim resistance in surface and wastewater is mediated by contrasting variants of the dfrB gene. *ISME Journal*, *17*(9), 1455–1466. https://doi.org/10.1038/s41396-023-01460-7

Koji, M., Mihajlovi, M., Marinovi, M., Petrovi, J., Katni, Đ., Krsti, A., Butulija, S., & Onjia, A. (2022). Calcium-pyro-hydrochar derived from the spent mushroom substrate as a functional sorbent of Pb 2 + and Cd 2 + from aqueous solutions. *Waste Management and Research*, *40*(11), 1629–1636. https://doi.org/10.1177/0734242X221093951

Kotabewatta, P. A., & Priyantha, N. (2024). Biosorption of Cd 2+ ions onto peel of artocarpus nobilis fruit: Intra-particle diffusion and isotherm studies. *Research*

Square, 1–28. https://doi.org/10.21203/rs.3.rs-4400981/v1

Kümmerer, K. (2010). Pharmaceuticals in the environment. *Annual Review of Environment and Resources*, *35*, 57–75. https://doi.org/10.1146/annurev-environ-052809-161223

Lach, J., Szymonik, A., & Ociepa-Kubicka, A. (2018). Adsorption of selected pharmaceuticals on activated carbons from water. *E3S Web of Conferences*, *44*(00089), 1–8. https://doi.org/10.1051/e3sconf/20184400089

Latif, W., Ciniglia, C., Iovinella, M., Shafiq, M., & Papa, S. (2023). Role of white rot fungi in industrial wastewater treatment : A review. *Applied Sciences*, *13*(14), 1–20. https://doi.org/10.3390/app13148318

Lestari, D. I., Yuliansyah, A. T., & Budiman, A. (2022). Adsorption studies of KOH-modified hydrochar derived from sugarcane bagasse for dye removal: Kinetic, isotherm, and thermodynamic study. *Communications in Science and Technology*, *7*(1), 15–22. https://doi.org/10.21924/cst.7.1.2022.669

Li, G., Guo, Y., & Zhao, W. (2017). Efficient adsorption removal of tetracycline by layered carbon particles prepared from seaweed biomass. *Environmental Progress & Sustainable Energy*, *36*(1), 59–65. https://aiche.onlinelibrary.wiley.com/doi/abs/10.1002/ep.12437

Li, J., Chen, Y., He, L., Liang, N., Wang, L., Zhao, J., & Pan, B. (2020). Sorption of sulfamethoxazole on biochars of varying mineral content. *Environmental Science: Processes and Impacts*, *22*(5), 1287–1294. https://doi.org/10.1039/d0em00102c

Li, J., Liang, N., Jin, X., Zhou, D., Li, H., Wu, M., & Pan, B. (2017). The role of ash content on bisphenol A sorption to biochars derived from different agricultural wastes. *Chemosphere*, *171*, 66–73.

https://doi.org/10.1016/j.chemosphere.2016.12.041

Li, Y., Shang, H., Cao, Y., Yang, C., Feng, Y., & Yu, Y. (2022). High performance removal of sulfamethoxazole using large specific area of biochar derived from corncob xylose residue. *Biochar*, *4*(11), 1–11. https://doi.org/10.1007/s42773-021-00128-9

Liu, J., Zhang, J., & Li, N. (2025). Environmentally friendly cellulose/lignin aerogel as adsorbent for efficiently adsorptive removal of trimethoprim from water. *Environmental Engineering Science*, *42*(6), 243–254. https://doi.org/10.1089/ees.2024.0335

Liu, R., Yu, H., Hou, X., Liu, X., Bi, E., Wang, W., & Li, M. (2022). Typical sulfonamide antibiotics removal by biochar-amended river coarse sand during groundwater recharge. *International Journal of Environmental Research and Public Health*, *19*(24), 1–12. https://doi.org/10.3390/ijerph192416957

Liu, X., Zhang, Y., Li, Z., Feng, R., & Zhang, Y. (2014). Characterization of corncob-derived biochar and pyrolysis kinetics in comparison with corn stalk and sawdust. *Bioresource Technology*, *170*, 76–82. https://doi.org/10.1016/j.biortech.2014.07.077

Loh, N. Y. L., Tee, W. T., Hanson, S., Chiu, W. S., Hiew, B. Y. Z., Khiew, S. P., & Lee, L. Y. (2024). Enhanced removal of lead and zinc by a 3D aluminium sulphate-functionalised graphene aerogel as an effective adsorption system. *Chemosphere*, *362*(142537), 1–12. https://doi.org/10.1016/j.chemosphere.2024.142537

López-Cabeza, R., Cox, L., Gámiz, B., Galán-Pérez, J. A., & Celis, R. (2024). Adsorption of sulfamethoxazole and ethofumesate in biochar- and organoclay-amended soil : Changes with adsorbent aging in the laboratory and in the field. *Science of the Total Environment*, *939*(173501), 1–11. https://doi.org/10.1016/j.scitotenv.2024.173501

Macherzyński, B., Wszelaka-Rylik, M., Włodarczyk-Makuła, M., & Andrzejewska-Górecka, D. (2021). Removal of chemotherapeutic agents in an integrated process of coagulation and sorption. *Desalination and Water Treatment*, *232*, 256–263. https://doi.org/10.5004/dwt.2021.27369

Maddodi, S. A., Alalwan, H. A., Alminshid, A. H., & Abbas, M. N. (2020). Isotherm and computational fluid dynamics analysis of nickel ion adsorption from aqueous solution using activated carbon. *South African Journal of Chemical Engineering*, *32*, 5–12. https://doi.org/10.1016/j.sajce.2020.01.002

Mahmoud, S. A., Atia, B. M., Amin, L. G., & Abdalla, M. (2025). Innovative preparation of multi-dentate Schiff base adsorbent for the adsorption of silver and its application on nano silver particles preparation from liquid photographic wastes. *Journal of Chemical Technology and Biotechnology*, *100*(2), 448–465. https://doi.org/10.1002/jctb.7787

Manila, R. M., Srinivasan, K., & Dutta, P. (2024). Experimental studies on the impact of adsorbent particle size on the adsorption chiller performance. *International Journal of Refrigeration*, *164*, 154–166. https://doi.org/https://doi.org/10.1016/j.ijrefrig.2024.04.021

Martins, M., Sanches, S., & Pereira, I. A. C. (2018). Anaerobic biodegradation of pharmaceutical compounds: New insights into the pharmaceutical-degrading bacteria. *Journal of Hazardous Materials*, *357*, 289–297. https://doi.org/https://doi.org/10.1016/j.jhazmat.2018.06.001

Matin, A., Jillani, S. M. S., Baig, U., Ihsanullah, I., & Alhooshani, K. (2023). Removal of pharmaceutically active compounds from water sources using nanofiltration and reverse osmosis membranes: Comparison of removal efficiencies and in-depth analysis of rejection mechanisms. *Journal of Environmental Management*, *338*(117682). https://doi.org/https://doi.org/10.1016/j.jenvman.2023.117682

Mayans, B., Camacho-Arévalo, R., García-Delgado, C., Antón-Herrero, R., Escolástico, C., Segura, M. L., & Eymar, E. (2021). An assessment of pleurotus ostreatus to remove sulfonamides, and its role as a biofilter based on its own spent mushroom substrate. *Environmental Science and Pollution Research*, *28*(6), 7032–7042. https://doi.org/10.1007/s11356-020-11078-3

Mendes, G. R., Modenez, I. D. A., Cagnani, G. R., Colombo, R. N. P., & Crespilho, F. N. (2023). Exploring enzymatic conformational dynamics at surfaces through μ-FTIR spectromicroscopy. *Analytical Chemistry*, *95*, 11254–11262. https://doi.org/10.1021/acs.analchem.3c00872

Mortazavian, S., Murph, S. E. H., & Jaeyun, M. (2022). Biochar nanocomposite as an inexpensive and highly efficient carbonaceous adsorbent for hexavalent chromium removal. *Materials*, *15*(6055), 1–16. https://doi.org/10.3390/ma15176055

Mshana, S. E., Sindato, C., Matee, M. I., & Mboera, L. E. G. (2021). Antimicrobial use and resistance in agriculture and food production systems in africa : A systematic review. *Antibiotics*, *10*(976), 1–21. https://doi.org/10.3390/ antibiotics10080976

Mukome, F. N. D., Zhang, X., Silva, L. C. R., Six, J., & Parikh, S. J. (2013). Use of chemical and physical characteristics to investigate trends in biochar feedstocks. *Journal of Agricultural and Food Chemistry*, *61*(9), 2196–2204. https://doi.org/10.1021/jf3049142

Musah, M., Azeh, Y., Mathew, J., Umar, M., Abdulhamid, Z., & Muhammad, A. (2022). Adsorption kinetics and isotherm models: A review. *Caliphate Journal of Science and Technology*, *4*(1), 20–26. https://doi.org/10.4314/cajost.v4i1.3

Musah, M., Mathew, T. J., Azeh, Y., Badeggi, M. U., Muhammad, I. A., & Muhammad, T. K. (2023). Intraparticle diffusion study of the adsorption of NI2+ and MN2+ onto chemically modified agricultural waste. *Development Journal of Science and*

Technology Research, *13*(1), 73–81. https://www.researchgate.net/publication/377063648_INTRAPARTICLE_DIFFUSION_STUDY_OF_THE_ADSORPTION_OF_Ni_2_AND_Mn_2_ONTO_CHEMICALLY_MODIFIED_AGRICULTURAL_WASTE

Musthofa, A. M. H., Syafila, M., & Helmy, Q. (2023). Effect of activated carbon particle size on methylene blue adsorption process in textile wastewater. *Indonesian Journal of Chemistry*, *23*(2), 461–474. https://doi.org/10.22146/ijc.79784

Mutegoa, E. (2024). Efficient techniques and practices for wastewater treatment : An update. *Discover Water*, *4*(69), 1–27. https://doi.org/10.1007/s43832-024-00131-8

N'diaye, A. D., Bollahi, M. A., & Kankou, M. S. (2019). Sorption of paracetamol from aqueous solution using groundnut shell as a low cost sorbent. *Journal of Materials and Environmental Sciences*, *10*(6), 553–562. https://www.researchgate.net/publication/371959888_Sorption_of_paracetamol_from_aqueous_solution_using_groundnut_shell_as_a_low_cost_sorbent

Nandiyanto, A. B. D., Ragadhita, R., & Aziz, M. (2023). How to calculate and measure solution concentration using uv-vis spectrum analysis: Supporting measurement in the chemical decomposition, photocatalysis, phytoremediation, and adsorption process. *Indonesian Journal of Science and Technology*, *8*(2), 345–362. https://doi.org/10.17509/ijost.v8i2.57783

Nayak, A. K., & Pal, A. (2019). Development and validation of an adsorption kinetic model at solid-liquid interface using normalized gudermannian function. *Journal of Molecular Liquids*, *276*, 67–77. https://doi.org/10.1016/j.molliq.2018.11.089

Ngumba, E., Gachanja, A., & Tuhkanen, T. (2016). Occurrence of selected antibiotics and antiretroviral drugs in Nairobi River Basin, Kenya. *Science of the Total Environment*, *539*, 206–213. https://doi.org/10.1016/j.scitotenv.2015.08.139

Ngumba, E., Kosunen, P., Gachanja, A., & Tuhkanen, T. (2016). A multiresidue analytical method for trace level determination of antibiotics and antiretroviral drugs in wastewater and surface water using SPE-LC-MS/MS and matrix-matched standards. *Analytical Methods*, *8*, 6720–6729. https://doi.org/10.1039/C6AY01695B

Nugraha, W. M., Kim, S., Roddick, F., Xie, Z., & Fan, L. (2025). A review of the recent advancements in adsorption technology for removing antibiotics from hospital wastewater. *Journal of Water Process Engineering*, *70*(106960), 1–17. https://doi.org/10.1016/j.jwpe.2025.106960

Nwabueze, B. I., Nwabueze, O. O., Isiuku, B. O., Njoku, V. O., Adindu, C. B., & John-Dewole, O. O. (2024). Biosorption of Methylene Blue from Aqueous Solution using Unmodified Plantain Stalk (UPS) Biomass. *Life Science Journal*, *21*(10). http://dx.doi.org/10.7537/marslsj211024.02

Oberoi, A. S., Jia, Y., Zhang, H., Khanal, S. K., & Lu, H. (2019). Insights into the fate and removal of antibiotics in engineered biological treatment systems : A critical review. *Environmental Science and Technology*, *53*, 7234–7264. https://doi.org/10.1021/acs.est.9b01131

Oginni, O., Singh, K., Oporto, G., Dawson-Andoh, B., McDonald, L., & Sabolsky, E. (2019). Effect of one-step and two-step H_3PO_4 activation on activated carbon characteristics. *Bioresource Technology Reports*, *8*(100307). https://doi.org/https://doi.org/10.1016/j.biteb.2019.100307

Otieno, O. A. (2023). *Nutrients and energy recovery from ecological sanitation system*. Unpublished doctorial dissertation, Jomo Kenyatta University of Agriculture and Technology.

Otoo, B. A., Amoabeng, I. A., Darko, G., & Borquaye, L. S. (2022). Antibiotic and analgesic residues in the environment – Occurrence and ecological risk study from

the Sunyani municipality, Ghana. *Toxicology Reports*, *9*, 1491–1500. https://doi.org/10.1016/j.toxrep.2022.07.003

Paredes-Laverde, M., Silva-Agredo, J., & Torres-Palma, R. A. (2018). Removal of norfloxacin in deionized, municipal water and urine using rice (oryza sativa) and coffee (coffea arabica) husk wastes as natural adsorbents. *Journal of Environmental Management*, *213*, 98–108. https://doi.org/10.1016/j.jenvman.2018.02.047

Patil, D., & Kadam, S. (2023). Basics of computational fluid dynamics: An overview. *IOP Conference Series: Earth and Environmental Science*, *1130*(1), 1–13. https://doi.org/10.1088/1755-1315/1130/1/012042

Pavlović, D. M., Ćurković, L., Macan, J., & Žižek, K. (2017). Eggshell as a new biosorbent for the removal of pharmaceuticals from aqueous solutions. *Clean*, *45*(12), 1–14. https://doi.org/10.1002/clen.201700082

Pouretedal, H. R., & Sadegh, N. (2014). Effective removal of amoxicillin, cephalexin, tetracycline and penicillin G from aqueous solutions using activated carbon nanoparticles prepared from vine wood. *Journal of Water Process Engineering*, *1*, 64–73. https://doi.org/https://doi.org/10.1016/j.jwpe.2014.03.006

Puhlmann, N., Olsson, O., & Kümmerer, K. (2024). How data on transformation products can support the redesign of sulfonamides towards better biodegradability in the environment. *Science of the Total Environment*, *921*(171027), 1–13. https://doi.org/10.1016/j.scitotenv.2024.171027

Putranto, A., Wei, Z. W. N., Hadibarata, T., Aziz, M., Yeo, J. Y. J., Ismadji, S., & Sunarso, J. (2022). Effects of pyrolysis temperature and impregnation ratio on adsorption kinetics and isotherm of methylene blue on corn cobs activated carbons. *South African Journal of Chemical Engineering*, *42*, 91–97. https://doi.org/10.1016/j.sajce.2022.07.008

Qais, D. S., Islam, M. N., Othman, M. H. D., Mahmud, H. N. M. E., Quayum, M. E., Isram, M. A., Ismail, I. M. I., & Habib, A. (2023). Nano-zinc oxide fibers: Synthesis, characterization, adsorption of acid blue 92 dye, isotherms, thermodynamics and kinetics. *Emerging Contaminants*, *9*(100224), 1–13. https://doi.org/10.1016/j.emcon.2023.100224

Ravindiran, G., Rajamanickam, S., Janardhan, G., Hayder, G., Alagumalai, A., Mahian, O., Lam, S. S., & Sonne, C. (2024). Production and modifications of biochar to engineered materials and its application for environmental sustainability : A review. *Biochar*, *6*(62), 1–27. https://doi.org/10.1007/s42773-024-00350-1

Reddy, C. A. (1995). The potential for white-rot fungi in the treatment of pollutants. *Current Opinion in Biotechnology*, *6*, 320–328. https://doi.org/10.1016/0958-1669(95)80054-9

Reza, M. S., Yun, C. S., Afroze, S., Radenahmad, N., Bakar, M. S. A., Saidur, R., Taweekun, J., & Abul, K. (2020). Preparation of activated carbon from biomass and its applications in water and gas purification , a review. *Arab Journal of Basic and Applied Sciences*, *27*(1), 208–238. https://doi.org/10.1080/25765299.2020.1766799

Rohde, M. (2019). The gram-positive bacterial cell wall. *Microbiol Spectrum*, *7*(3), 1–21. https://doi.org/10.1128/microbiolspec.GPP3-0044-2018.Correspondence

Roy, N., Roy, S., Debroy, A., & Mukherjee, A. (2024). Chlorella sp. EPS loaded alginate microsphere: A novel bionanomaterial for adsorptive removal of sulfamethoxazole from the aqueous solutions. *Environmental Technology and Innovation*, *33*(103513), 1–17. https://doi.org/10.1016/j.eti.2023.103513

Rudakiya, D. M., & Gupte, A. (2019). Assessment of white rot fungus mediated hardwood degradation by FTIR spectroscopy and multivariate analysis. *Journal of Microbiological Methods*, *157*, 123–130.

https://doi.org/https://doi.org/10.1016/j.mimet.2019.01.007

Samimi, M., Zakeri, M., Alobaid, F., & Aghel, B. (2023). A brief review of recent results in arsenic adsorption process from aquatic environments by metal-organic frameworks: Classification based on kinetics, isotherms and thermodynamics behaviors. *Nanomaterials*, *13*(60), 1–12. https://doi.org/10.3390/nano13010060

Sanusi, I. O., Olutona, G. O., Wawata, I. G., & Onohuean, H. (2023). Occurrence, environmental impact and fate of pharmaceuticals in groundwater and surface water: A critical review. *Environmental Science and Pollution Research*, *30*(39), 90595–90614. https://doi.org/10.1007/s11356-023-28802-4

Saravanan, A., Kumar, P. S., Jeevanantham, S., Karishma, S., Tajsabreen, B., Yaashikaa, P. R., & Reshma, B. (2021). Effective water / wastewater treatment methodologies for toxic pollutants removal : Processes and applications towards sustainable development. *Chemosphere*, *280*, 1–15. https://doi.org/10.1016/j.chemosphere.2021.130595

Sarfaraz, Q., Souza da Silva, L., Drescher, G. L., Zafar, M., Severo, F. F., Molin, G. D., Shafi, M. I., Shafique, Q., & Solaiman, Z. M. (2021). Characterization and carbon mineralization of biochars produced from different animal manures and plant residues. *Scientific Reports*, *10*(955), 1–9. https://doi.org/10.1038/s41598-020-57987-8

Sikder, S., Toha, M., Anik, A. H., Sultan, M. B., Alam, M., Parvin, F., & Tareq, S. M. (2024). A comprehensive review on the fate and impact of antibiotic residues in the environment and public health: A special focus on the developing countries. *Water Environment Research*, *96*(2), e10987. https://doi.org/10.1002/wer.10987

Silori, R., & Tauseef, S. M. (2021). A review of the occurrence of pharmaceutical compounds as emerging contaminants in treated wastewater and aquatic

environments. *Current Pharmaceutical Analysis*, *18*(4), 345–379. https://doi.org/10.2174/1573412918666211119142030

Silva, F., RR Almeida, W., R Paula, F., LH Müller, A., MM Flores, É., & F Ferrão, M. (2017). The effect of pH on the simultaneous determination of sulfamethoxazole and trimethoprim by ultraviolet spectrophotometry and multivariate calibration. *Drug Analytical Research*, *1*(2), 15–23. https://doi.org/10.22456/2527-2616.79218

Stando, K., Czyż, A., Gajda, M., Felis, E., & Bajkacz, S. (2022). Study of the phytoextraction and phytodegradation of sulfamethoxazole and trimethoprim from water by limnobium laevigatum. *International Journal of Environmental Research and Public Health*, *19*(24), 1–18. https://doi.org/10.3390/ijerph192416994

Sudaryanto, A., Witama, R. O., Nosaki, K., Tanoue, R., Suciati, F., Sachoemar, S. I., Hayami, Y., Morimoto, A., Nomiyama, K., & Kunisue, T. (2023). Occurrence of emerging contaminants in Jakarta Bay, Indonesia: Pharmaceuticals and personal care products. *IOP Conference Series: Earth and Environmental Science*, *1137*(012050), 1–7. https://doi.org/10.1088/1755-1315/1137/1/012050

Sumbe, R., Gawade, A., Bhingare, C. ., & Kuchekar, A. (2021). Development and validation of UV visible spectrophotometric method for estimation of quercetin in tagetes erecta extract. *International Journal of Recent Scientific Research*, *12*(01(A)), 40465–40468. https://doi.org/10.24327/IJRSR

Sun, Y., & Webley, P. A. (2010). Preparation of activated carbons from corncob with large specific surface area by a variety of chemical activators and their application in gas storage. *Chemical Engineering Journal*, *162*, 883–892. https://doi.org/10.1016/j.cej.2010.06.031

Swedberg, G., & Sundström, L. (2010). *Diaminopyrimidines* (pp. 250–258). https://doi.org/10.1016/B978-0-7020-4064-1.00017-8

Syafiuddi, A., Salmiati, S., Jonbi, J., & Fulazzaky, M. A. (2018). Application of the kinetic and isotherm models for better understanding of the behaviors of silver nanoparticles adsorption onto different adsorbents. *Journal of Environmental Management*, *218*, 59–70. https://doi.org/10.1016/j.jenvman.2018.03.066

Torres-Farradá, G., Thijs, S., Rineau, F., Guerra, G., & Vangronsveld, J. (2024). White rot fungi as tools for the bioremediation of xenobiotics : A review. *Journal of Fungi*, *10*(167), 1–41. https://www.frontiersin.org/journals/microbiology/articles/10.3389/fmicb.2024.1374974/full

Tsarpali, M., Kuhn, J. N., & Philippidis, G. P. (2024). Activated carbon production from algal biochar : Chemical activation and feasibility analysis. *Fuel Communications*, *19*(100115), 1–10. https://doi.org/10.1016/j.jfueco.2024.100115

Varela, C. F., Moreno-Aldana, L. C., & Agámez-Pertuz, Y. Y. (2024). Adsorption of pharmaceutical pollutants on ZnCl 2-activated biochar from corn cob : Efficiency, selectivity, and mechanism. *Journal of Bioresources and Bioproducts*, *9*, 58–73. https://doi.org/10.1016/j.jobab.2023.10.003

Vona, A., di Martino, F., Garcia-Ivars, J., Picó, Y., Mendoza-Roca, J.-A., & Iborra-Clar, M.-I. (2015). Comparison of different removal techniques for selected pharmaceuticals. *Journal of Water Process Engineering*, *5*, 48–57. https://doi.org/https://doi.org/10.1016/j.jwpe.2014.12.011

Vuong, T. X., Stephen, J., Nguyen, T. T. T., Cao, V., & Pham, D. T. N. (2023). Insight into the speciation of heavy metals in the contaminated soil incubated with corn cob-derived biochar and apatite. *Molecules*, *28*(2225), 1–23. https://doi.org/10.3390/molecules28052225

Weber, K., & Quicker, P. (2018). Properties of biochar. *Fuel*, *217*, 240–261.

https://doi.org/https://doi.org/10.1016/j.fuel.2017.12.054

Wei, W., Zhang, C., Chen, Z., Chen, W., Ran, G., Pan, G., Zhang, W., Müller-Buschbaum, P., Bo, Z., Yang, C., & Luo, Z. (2024). Precise methylation yields acceptor with hydrogen-bonding network for high-efficiency and thermally stable polymer solar cells. *Angewandte Chemie - International Edition*, *63*(6), 1–14. https://doi.org/10.1002/anie.202315625

Wha, J., Euijin, L., & Raghu, H. (2022). True value , error , and measurement uncertainty : Two views. *Accreditation and Quality Assurance*, *27*(4), 235–242. https://doi.org/10.1007/s00769-022-01508-9

Wilberforce, T., Ijaodola, O., Emmanuel, O., Thompson, J., Olabi, A. G., Abdelkareem, M. A., Sayed, E. T., Elsaid, K., & Maghrabie, H. M. (2021). Optimization of fuel cell performance using computational fluid dynamics. *Membranes*, *11*(146), 1–20. https://doi.org/10.3390/ membranes11020146

Wilkinson, J. L., Boxall, A. B. A., Kolpin, D. W., Leung, K. M. Y., Lai, R. W. S., Wong, D., Ntchantcho, R., Pizarro, J., Mart, J., Echeverr, S., Garric, J., Chaumot, A., Gibba, P., Kunchulia, I., Seidensticker, S., Lyberatos, G., Morales-salda, J. M., & Kang, H. (2022). Pharmaceutical pollution of the world ’s rivers. *PNAS*, *119*(8), 1–10. https://doi.org/10.1073/pnas.2113947119/-/DCSupplemental.Published

Wilkinson, J. L., Thornhill, I., Oldenkamp, R., Gachanja, A., & Busquets, R. (2023). Pharmaceuticals and personal care products in the aquatic environment: How can regions at risk be identified in the future? *Environmental Toxicology and Chemistry*, *43*(3), 575–588. https://doi.org/10.1002/etc.5763

Wu, Q., Xian, Y., He, Z., Zhang, Q., Wu, J., Yang, G., & Zhang, X. (2019). Adsorption characteristics of Pb (II) using biochar derived from spent mushroom substrate. *Scientific Reports*, *9*(15999), 1–11. https://doi.org/10.1038/s41598-019-52554-2

Wu, S., Li, Y., Zhao, X., Du, Q., Wang, Z., Xia, Y., & Xia, L. (2015). Biosorption behavior of ciprofloxacin onto enteromorpha prolifera: Isotherm and kinetic studies. *International Journal of Phytoremediation*, *17*(10), 957–961. https://doi.org/10.1080/15226514.2014.935288

Xu, D., Cao, J., Li, Y., Howard, A., & Yu, K. (2019). Effect of pyrolysis temperature on characteristics of biochars derived from different feedstocks : A case study on ammonium adsorption capacity. *Waste Management*, *87*, 652–660. https://doi.org/10.1016/j.wasman.2019.02.049

Xu, L., Campos, L. C., Li, J., Karu, K., & Ciric, L. (2021). Removal of antibiotics in sand, GAC, GAC sandwich and anthracite/sand biofiltration systems. *Chemosphere*, *275*(130004). https://doi.org/https://doi.org/10.1016/j.chemosphere.2021.130004

Yang, C., Wu, H., Cai, M., Li, Y., Guo, C., Han, Y., Zhang, Y., & Song, B. (2023). Valorization of food waste digestate to ash and biochar composites for high performance adsorption of methylene blue. *Journal of Cleaner Production*, *397*(136612), 1–9. https://doi.org/10.1016/j.jclepro.2023.136612

Yang, X., Zhang, S., Ju, M., & Liu, L. (2019). Preparation and modification of biochar materials and their application in soil remediation. *Applied Sciences*, *9*(7), 1–25. https://doi.org/10.3390/app9071365

Yekeen, N., Ali Elakkari, A. M., Khan, J. A., Ali, M., Al-Yaseri, A., & Hoteit, H. (2023). Experimental and computational fluid dynamics investigation of mechanisms of enhanced oil recovery via nanoparticle-surfactant solutions. *Energy and Fuels*, *37*(7), 5114–5129. https://doi.org/10.1021/acs.energyfuels.3c00136

Yu, L., Bi, J., Song, Y., & Wang, M. (2022). Isotherm, thermodynamics, and kinetics of methyl orange adsorption onto magnetic resin of chitosan microspheres. *International Journal of Molecular Sciences*, *23*(22), 1–18.

https://doi.org/10.3390/ijms232213839

Yusuff, A. S., Ajayi, O. A., & Popoola, L. T. (2021). Application of taguchi design approach to parametric optimization of adsorption of crystal violet dye by activated carbon from poultry litter. *Scientific African*, *13*(e00850), 1–13. https://doi.org/10.1016/j.sciaf.2021.e00850

Zambrano, J., García-Encina, P. A., Hernández, F., Botero-Coy, A. M., Jiménez, J. J., & Irusta-Mata, R. (2021). Removal of a mixture of veterinary medicinal products by adsorption onto a scenedesmus almeriensis microalgae-bacteria consortium. *Journal of Water Process Engineering*, *43*(102226), 1–11. https://doi.org/10.1016/j.jwpe.2021.102226

Zhang, Y., Qin, Z., & Zhao, K. (2026). Application of gaussian curve fitting method in gamma energy spectrum overlapping peak identification. *Radiation Physics and Chemistry*, *239*(113362). https://doi.org/https://doi.org/10.1016/j.radphyschem.2025.113362

Zhang, Z., Wu, J., & Chen, W. (2014). Review on prepation and application of biochar. *Advanced Materials Research*, *898*, 456–460. https://doi.org/10.4028/www.scientific.net/AMR.898.456

Zhao, J., Gao, F., Sun, Y., Fang, W., Li, X., & Dai, Y. (2021). New use for biochar derived from bovine manure for tetracycline removal. *Journal of Environmental Chemical Engineering*, *9*(4). https://doi.org/https://doi.org/10.1016/j.jece.2021.105585

Zhao, X., Zhu, G., Liu, J., Wang, J., Zhang, S., Wei, C., & Cao, L. (2024). Efficient removal of tetracycline from water by one-step pyrolytic porous biochar derived from antibiotic fermentation residue. *Nanomaterials*, *14*(1377), 1–18. https://doi.org/10.3390/nano14171377

Zhou, T., Yu, Z., Zhang, L., Gong, C., & Yan, C. (2024). Removal of sulfonamides from water by wetland plants : Performance , microbial response and mechanism. *Science of the Total Environment*, *916*(170181), 1–11. https://doi.org/10.1016/j.scitotenv.2024.170181

Zhu, Q., Moggridge, G. D., & D'Agostino, C. (2016). Adsorption of pyridine from aqueous solutions by polymeric adsorbents MN 200 and MN 500. Part 2: Kinetics and diffusion analysis. *Chemical Engineering Journal*, *306*, 1223–1233. https://doi.org/https://doi.org/10.1016/j.cej.2016.07.087

APPENDICES

Appendix I: Adsorption Data for Sulfamethoxazole (SMX) and Trimethoprim (TMP) onto White-Rot Fungus Biochar (WR700) and Corncob Biochar (CB700) at an Initial Concentration of 1 mg/L

Table A1: Adsorption Data for SMX onto WR700

Time (minutes)	C_0 (mg/L)	C_t (mg/L)	q_t (mg/g)	Removal (%)	STD Deviation
0	0.88	0.88	0	0	0.97
4	0.88	0.45	0.10	48.68	3.49
10	0.88	0.31	0.14	64.35	2.56
30	0.88	0.08	0.20	91.21	2.56
60	0.88	0.04	0.21	95.13	8.45
90	0.88	0.05	0.21	94.29	2.56
120	0.88	0.04	0.21	95.69	2.56

Table A2: Adsorption Data for TMP onto WR700

Time (minutes)	C_0 (mg/L)	C_t (mg/L)	q_t (mg/g)	Removal (%)	STD Deviation
0	0.86	0.86	0	0	0
6	0.86	0.65	0.21	24.05	0.71
10	0.86	0.41	0.45	52.53	1.11
20	0.86	0.26	0.6	69.62	5.55
30	0.86	0.17	0.68	79.75	1.11
40	0.86	0.1	0.76	88.61	4.44
60	0.86	0.02	0.84	97.47	2.27
80	0.86	0.05	0.8	93.67	7.37
100	0.86	0.02	0.84	97.47	4.62

Table A3: Adsorption Data for SMX onto CB700

Time (minutes)	C_0 (mg/L)	C_t (mg/L)	q_t (mg/g)	Removal (%)	STD Deviation
0	0.92	0.92	0	0	1.76
4	0.92	0.54	0.1	41.56	4.65
10	0.92	0.31	0.15	66.90	2.32
20	0.92	0.20	0.18	78.05	1.76
30	0.92	0.22	0.18	76.03	7.19
60	0.92	0.16	0.19	82.62	3.17

Table A4: Adsorption Data of TMP onto CB700

Time (minutes)	C_0 (mg/L)	C_t (mg/L)	q_t (mg/g)	Removal (%)	STD Deviation
0	1.11	1.11	0	0	0
4	1.11	0.75	0.09	33.07	1.75
10	1.11	0.43	0.17	61.41	2.54
20	1.11	0.18	0.23	83.46	5.43
30	1.11	0.08	0.26	92.91	0.46
40	1.11	0.13	0.25	88.19	5.21
60	1.11	0.13	0.25	88.19	5.21
80	1.11	0.11	0.25	90.55	2.68

Appendix II: Zeta Potential Data for White-Rot Fungus Biochar (WR700) and Corncob Biochar (CB700)

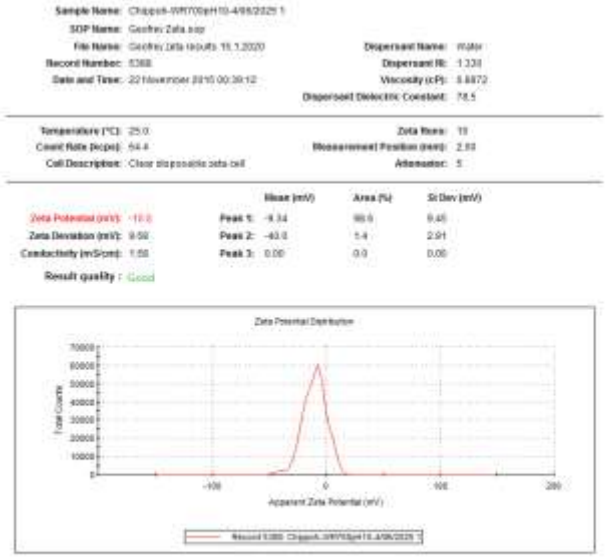

Figure B1: Zeta potential Data for WR700 at pH10

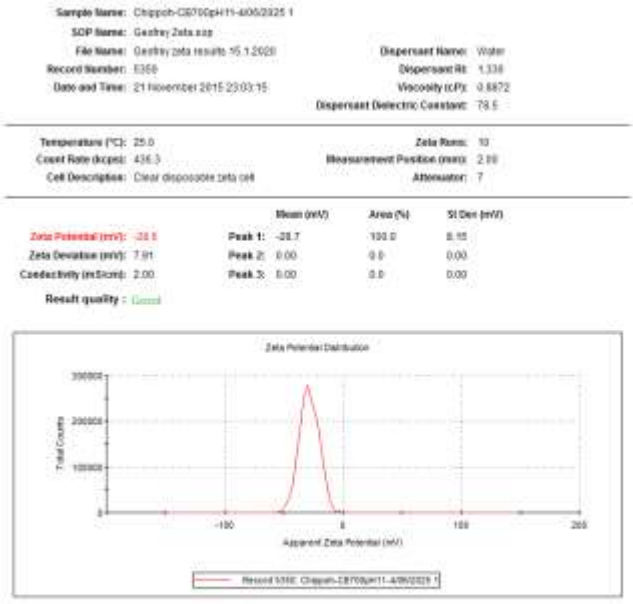

Figure B2: Zeta potential Data for CB700 at pH11

Appendix III: Pictures of Equipment and Samples Used in the Study

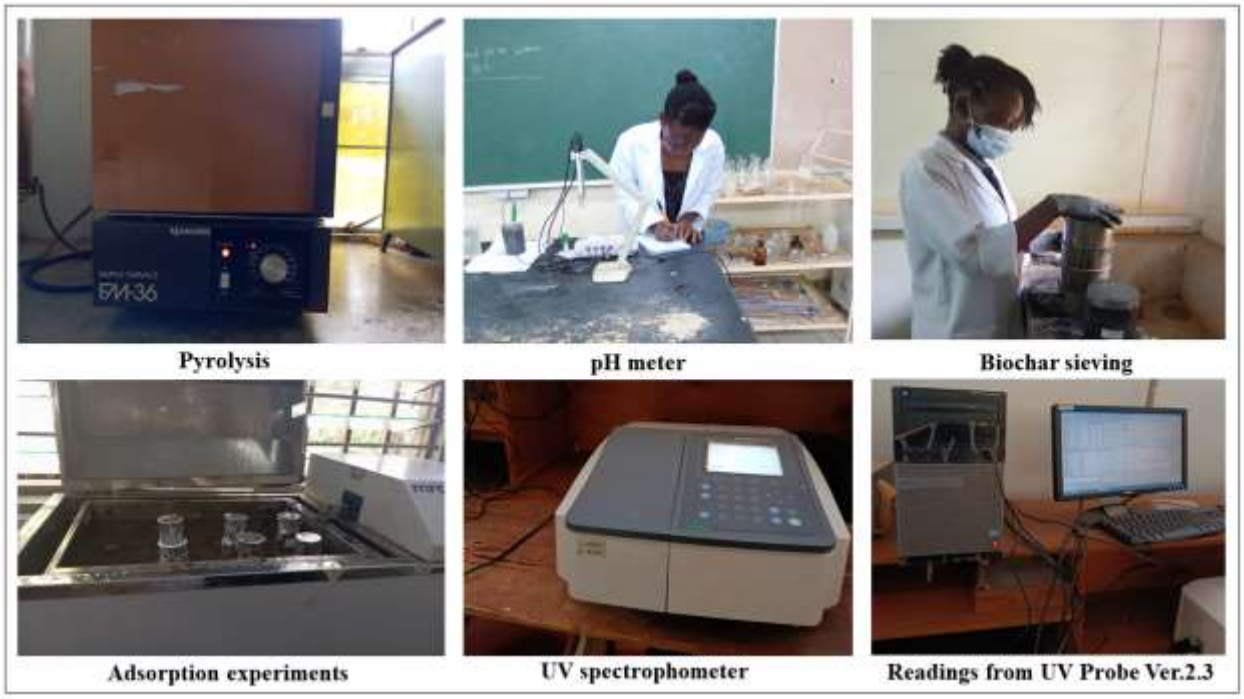

Figure C1: Equipment used in Biochar Preparation and Adsorption studies

Figure C2: Image of White-Rot Fungus (*Ganoderma applanatum*)

Figure C3: Image of Corncobs

Figure C4: Image of Corncob Biochar

Figure C5: Image of White-Rot Fungus Biochar